

Pavement Performance Prediction Using Machine Learning and Instrumentation in Smart Pavement

by

Jianqi Kang

A thesis

presented to the University of Waterloo

in fulfillment of the

thesis requirement for the degree of

Master of Applied Science

in

Civil Engineering

Waterloo, Ontario, Canada, 2022

© Jianqi Kang 2022

Author's Declaration

I hereby declare that I am the sole author of this thesis. This is a true copy of the thesis, including any required final revisions, as accepted by my examiners.

I understand that my thesis may be made electronically available to the public.

Abstract

The optimization of pavement Maintenance and Rehabilitation (M&R) planning and costs has been historically proven as a complex task. In recent years, Artificial Intelligence (AI) and Machine Learning (ML) applications in pavement engineering data analytics have been gaining momentum. These advanced techniques have shown promising results in civil engineering and transportation asset management. Therefore, designing a smart pavement framework that relies on the actual pavement responses and in-service condition can help with utilising the ML approach toward better understanding the performance of pavements. To implement the concept of “Smart Pavement”, constructing an interactive pavement pilot section that provides the necessary data feedback to improve the decision-makings of M&R would be needed. This thesis focuses on some aspects of the design of in-situ pavement monitoring and the applying selected machine learning techniques for pavement performance prediction. In order to design an effective pavement instrumentation plan, a literature review was conducted to identify and evaluate the major in-situ monitoring devices and previous case studies. Innovative technologies of Structural Health Monitoring (SHM) were also discussed as a part of the sensory system. A potential pilot section was identified by the Region of Waterloo, for which the pavement structure and technical details were retrieved. Based on the results from the literature review and the evaluation of the proposed section details, a preliminary instrumentation layout has been proposed. Next, the interaction between the proposed embedded sensors and surrounding pavement structure under traffic loading was further studied to evaluate the effect of pavement instrumentation on actual structural responses. Therefore, a series of finite element analysis (FEA) scenarios were defined, and modelling was conducted using ABAQUS to quantify the artefact impacts of the sensors on the pavement responses. Based on the FEA results, high stress- and strain-concentration areas were located which can be used to optimize the design of sensor layout, leading to capturing representative critical pavement responses. Consequently, sensor spacing criteria were suggested to avoid device interference for the response measurement.

Furthermore, it would be informative to know how, and which AI/ML methods have been previously used for pavement performance prediction purposes. A systematic literature review was conducted indicating that majority of studies used Artificial Neural Network (ANN) of which the prediction process is unexplainable to predict International Roughness Index (IRI) resulting in high prediction accuracies ($R^2 \geq 0.9$). A Decision Tree (DT) model and a Random Forest (RF) model were developed using the most commonly used input data retrieved from the Long-Term Pavement Performance (LTPP) database to predict IRI. Finally, after the pruning process, the DT model and RF model resulted in a cross-validation accuracy (R^2) of 0.846 and 0.859, respectively. The single tree from the DT model is less complex than the trees from the RF model. Further studies on machine learning model development should be conducted to refine prediction accuracy. Finally, recommendation for future data collection standards from pilot sections were provided to help with developing a pavement response database that can overcome the inconsistencies in the existing LTPP database and potentially improve the reliability of the future pavement performance modelling.

Acknowledgements

I would like to acknowledge the AI for Logistics program of the National Research Council of Canada (NRC) for funding this project and the collaboration of the Construction Research Centre of the NRC.

I would like to express my special thanks to my advisor and mentor Prof. Pezhouhan Tavassoti-Kheiry, and my supervisors Prof. Moojan Ghafurian and Prof. Hassan Baaj for giving me the golden opportunity to conduct this wonderful research project as well as their full support and patient guidance throughout my master's journey.

I would like to sincerely thank the Readers of my master's thesis, Prof. Shunde Yin and Prof. Liping Fu, for their invaluable suggestions to this thesis.

Finally, I would specially thank to my beautiful parents and grandparents for their forever trust and support, and my life partner for her patience. Without any of you, this perilous journey would be impossible.

Table of Contents

| | |
|---|------------|
| Author’s Declaration | ii |
| Abstract | iii |
| Acknowledgements | v |
| Chapter 1 Introduction | 1 |
| <i>1.1 Background</i> | <i>1</i> |
| <i>1.2 Problem Statement</i> | <i>3</i> |
| <i>1.3 Research Objectives</i> | <i>4</i> |
| <i>1.4 Summary of Contributions</i> | <i>5</i> |
| <i>1.5 Thesis Organization</i> | <i>6</i> |
| Chapter 2 Review of Relevant Work | 7 |
| <i>2.1 Pavement Performance Prediction</i> | <i>7</i> |
| 2.1.1 AI/ML-Aided Predictions Approaches | <i>8</i> |
| <i>2.2 Pavement Instrumentation Practices</i> | <i>18</i> |
| Chapter 3 Data Analysis and Machine Learning Modelling | 39 |
| <i>3.1 Introduction</i> | <i>39</i> |
| 3.1.1 Pavement Databases | <i>40</i> |
| 3.1.2 International Roughness Index..... | <i>43</i> |
| <i>3.2 Data Preparation</i> | <i>44</i> |
| 3.2.1 Data Selection | <i>44</i> |
| 3.2.2 Data Cleaning and Assembly | <i>47</i> |
| 3.2.3 Challenges..... | <i>50</i> |
| 3.2.4 Final Input Data Selection..... | <i>56</i> |

| | |
|---|------------|
| 3.3 <i>Decision Tree and Random Forest Modelling</i> | 58 |
| 3.3.1 Background | 58 |
| 3.3.2 Model Training and Evaluation | 64 |
| 3.3.3 Model Pruning and Hyperparameter Optimization | 69 |
| 3.4 <i>Discussion and Conclusion</i> | 78 |
| Chapter 4 Design and Finite Element Modelling of Pilot Section | 81 |
| 4.1 <i>Overview</i> | 81 |
| 4.2 <i>Geometry and Pavement Structure Design Review</i> | 81 |
| 4.3 <i>Instrumentation Layout Design</i> | 82 |
| 4.4 <i>Finite Element Modelling</i> | 84 |
| 4.4.1 Model Geometry | 84 |
| 4.4.2 Material Property | 93 |
| 4.4.3 Boundary Conditions, Loading, Interaction, and Final Models | 98 |
| 4.4.5 Meshing Techniques and Mesh Independence | 100 |
| 4.4.6 Result Discussion | 101 |
| 4.5 <i>Conclusion</i> | 109 |
| Chapter 5 Conclusions and Future Work | 112 |
| 5.1 <i>Summary of Findings and Conclusions</i> | 112 |
| 5.2 <i>Research Contributions</i> | 114 |
| 5.3 <i>Recommendations for Future Work</i> | 115 |
| Letter of Copyright Permissions | 117 |
| References | 121 |
| Appendix | 139 |

List of Figures

| | |
|--|----|
| Figure 2-1 Horizontal (a) and Vertical (b) Asphalt Strain Gauges (Courtesy of CTLGroup)..... | 21 |
| Figure 2-2 Example of BAsT pavement stress and strain due to wheel loading and the measuring equipment (pressure cells and strain gauges) (Rabe 2013)..... | 23 |
| Figure 2-3 Road layer and sensors distribution (Maadani et al, 2015)..... | 23 |
| Figure 2-4 Example of BAsT 2nd generation aluminum soil pressure cell (Rabe 2007) | 23 |
| Figure 2-5 Type-T Thermocouple (Courtesy of IQS Directory) | 24 |
| Figure 2-6 Thermocouple installation (Maadani, 2015)..... | 25 |
| Figure 2-7 In-situ water content reflectometer (Maadani, 2015) | 26 |
| Figure 2-8 In-situ CRREL resistivity probe (Maadani, 2015)..... | 27 |
| Figure 2-9 Data acquisition system hardware architecture (Mohammad et al, 1994)..... | 28 |
| Figure 2-10 Example data acquisition system layout (Maadani et al, 2015)..... | 29 |
| Figure 2-11 Example data acquisition system layout (Dong et al., 2017)..... | 30 |
| Figure 2-12 Data acquisition and control system panel..... | 30 |
| Figure 2-13 Sensor overview and installation for pavement instrumentation. | 32 |
| Figure 2-14 Layout of the sensors in the second Smart Pavement Project in Virginia in 2011 | 34 |
| Figure 2-15 Pavement monitoring system outlook of the second Smart Pavement Project in Virginia in 2011 (Wang et al., 2012) | 35 |
| Figure 2-16 Optical fiber sensor configurations and functioning (Ansari, 2007) | 36 |
| Figure 2-17 A typical fiber optic sensor for embedment in concrete (Left); Embedded fiber optic sensors during concreting operations (Right). (Ansari, 2007) | 37 |
| Figure 3-1 Types of data included on LTPP..... | 42 |
| Figure 3-2 LTPP database structure | 43 |
| Figure 3-3 LTPP data selection using web operations | 45 |
| Figure 3-4 LTPP data selection using SQL | 46 |
| Figure 3-5 LTPP data entity relationship example illustration..... | 48 |
| Figure 3-6 Detailed LTPP data entity relationship between AADTT, pavement age and annual temperature | 49 |
| Figure 3-7 Climate regions on LTPP for pavement test sections (Zhang et al, 2017)..... | 52 |
| Figure 3-8 Change of IRI over time with M&R activities..... | 55 |
| Figure 3-9 Illustration of Decision Tree classification | 60 |

| | |
|--|-----|
| Figure 3-10 Illustration of Decision Tree regression..... | 60 |
| Figure 3-11 Illustration of a Random Forest model | 63 |
| Figure 3-12 Initial decision tree training (a) and testing (b) results | 66 |
| Figure 3-13 Learning curve of training data..... | 66 |
| Figure 3-14 Visualization of a part of the initial decision tree | 67 |
| Figure 3-15 The number of trees in initial random forest model vs. accuracies | 69 |
| Figure 3-16 Training and testing accuracy as a function of alpha value | 71 |
| Figure 3-17 The number of nodes (a) and the depth of the tree (b) as a function of alpha value..... | 71 |
| Figure 3-18 Pruned decision tree training (a) and testing (b) results | 73 |
| Figure 3-19 Visualization of the full pruned decision tree | 74 |
| Figure 3-20 Visualization of hyperparameter tuning results when the num of trees is 3 | 76 |
| Figure 3-21 Hyperparameter selection based on accuracy scores | 76 |
| Figure 3-22 Optimized RF model with a total number of 3 trees..... | 78 |
| Figure 4-1 Pilot section instrumentation layout design (top view)..... | 83 |
| Figure 4-2 Pilot section instrumentation layout design (cross-section view)..... | 84 |
| Figure 4-3 Actual tire contact area (a) and rectangular tire contact area (b)..... | 86 |
| Figure 4-4 Tire loading pressure and dimension used for ABAQUS input..... | 87 |
| Figure 4-5 Pavement layer surface partitioning geometry with respect to tire loading. (Unit: mm)..... | 88 |
| Figure 4-6 Dynatest PAST-II AC strain gauge (Dynatest, 2022)..... | 89 |
| Figure 4-7 The Dimension of Dynatest PAST-II AC strain gauge used in ABAQUS..... | 89 |
| Figure 4-8 RST Total Earth Pressure Load Cells 9” | 90 |
| Figure 4-9 The dimension RST Total Earth Pressure Load Cells 9” used in ABAQUS..... | 90 |
| Figure 4-10 Pavement structure geometry without instrumentation sensors..... | 91 |
| Figure 4-11 Horizontal layout design of asphalt strain gauge | 92 |
| Figure 4-12 Horizontal layout design of pressure cell..... | 93 |
| Figure 4-13 Vertical layout design of strain gauge and pressure cell..... | 93 |
| Figure 4-14 Instrumented and non-instrumented models: (a) Both strain gauge and pressure cell, (b) no sensors, (c) only strain gauge, and (d) only pressure cell | 99 |
| Figure 4-15 Boundary conditions and loading of the model | 100 |
| Figure 4-16 Mesh for the instrumented model | 101 |
| Figure 4-17 Von Mises stress distribution of the uninstrumented model..... | 102 |

| | |
|---|-----|
| Figure 4-18 Referencing areas for the ABAQUS output results | 103 |
| Figure 4-19 Stress results comparison of all reference areas in four models | 106 |
| Figure 4-20 Strain results comparison of all reference areas in four models | 107 |
| Figure 4-21 Stress and strain comparison between the models with and without strain gauge | 108 |
| Figure 4-22 Specific location of the strain gauge (yellow) at the bottom of the SP 19 layer (blue) and above the Granular A layer (green) | 109 |

List of Tables

| | |
|---|----|
| Table 2-1 The inclusion and exclusion criteria of systematic review | 10 |
| Table 2-2 Set of keywords and number of studies for each database | 12 |
| Table 2-3 PRISMA Chart of the data selection process | 13 |
| Table 2-4 Commonly used algorithm types and their discussions | 14 |
| Table 2-5 Commonly used input variables for performance predictions | 17 |
| Table 2-6 Commonly used output variables as performance indicators..... | 17 |
| Table 3-1 LTPP data relational fields | 47 |
| Table 3-2 An example showing data inconsistency on LTPP | 51 |
| Table 3-3 Digitized climate zoning for LTPP data..... | 53 |
| Table 3-4 Traffic data table comparison..... | 54 |
| Table 3-5 Example of defining initial IRI (MRI0), age since last M&R (AGE0), and the number of constructions (CONSTRUCTION_NO)..... | 56 |
| Table 3-6 Final data for pavement structure and construction | 56 |
| Table 3-7 Final data for climate..... | 57 |
| Table 3-8 Final data for traffic..... | 57 |
| Table 3-9 Final data for pavement performance..... | 58 |
| Table 3-10 Advantages and limitations of decision tree algorithm | 61 |
| Table 3-11 Advantages and limitations of random forest algorithm | 63 |
| Table 3-12 Initial decision tree model parameters..... | 65 |
| Table 3-13 Prediction result summary from the initial decision tree model | 65 |
| Table 3-14 Prediction result summary from the pruned decision tree model..... | 71 |
| Table 3-15 Pruned tree model parameters | 72 |
| Table 3-16 Hyperparameters for the RF grid search | 75 |
| Table 3-17 RF grid search results..... | 77 |
| Table 4-1 Pavement structural and material design of the test section..... | 82 |
| Table 4-2 AASHTOWare Pavement ME Design Defaults Axle Configuration | 85 |
| Table 4-3 Ontario Typical Defaults for Axle Spacing..... | 85 |
| Table 4-4 Measured tire pressure, wheel loading, contact area, and mean contact pressure (Nega, 2017) | 87 |
| Table 4-5 Material property summary | 94 |
| Table 4-6 Ontario Superpave properties (MTO, 2019) | 96 |

| | |
|--|-----|
| Table 4-7 Modulus of asphalt mixes used in this study..... | 96 |
| Table 4-8 Ontario subgrade moduli and soil classification | 97 |
| Table 4-9 Dynatest PAST-II AC strain gauge material property | 98 |
| Table 4-10 Average peak Von Mises stress and tensile strain | 104 |
| Table 4-11 Average peak Von Mises stress and vertical pressure | 105 |

List of Abbreviations

| | |
|------------------------|--|
| <i>AADT</i> | Annual Average Daily Traffic |
| <i>AADTT</i> | Annual Average Daily Truck Traffic |
| <i>AASHTO</i> | American Association of State Highway and Transportation Officials |
| <i>AC</i> | Asphalt Concrete |
| <i>AI</i> | Artificial Intelligence |
| <i>ANN (NN)</i> | Artificial Neural Network Algorithm |
| <i>ASTM</i> | American Society for Testing and Materials |
| <i>CPATT</i> | Centre for Pavement and Transportation Technology |
| <i>DOT</i> | Department of Transportation |
| <i>DT</i> | Decision Tree Algorithm |
| <i>ESAL</i> | Equivalent Single Axle Load |
| <i>FEA</i> | Finite Element Analysis |
| <i>FWD</i> | Falling Weight Deflectometer |
| <i>GPR</i> | Ground Penetration Radar |
| <i>HMA</i> | Hot Mix Asphalt |
| <i>IRI</i> | International Roughness Index |
| <i>LCCA</i> | Life Cycle Cost Analysis |
| <i>LTPP</i> | Long-Term Pavement Performance |
| <i>M&R</i> | Pavement Maintenance and Rehabilitation |
| <i>MEPDG</i> | Mechanistic-Empirical Pavement Design Guide |
| <i>ML</i> | Machine Learning |
| <i>MTO</i> | Ministry of Transportation Ontario |
| <i>OPS</i> | Optic Fibre Sensor |
| <i>OPSS</i> | Ontario Provincial Standards |
| <i>PCC</i> | Portland Cement Concrete |
| <i>PCI</i> | Pavement Condition Index |
| <i>PCR</i> | Pavement Condition Rating |
| <i>PMS</i> | Pavement Management System |
| <i>PSI</i> | Pavement Serviceability Index |
| <i>RF</i> | Random Forest Algorithm |
| <i>RMSE</i> | Root-Mean-Square Error |
| <i>SN</i> | Structure Number |
| <i>SHM</i> | Structural Health Monitoring |
| <i>SVM</i> | Support Vector Machine Algorithm |

Chapter 1

Introduction

1.1 Background

Pavement networks are multi-billion-dollar assets that play a vital role in the national transportation infrastructure and economic growth of countries through enabling movement of goods, services, and people in a safe, fast, and economic manner. Understanding pavement performance evolution with time and accordingly optimizing Maintenance and Rehabilitation (M&R) costs have been historically proven to be complex tasks. This has been especially challenging due to the large number of variables that contribute to the overall pavement performance and the considerably high level of uncertainty in predicting traffic patterns, climate conditions, deteriorations, and material property changes. Poorly performing pavements result in increased construction costs, adverse environmental impacts, higher maintenance fees, complaints from road-users, and a risk to damaging vehicles and provoking accidents. In Canada, there are over 415,600 km of paved and 626,700 km of unpaved public roadway network as of December 31, 2019 (Transport Canada, 2019). Meanwhile, new roadways are continuously being designed and constructed every year with an increasing growth trend. After the roadways have been constructed, in order to maintain the proper functioning of pavement, systematic management of the pavement conditions and performance are crucial. Inadequate pavement maintenance strategies can result in unexpected cost due to potential failures and shortening of the designed service life. This price metric solely considers the impacts on material selection for pavement costs without taking other internal factors such as the costs imposed to municipalities for landfilling the milling products or repairing and replacing old road sections due to poor pavement performance into account.

Typically, pavement deteriorations are monitored by project-level and network-level pavement management system (PMS). Current PMS is constructed based on condition surveys such as Pavement Condition Index (PCI) survey, surface roughness profiling, and Ground Penetrating Radar (GPR) and borehole drilling for existing pavement structure characterization. Such non-destructive and destructive assessments require significant costs for PMS implementation in

order to properly monitor pavement conditions and plan necessary M&R actions. In addition, conditions surveys focus on the analysis of the deterioration output results due to damaging factors such as heavy vehicle loading and extreme climate conditions. Yet, there is a lack of interpretation in the pavement deterioration process, i.e., how the pavement structure will respond to each type of damaging factors is yet uncertain. To this end, in-situ pavement instrumentation collects mechanistic pavement response data subjected to traffic loading and undergoing actual climatic condition. Such data can be utilized for quantitative analysis of structural and material performance. For example, when stress and strain at the bottom of asphalt layer are constantly above the maximum threshold values due to a large volume of heavy vehicles, bottom-up cracking may occur. Therefore, by accurately analyzing the stress and strain data, cracking occurrence and propagation can be predicted to reduce the need of costly condition surveys. The Smart Pavement project at the University of Waterloo implements a set of in-situ sensory system to monitor the long-term pavement performance, and this thesis seeks to conduct the design and analysis of instrumentation setting in a pilot section that will be constructed in the Region of Waterloo.

In recent decades, Artificial Intelligence (AI) and Machine Learning (ML) methods have shown promising results in civil and infrastructure engineering data analysis. As a result of their growing application in different domains, AI and ML methods have been also introduced in pavement performance prediction models in recent years which can be noted from several existing studies. Many of those studies have stated that the prediction accuracy and efficiency of AI and ML-based models can exceed the accuracy of traditional models. A better performing model provides an opportunity to decrease costs associated with M&R of these valuable network of transportation assets by a better premise for decision-making. Therefore, this thesis first evaluates the types and characteristics of the AI/ML techniques used in the existing literature for the purpose of pavement performance predictions, and then utilizing the selected ML models and the currently available pavement performance database, to facilitate ML framework development for future applications of instrumentation data analysis.

1.2 Problem Statement

In-situ Pavement Monitoring

In this project, in-situ pavement monitoring will be implemented for the data collection. However, to design and install a proper monitoring system for the pilot section, there are many factors to consider which can be quite challenging. Of instrumentation layout design, sensory system selection, and data collection schemes, each aspect should be tailored for the pilot section in order to collect key types of data and maximize data quality and data quantity. Excessively sophisticated sensory system may result in unnecessary costs, whereas some key performance data may be neglected due to insufficiently designed instrumentation layout and inappropriate equipment selection. Currently, in-situ pavement monitoring has not been widely applied in Canada since most PMS rely on condition surveys. There is a lack of well-established instrumentation practices with specific procedures and regulations for mechanistic data collection in Canada. A thorough review of recent instrumentation methods and case studies should be conducted in order to fill this knowledge gap by identifying the primary sensor types, layout plans, and common issues.

Although there are some recent instrumentation practices in Virginia (Al-Qadi et al., 2004), Maine (Swett et al., 2008), France (Gaborit et al., 2013), and China (Wang et al., 2012) that have discussed about the sensory system layout and device usage, another important aspect has not yet been thoroughly investigated which is the interaction between embedded sensors and surrounding pavement structure. In other words, the artefacts of embedding sensors for the pavement structural response under loadings need to be identified. The material property difference between sensors and pavement material may result in uneven stress and strain distribution that can affect the accuracy of measurements. In addition, in order to capture critical pavement responses, sensors should be located in the highly concentrated areas of stress and strain. However, the effect of embedded instrumentation on these critical response points varies from a pavement structure to another and from a layer to another. These questions should be answered via running analysis using numerical modelling approaches such as finite element Analysis (FEA).

AI/ML-aided Data Analysis

In recent years, there is a growing trend of AI/ML-aided predictive modelling for pavement performance prediction. The methodology in each study varies in terms of algorithm and data. A thorough review that summarizes the state of the practice and state of the art in application of AI and ML for pavement performance prediction and identify the underlying problems can be highly informative for the future research.

However, in the field of pavement management, the M&R decision-makings, it can be informative for users to also understand the decision-process. Algorithms such decision tree are considered as explainable machine learning algorithm as the decision-making process is interpretable. Hence, in this thesis, decision trees are used and compared with random forests with limited number of trees to evaluate their performance.

In addition, there has been a lack of transparency of pavement data processing and cleaning methods in previous studies that used AI and ML methods to predict pavement performance. Model prediction accuracy can rely heavily on data quality and quantity. Although many studies may have used the same data source and similar methodologies, their datasets used can be different as well as data quality, which is difficult for model performance comparison. Without clear data preparation instructions, it is challenging for other researchers to reproduce or replicate high quality datasets allowing for model advancements. Therefore, this study should also focus on the detailed illustration of data processing and cleaning.

1.3 Research Objectives

Corresponding to the problems addressed in section 1.2, the following research objectives are set:

- To synthesize the results of current AI/ML applications in pavement performance prediction by identifying the most commonly used algorithms, input variables, output variables, pavement types, and data sources.

- To prepare a dataset from a publicly accessible data source while clarifying the data processing procedures.
- To implement tree-based algorithms on the prepared dataset and evaluate the results and accuracy.
- To review and evaluate recent in-situ pavement instrumentation and structural health monitoring practices in terms of sensory system layout design, proper equipment selection, and data collection techniques.
- To identify the impact of embedded instrumentation sensors on surrounding pavement structure under loading using FEA
- To optimize the instrumentation layout for the pilot section construction of the smart pavement project in the future.

1.4 Summary of Contributions

The following major contributions can be listed for this thesis:

- This thesis provides a systematic review of the studies that focused on AI/ML-aided pavement performance prediction of which the outcomes help future researchers determine effective predictive modelling strategies efficiently by reducing random errors and biases and highlighting underlying problems.
- The results of the IRI prediction models have demonstrated the capability of Decision Tree and Random Forest algorithms to achieve promising accuracy while providing clear decision-making visualization based on pavement dataset.
- This study provides concise instructions of LTPP data preparation allowing future researchers to reproduce/replicate high quality datasets for prediction model advancement.
- The study would contribute to improving data collection practices for better pavement performance modelling purposes.
- The impacts of embedded sensor on pavement structure have been identified informing pavement engineers to optimize the instrumentation layout design to avoid device interference and measurement errors.

1.5 Thesis Organization

This article consists of five main chapters to explicitly discuss the different aspects of the smart pavement project:

- Chapter 1 - Introduction

In this part, the background of the project, problem statement, research objectives, and summary of contributions are discussed.

- Chapter 2 - Review of the relevant work

The review was divided into two aspects: a systematic literature review of previous studies using AI/ML applications in pavement performance prediction and a review of pavement instrumentation practices.

- Chapter 3 - Data analysis and machine learning modelling

Detailed data preparation procedures are documented along with the challenges in the database. Machine learning framework and example models are established using LTPP database and the results are discussed.

- Chapter 4 – Design and finite element modelling of the pilot section

A set of finite element models in ABAQUS were constructed to investigate subsurface condition of pavement structure with embedded sensors under vehicle loading.

- Chapter 5 - Conclusion and future work

This Chapter includes a summary of the findings, conclusions, the major contributions of this research, and suggestions for future work.

Chapter 2

Review of Relevant Work

As an initial part of Smart Pavement project, the scope of review of this thesis fell into these two categories: pavement performance prediction using AI/ML techniques and in-situ pavement monitoring.

2.1 Pavement Performance Prediction

In pavement engineering management, pavement performance prediction is an essential component of Pavement Management System which aids the M&R decision-makings by estimating timeline when the performance indices will reach the threshold values (Haas et al., 2015). Based on the parameters used, prediction models can be divided into four types (Haas et al., 2015):

- Purely mechanistic, based on structural response such as stress and strain
- Mechanistic-empirical that includes both structural parameter and functional parameter such as surface roughness
- Regression, where input variables can be mathematically related to output variable(s)
- Subjective, where the development of prediction models is based on experience

Traditionally, the prediction methods behind these models are typically based on statistical approaches such as regressions using developed equations. For example, Karan in 1983 has developed a Riding Comfort Index (RCI) prediction model base on direct regression equation with a squared correlation coefficient (R^2) of 0.84 and a standard error of estimate of 0.38 (Equation 2.1)

$$RCI = - 5.998 + 6.870 \cdot LOG_e(RCI_B) - 0.162 \cdot LOG_e(AGE^2 + 1) + 0.185 \cdot AGE - 0.084 \cdot AGE \cdot LOG_e(RCI_B) - 0.093 \cdot \Delta AGE \quad (\text{Equation 2.1})$$

RCI = Riding Comfort Index

RCI_B = Previous RCI

AGE = Age in years

Δ AGE = Time period between the data collections

Another example of cracking prediction developed by Queiroz in 1983 is also based on a regression model yet only has a coefficient of determination (R^2) of 0.54 and a standard error of the residuals of 15.4 (Equation 2.2).

$$CR = -8.70 + 0.258 HST \cdot LOG(N) + 1.006 \cdot 10^{-7} HSTI \cdot N \quad (\text{Equation 2.2})$$

CR = Percent of pavement area cracked

HST = Horizontal tensile stress at the bottom of the asphalt layer (kgf/cm²)

N = ESAL

Although these models may have shown some satisfactory accuracies, they typically have difficulties adapting to noisy datasets. In addition, Markov chain method is another common practice used in the prediction models (Zeiada, 2020; Pulugurta, 2009; and Li et al., 1996). However, Markov chain may suffer from the fact that the prediction of the future period is based on the most recent time period, and it is difficult to include historical data and trace the long-term history (Haas et al., 2015). Furthermore, Federal Aviation Administration (FAA) has developed a robust finite-element-based model (FEAFAA) to predict airport pavement structural response associated with top-down cracking (Tarahomi et al., 2020). However, the huge computational cost of this model's processing time which may take up to weeks is the major limitation of this finite element-based approach (Tarahomi et al., 2020).

2.1.1 AI/ML-Aided Predictions Approaches

In recent decades, AI and ML applications have been gaining momentum in the field of infrastructure asset management and pavement engineering. Common practices of AI/ML have been applied into image processing such as pavement crack detection and object recognition used in computer vision (Ju et al., 2019), predictive modelling such as asset deterioration and material behaviour predictions. Not only these practices have shown superior accuracy and precision, task efficiency has also been improved with the use of AI-aided techniques.

There are a significant number of studies that have investigated the application of AI/ML in pavement performance prediction. However, the data and algorithm used in each study are different from other studies. There are many pavement performance indicators from condition indices such as Pavement Condition Index (PCI) and International Roughness Index (IRI) to specific distress measurements such as longitudinal cracking length and rutting depth. All those indicators could be used as the prediction output variables. In terms input variable, it is still uncertain that which types of data should be included that have significant impacts on pavement deterioration. As for modelling approaches, each type of algorithm has its advantages and limitations which may be suitable for different datasets and prediction scenarios. Different combinations of dataset and algorithm result in a wide distribution of prediction accuracy. As a result, in this part, a systematic literature review has been conducted to determine and discuss what input variables and output targets were used in the models in addition to the algorithms implemented for model training and testing.

Research Questions

The research questions have been specified as the followings in order to provide clear guidance for the review:

- What are the most commonly used AI and ML algorithms that have been specifically used for the purpose of pavement performance prediction?
- How do these different algorithms compare with each other in terms of accuracy and precision of the predictions?
- What are the main input (predictors) and output parameters used for the purpose of performance prediction modelling?
- What are the characteristics of the databases used for training and testing the AI based models?
- What are the most promising algorithms for the purpose of pavement performance prediction?

Scope of Review and Inclusion/Exclusion criteria

Unlike the studies that focused on damage detection in pavement structure and correlation of constituents and mix design to the engineering properties of paving materials, the scope of this systematic review covers the performance prediction of pavements in terms of performance indices, stress and strain, and correlating the contributing factors to the damage evolution rather than detecting existing damages. Pavement performance prediction requires a wide range of parameters for its input data, which can be mainly categorized under traffic data, material properties, and climate conditions. There are many specific parameters included in each of these main categories. Selection of the parameters can affect prediction results as well as the feasibility of prediction model comparison.

In addition, the selection of machine learning method and algorithms should also be carefully considered. Since this study focuses on the analysis of labelled pavement data, supervised ML methods were included, and unsupervised and semi-supervised learning methods were excluded. When selecting the review articles, the exclusion/inclusion criteria are:

Table 2-1 The inclusion and exclusion criteria of systematic review

| Inclusion criteria | Exclusion criteria |
|---|---|
| <ul style="list-style-type: none">• Studies using supervised ML algorithm to predict pavement performance• Studies evaluating performance of ML models on datasets and reports pertaining to the accuracy and precision of the results• Studies using flexible, Rigid, and composite pavements including either Hot Mix Asphalt (HMA) and/or concrete properties prediction• Peer reviewed articles published in conferences, journals, and as technical reports | <ul style="list-style-type: none">• Studies predicting pavement performance using image processing and computer vision• Studies using semi-supervised learning and unsupervised learning approaches• Studies written in a language other than English |

Information Sources

In this systematic literature review, articles were searched from the following four databases: Association for Computing Machinery (ACM), Institute of Electrical and Electronics Engineers (IEEE), Transport Research International Documentation (TRID), and Scopus. All of the databases were accessed online.

Search Strategy and Keywords

The search keywords covered both pavement engineering and machine learning aspects. In terms of the pavement side, the keywords can be summarized as: “pavement performance prediction”, “stresses/distresses”, “rutting”, “fatigue cracking”, “International Roughness Index (IRI)”, etc. The selected keywords for the machine learning aspect included: “supervised/unsupervised/semi-supervised learning”, “Artificial Neural Network (ANN)”, “decision trees”, “Artificial Intelligence (AI)”, and other types of supervised algorithms. Table 2.2 summarizes specific set of keywords and number of search results for each database. Finally, a total of 1,606 studies have been selected from these libraries.

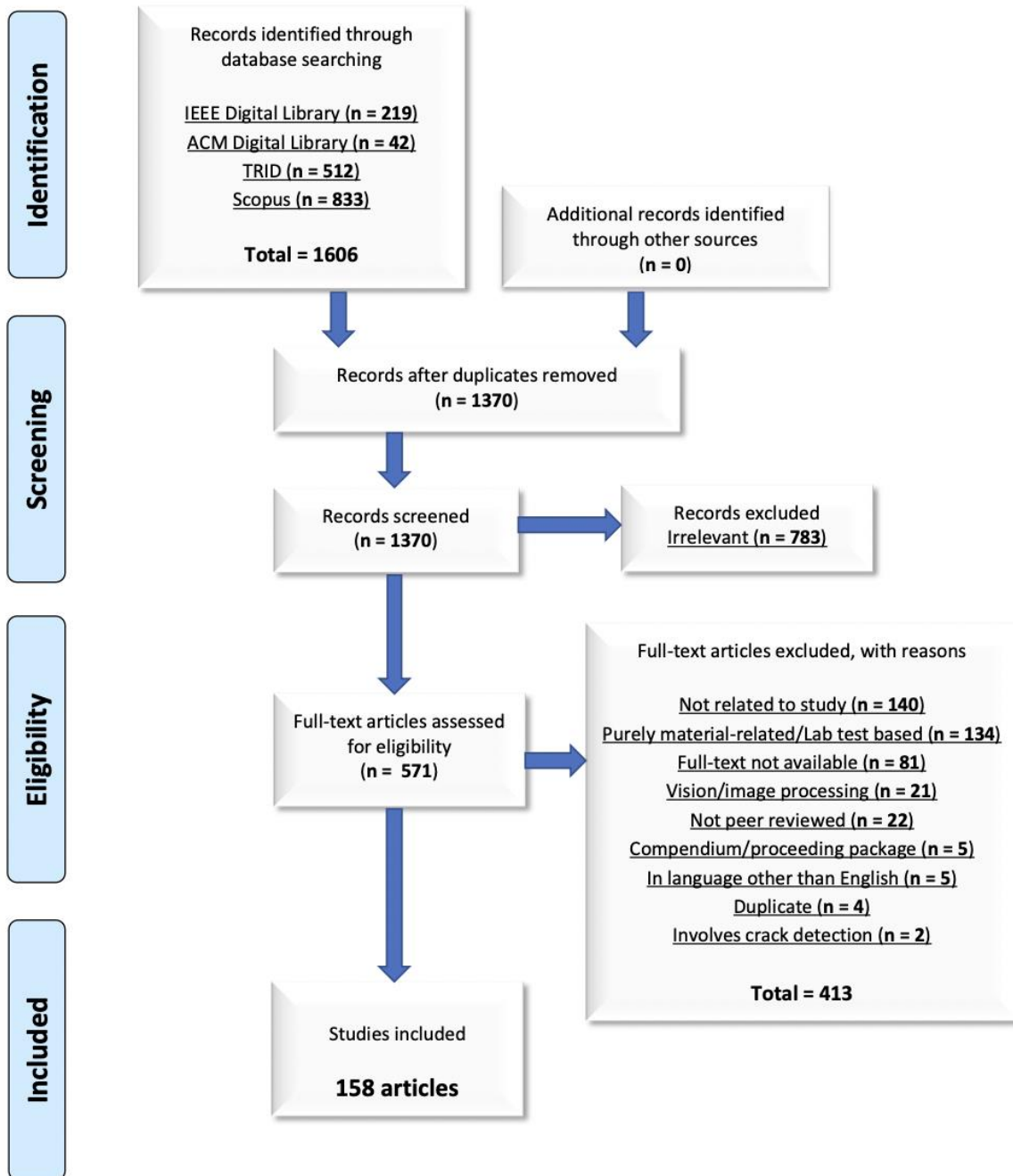
Table 2-2 Set of keywords and number of studies for each database

| Database | Number of Results | Keywords Used |
|----------|-------------------|---|
| IEEE | 219 | "All Metadata":pavement performance modelling OR "All Metadata":pavement performance prediction" OR "All Metadata":pavement condition assessment OR "All Metadata":pavement deterioration |
| ACM | 42 | Abstract:(pavement*) OR Title:(pavement*) OR Keyword:(pavement*) |
| Scopus | 833 | (TITLE-ABS-KEY (pavement*) AND TITLE-ABS-KEY (perform* OR condition OR deteriorat*) AND TITLE-ABS-KEY ("Machine Learning" OR "supervised learning" OR "neural network*" OR "deep learning" OR "artificial intelligence" OR "decision tree*") AND TITLE-ABS-KEY (model* OR predict* OR assess*)) |
| TRID | 512 | (pavement*) AND ("Machine Learning" OR "supervised learning" OR "neural network*" OR "deep learning" OR "artificial intelligence" OR LSTM OR CNN OR "decision tree*") AND (perform* OR deteriorat* OR condition) AND (model* OR assess* OR predict*) |

Data Selection

After the studies were collected from the four databases, two following processes were established to filter the articles: title and abstract screening and full-text assessment. Studies were screened independently, adhering to the inclusion and exclusion criteria as previously mentioned. A total of four reviewers participated in the screening of the literature. The title and abstract screening was used to include or exclude the studies based on the abstracts' relevance. After removing the duplicates and conducting the first screening process, selected articles were moved onto full-text assessment stage. At the full-text screening process, each article was reviewed based on its entire content to make the more accurate judgment to check its eligibility. All the screening processes involved at least two reviewers' consensus to minimize the decision conflict thus ensuring the accuracy of the synthesis. At the end of the full-text screening, there were 158 articles that passed all the inclusion and exclusion criteria and were agreed by the reviewers' consensus to be included as the ultimate references. Thus, those 158 articles were transferred to the data extraction stage. The PRISMA chart below summarizes the selection process with the number of articles at each step.

Table 2-3 PRISMA Chart of the data selection process



Discussion and Conclusion

A total number of 158 articles have been included for the data extraction at the end of selection process. A set of assessing parameters were generated to extract the key information from each article which are: algorithm type(s), input variable(s), output variable(s), data source, data size, and model fit/accuracy.

Table 2-4 Commonly used algorithm types and their discussions

| Algorithm types | Main advantages | Main limitations |
|-----------------------------------|---|--|
| NN* | <ul style="list-style-type: none"> - Superior prediction accuracy and efficiency - Able to learn complex and non-linear relationships | <ul style="list-style-type: none"> - Uninterpretable decision-making process - Dependent on the hardware to support the parallel processing |
| RF and DT | <ul style="list-style-type: none"> - Great visualization ability of the decision-making processing - Able to include both categorical and continuous variable | <ul style="list-style-type: none"> - Prone to overfitting - Requires large datasets |
| SVM | <ul style="list-style-type: none"> - Highly effective in high-dimensional data and unstructured data | <ul style="list-style-type: none"> - Long training time when the datasets are large and/or noisy - Difficult to choose kernel function |
| FL | <ul style="list-style-type: none"> - Easy to understand - Flexible with vague and imprecise data | <ul style="list-style-type: none"> - May not scale well to large and complex problems - Difficult to determine the exact fuzzy rules |
| Linear and non-linear regressions | <ul style="list-style-type: none"> - Good generalization ability - Easy to understand | <ul style="list-style-type: none"> - Tendency to overfit - May have high precision but low accuracy - Cannot describe complex relationships |

**Note: mostly used*

Among those 158 studies, commonly used types of algorithms have been identified as Neural Networks (NN), Random Forest (RF) and Decision Tree (DT), Fuzzy Logic (FL), Support

Vector Machine (SVM), linear and non-linear regressions, which predicted a factor related to pavement performance, including IRI as used in this study (Table 2.1). In addition, the advantages, and disadvantages of each type of algorithm have been discussed (Table 2.1). Neural networks were used in the majority of the studies, where a wide range of input variable type were included (e.g., Yamany et al., 2020; Zeiada et al., 2019; and Hossain et al., 2017). Among the studies that have used NN, typical prediction accuracy (R^2) ranges are higher than 90% (e.g., Ullah et al., 2020; Radwan et al., 2019; and Gu et al., 2018) while the model training times are very minimum (e.g., Tarahomi et al., 2020 and Marcelino et al., 2021). However, the major disadvantage of NN is its black-box nature, i.e., the decision-making process is unexplainable.

Since one of the objectives of this research is to develop machine learning models that is capable of explaining the decision-making process yet maintaining good prediction accuracy with complex datasets, there is another type of tree-based algorithms of thought that possess such capabilities: DT and RF. DT and RF has been used in some studies predicting IRI and PCI (e.g., Gong et al., 2018; Pirayonesi and El-Diraby 2018; Pirayonesi and El-Diraby 2020; and Pirayonesi and El-Diraby 2021). In this review, DT and RF has been classified as one type of algorithm due to their similar decision-making principles. Well-developed RF models based on large datasets (> 10000 data points) have also resulted in high prediction accuracies ($R^2 > 0.90$) (Gong et al., 2018; Jia et al., 2019; Pirayonesi and El-Diraby 2020; and Pirayonesi and El-Diraby 2021).

For example, Gong et al. (2018) has achieved a train accuracy (R^2) of 0.998 and a test accuracy (R^2) of 0.974 based on a tuned RF model for IRI prediction. The RF model consists of 500 trees and has 18 types of input variable including initial IRI, age, AC thickness, temperature, transverse cracking, rutting, potholing, etc. The data were solely retrieved from LTPP database. The has also included single decision tree visualization for illustration purpose (Figure 2.1). However, the final RF model had a very complex structure having 500 single trees and a complicated set of input variables requiring many specific types of distress such as block cracking area and patching area. Therefore, the actual implementation of the model can be

difficult because it needs a variety of surface condition survey data and selecting an optimum tree to represent model overall visualization is challenging when each tree can be unique.

A study from Pirayonesi and El-Diraby (2018) used a single tree DT model for PCI prediction and PCI prediction. The data set was simple consisting of 8 input variables (initial PCI, age, pavement type, freeze index, maximum mean annual temperature, minimum mean annual temperature, total annual precipitation, and road functional class) with a total size of 705. Due to insufficient training data, the model has only achieved an overall accuracy (R^2) of 58%. 3 years later, another study from Pirayonesi and El-Diraby (2021) utilized RF algorithm based on 100 base learners for IRI and PCI predictions. The data size was significantly improved to more than 30,000 and the highest cross-validation accuracy (R^2) for IRI and PCI prediction increased to 0.95 and 0.84, respectively. However, the RF model visualization feasibility was not discussed, and the data sources were unclear. Therefore, there is a need of developing highly accurate prediction models using tree-based algorithm and based on less complex input data.

The mostly used pavement type has been identified as flexible (asphalt concrete), while the studies of other pavement types such as rigid and composite are the minorities. A large range of input variable types have been used in the previous models, including traffic, construction history, climate, and historical distress records (Table 2.2). For example, for the prediction of IRI, Marcelino et al. (2021) and Hossain et al. (2019) used traffic (AADT, AADTT, and ESAL), construction history (M&R numbers, age and AC thickness), climate (temperature and precipitation), and initial IRI value as their input variables. In conclusion, initial IRI, pavement age, temperature, and thickness (AC layer or total layer) were the most frequently used input variables (Table 2.2). In addition, temperature, material properties and structural properties such as AC bearing capacity and resilient modulus were the primary inputs for cracking and rutting predictions (e.g., Okuda et al., 2017; Thube, 2012; and Taddesse, 2017). To explain such, asphalt cracking and rutting trends significantly depend on viscoelastic binder properties, which is a function of temperature change (Huang, 2004). Table 2.2 also summarizes the common databases for providing the input data.

Table 2-5 Commonly used input variables for performance predictions

| Input variable | Description | Major retrieval database |
|-------------------------|---|---------------------------------|
| Initial IRI* | Initial IRI value after the original construction of the pavement | LTPP and State/Provincial DOTs |
| Age * | Age of pavement | LTPP and State/Provincial DOTs |
| Layer Thickness* | The thickness of AC layers and/or base layers | LTPP and State/Provincial DOTs |
| Initial PCI | Initial PCI after the original construction of the pavement or major M&R | State/Provincial DOTs |
| Temperature* | Annual average air temperature | LTPP |
| ESAL | Annual equivalent single axle load | LTPP and State/Provincial DOTs |
| AADT | Includes annual AADT and/or monthly AADT | LTPP and State/Provincial DOTs |
| AADTT | Includes annual AADTT and/or monthly AADTT. May include values for specific truck classes (e.g., AADTT of Class 9 truck) | LTPP and State/Provincial DOTs |
| Precipitation | Annual average precipitation | LTPP |
| Freeze Index | Annual freeze index | LTPP |
| Humidity | Annual air humidity | LTPP |
| Material Property | Asphalt material properties and/or base/subgrade material properties | Field and/or laboratory data |

**Note: mostly used*

Table 2-6 Commonly used output variables as performance indicators

| Output variable | Description |
|------------------------|---|
| IRI* | Future IRI values |
| PCI | Future PCI values |
| Cracking | Future cracking lengths and/or cracking index |
| Rutting | Future rutting depth |

| | |
|-------------------|-----------------------------------|
| Material property | Future AC layer resilient modulus |
|-------------------|-----------------------------------|

**Note: mostly used*

Table 2.3 summarizes the most commonly used output variable for pavement performance indicator. IRI was one of the most commonly used ones in many studies such as Abdelaziz et al. (2014), Jia et al. (2019), Hossain et al., 2019, and Ziari (2016). Studies such as Ling (2019), Lou (2001), Kaya (2020), and Owusu-Ababio (1998) have used cracking lengths and cracking index as their output predictors.

Most studies have used governmental pavement databases such as U.S. State Department of Transportation (DOT) database and national-wide Long-Term Pavement Performance (LTPP) database (Table 2.2). LTPP has been selected as the primary data source for the majority of the studies such as Abo-Hashema (2013), Lucey et al.(2021), and Radwan et al. (2019). Studies that have used State DOT databases tend to focus on a smaller and regional data analysis such as Lou et al. (2001), Piryonesi and El-Diraby (2021), and Roberts and Atttoh-Okine (1998). Other less used databases that have used include Federal Aviation Administration (FAA) for airport pavement (Gopalakrishnan et at., 2009) and other countries' databases such as Swedish National Road Administration (Braban-Ledoux and Sundin, 2000).

In conclusion, most literature review studies have focused on flexible pavement and used ANN algorithm with the input variables shown on table 2.2 to predict IRI, PCI, cracking, and rutting based on LTPP database and/or State/Provincial DOT databases. Prediction accuracy has always been a focus of those studies

2.2 Pavement Instrumentation Practices

Recent practice of pavement design relies on proper understanding of the mechanistic response of pavement structures under varying climatic condition, traffic, and construction practices. Although purely analytical tools such as finite element software provide a valuable resource to

predict the pavement response, the results are not always representative of the actual in-situ performance of pavement structures. Therefore, verification of the analysis results can significantly help with better understanding the role of various factors in the way a pavement structure may perform in long-term, and hence can help advance the current state of mechanistic-empirical pavement design and transportation infrastructure asset management (Tabatabaee and Sebaaly, 1990; Tabatabaee et al., 1992). To this end, pavement instrumentation can help pavement engineers and researchers better understand the actual response of the structure through measuring the in-situ parameters and responses.

Typically, in-situ pavement monitoring can be conducted via two methods: 1) instrumentation and monitoring of an actual in-service pavement section with live traffic conditions, or 2) use of Accelerated Pavement Testing (APT) facility which typically uses controlled traffic loading volume and contact pressure (Guan et al., 2018). According to Willis (2008), there were 45 APT experiments reported in 2002 worldwide. The nature of the traffic specifically differs when looking at the live traffic versus closely controlled traffic conditions. The first type will be the focus of the ongoing Smart Pavement project.

This review provides a summary of the existing literature and past practices on the use of pavement instrumentation to monitor the pavement performance. The main focus will be on the major aspects including strain, stress, moisture, temperature, and frost penetration at different levels within a pavement structure.

Strain Measurements

Strain-based thresholds for pavement design have been commonly used in several pavement design methods such as AASHTO 1993, Asphalt Institute (AI) method, MEPDG, and many others. Measurement of strain distribution within a pavement structure, especially at critical response locations, is one of the most commonly used goals of pavement instrumentation. To this end, horizontal strain measurements at the bottom of the asphalt concrete layer and vertical strain measurement on top of the subgrade soil are two of the major points of interest. Figure 2.3 shows

examples of asphalt strain-gauges that can be used in pavement instrumentation. In general, the strain gauges used for flexible pavements application need to be robust enough to withstand the compaction loads and high temperatures induced during the construction process as well as any erosion due to long-term service.

Three major categories of strain gauges include: strain coils, foil gauges, and H-shaped gauges. The foil type and some of the coil gauges need to be cemented to a carrier block which is considered as a downside from the complexity of construction perspective. However, the coil type can also be attached to the layer of interest using tack coat material. The H-Shaped strain gauges are one of the most commonly used types in pavement applications (Figure 2.3a). Review of the pavement instrumentation research indicates that there are a handful of manufacturers with trackable record of successful use of their strain gauges for pavement projects. Willis (2008) performed a survey of available manufacturers that seems to be valid to date including Dynatest, Tokyo Sokki, Kyowa, TMK, Vishay, and CTL Group.

Furthermore, when selecting a proper strain gauge depending on the project expectations and cost, one should carefully consider the costs and performance changes associated with using a full-bridge gauge versus half-and-quarter bridge counterparts, which would need additional signal conditioning and/or more sophisticated data acquisition systems (Pallas-Areny and Webster, 2012).



Figure 2-1 Horizontal (a) and Vertical (b) Asphalt Strain Gauges (Courtesy of CTLGroup)

Stress Measurements

Stress measurement is also another pavement structural response factor due to traffic loadings. In most cases, pavement design methods and distress analysis require that the stress measurements also need to be coupled with strain measurements simultaneously. The stresses can be assessed through total earth pressure cells (TEPCs) as an indication of the vertical stresses due to the pavement loading from traffic. In order to measure the vertical and horizontal pressures, in the vertical direction along with the progression of the depth, a series of pressure cells are installed in the soil layers including the granular base and other unbound layers underneath the AC layer (Figure 2.4, 2.5 and 2.6).

Soil pressure cells commonly consist of two circular metal plates, which can be made of steel or aluminum. The diameter of pressure cells typically ranges from 150mm to 250mm with a thickness 10mm to 15mm. Pressure cells with smaller-sized loading plates (150mm) are typically installed in HMA layers, whereas the larger ones (225mm) fit better for base layers and subgrade. Based on the hydraulic principles, the space between the two plates is filled with liquids, such as silicon oil (Rabe, 2013), which measures the pressure based on the volumetric change. Also, to avoid the expansion of the pressure cell diaphragm, the boiling point (typically around 200°C) of the hydraulic oil needs to be higher than the temperature of HMA at its paving

phase. (Al-Qadi et al., 2001) The common manufacturers of pressure cells include but not limited to: RST Instruments, GEOKON, Sisgeo, Tokyo Measuring Instruments, and KYOWA.

However, traditional oil-filled pressure cells have a major disadvantage: temperature change may result in the slight thermal expansion or contraction of the filling oils. Therefore, long-term soil pressure monitoring should also consider seasonal temperature variations and calibration based on spot temperature measurements.

The longitudinal and transverse positioning of strain gauges and pressure cells is yet sophisticated to be carefully considered. For example, in a single direction, if the strain gauges are positioned too densely, not only the number of the sensors will increase, the strain value interference may also occur if the sensors are too loosely distributed with large spacings, some peak strain values at specific locations may not be able to captured or this might cause some installation practicality in terms of wires collection and redirection during the construction.

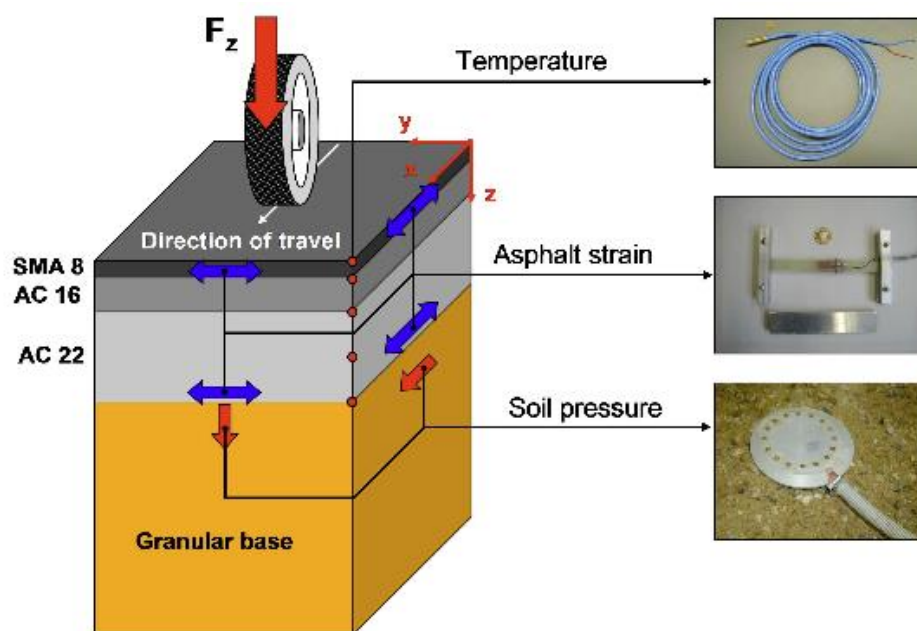


Figure 2-2 Example of BAST pavement stress and strain due to wheel loading and the measuring equipment (pressure cells and strain gauges) (Rabe 2013)

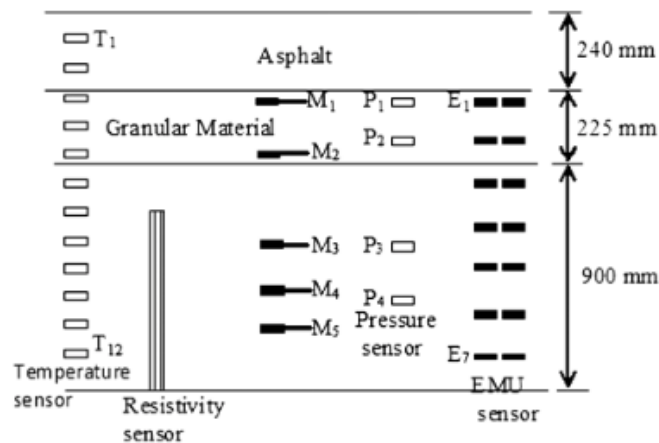


Figure 2-3 Road layer and sensors distribution (Maadani et al, 2015)

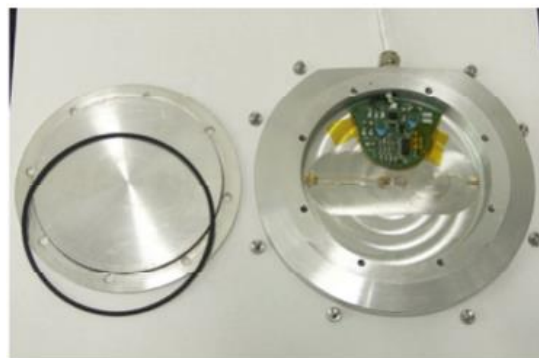


Figure 2-4 Example of BAST 2nd generation aluminum soil pressure cell (Rabe 2007)

Temperature Monitoring

In addition to the traffic loadings, environmental conditions such as temperature and moisture level are also major factors affecting the pavement performance. Pavement surface rutting may occur as the high temperatures in summer lower the stiffness and the stability asphalt concrete layers. On the other hand, base layers with poor drainage characteristics such as clayey material suffer from heavy precipitation resulting in a decrease in overall structural capacity. Temperature

variations and freeze-thaw cycles can also accelerate pavement deterioration such as block cracking and thermal cracking. Therefore, to better understand the pavement distress, mechanistic response monitoring needs to be paired with environment condition monitoring concurrently.

There are several types of temperature data collection methods and equipment such as thermocouples, thermistor probes, monolithic integrated circuits, and photoelectric system. Thermocouples are one of the most commonly used temperature sensors due to their simple design, robustness, and cost-efficiency (Tabatabaee and Sebaaly, 1990). Type-T thermocouples (Figure 2.7), which are made of copper and constantan, have temperature measuring range from below zero to about 370°C (700 °F) and a measuring accuracy of about $\pm 1.8^{\circ}\text{F}$ (Tabatabaee and Sebaaly, 1990).

Since the heat transfer is based on layer thickness and material property, thermocouples are required to be installed in surface layers and soil layers in various depths. In the soil layers, consistent intervals (100mm) between thermocouples in vertical directions were suggested (Figure 2.6) (Maadani et al, 2015).

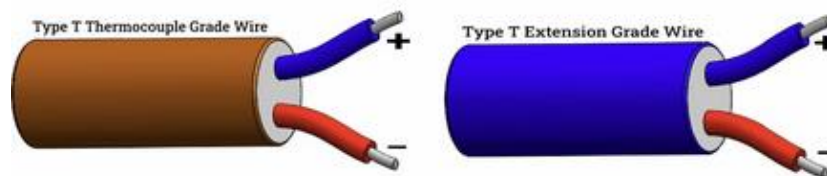


Figure 2-5 Type-T Thermocouple (Courtesy of IQS Directory)



Figure 2-6 Thermocouple installation (Maadani, 2015)

Moisture and Frost Monitoring

Freeze-thaw cycles represented by cold winters and warm summers are more common in Eastern Canada and in other similar climate zones. In winter, the water molecules in soil freezes when the temperature drops below freezing point. Then, the frozen water molecule expands in its volume, thus increasing the void ratios of granular layers and subgrade. However, when spring begins and temperature increases, the stability of the base layers and subgrade will be reduced due to the thawing process. In addition, frost penetration depth fluctuates depending on air temperature and solar radiation. Therefore, moisture monitoring and frost penetration monitoring are crucial to the in-situ pavement instrumentation, especially in cold regions such as in Canadian climate. Such monitoring also provides feedback to the drainage design to avoid the excessive soil moisture and thereby improving the structural stability.

Water-content reflectometer sensor (Figure 2.9) is one of the most commonly used probes for the moisture content monitoring. This type of sensor measures the unfrozen water content by volume in soil (Maadani, 2015). Common water-content reflectometer sensors are CS615 and CS616 manufactured by Campbell Scientific.

Resistivity Probe Sensors (Figure 2.10), typically made from PVC rods, are used to detect frost depth. The probe identifies soil resistance change due to freezing or thawing, and the paired data logger record such resistance changes.



Figure 2-7 In-situ water content reflectometer (Maadani, 2015)



Figure 2-8 In-situ CRREL resistivity probe (Maadani, 2015)

Data Acquisition System

To ensure the data quality and quantity, a well-fit data acquisition and control system is critical component of the instrumentation setting. Typically, the data acquisition systems collect, store, organize, and digitize the raw data transmitted from embedded sensors. The data acquisition system consists of hardware units and data processing software (Figure 2.11). The primary purposes of the data acquisition and control system are: signal conditioning, isolation, analog-to-digital conversion, digital-to-analog conversion for the hardware units; the data processing software is responsible for data reduction and analysis, control algorithms, and permanent data storage (Mohammad et al, 1994). Depending on the specific instrumentation setting and data requirements, the data acquisition and control system varies (Figure 2.12 and 2.13).

Typical data acquisition hardware including sets of static and dynamic data loggers, and communication devices are assembled in a weather-proof panel (Figure 2.14) near the instrumented pavement section. Static data loggers, which are often used to record environmental data, may require long durability, versatile operation conditions in terms of climates and fewer calibration needs. Model CR10X is an example of such equipment that is manufactured by Campbell Scientific (Maadani, 2015). On the other hand, dynamic data loggers that are commonly used to record stress and strain, require fast and yet precise readings, agile sensitivity, high reading consistency, and also long durability. Model CR9000 manufactured by Campbell Scientific is an example of such system (Maadani, 2015).

When one is designing the hardware system, some important aspects need to be considered: the instrumentation sensor properties and output range, the data reading frequency, finding the optimum number of sensors that is optimum for the data sampling rate (large number of sensors may lower the sampling rate due to the limited system capacity) (Maadani, 2015).

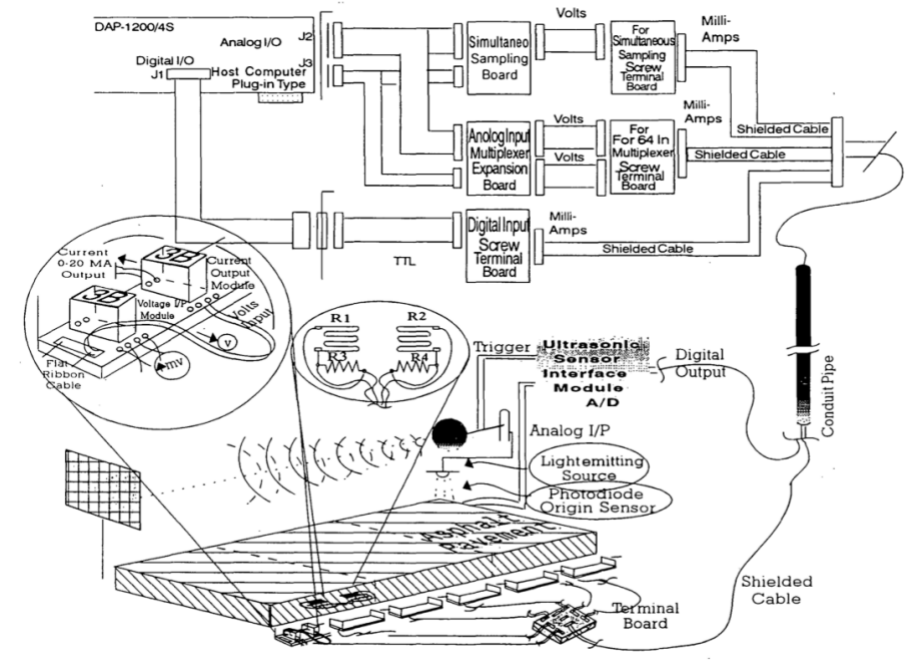


Figure 2-9 Data acquisition system hardware architecture (Mohammad et al, 1994)

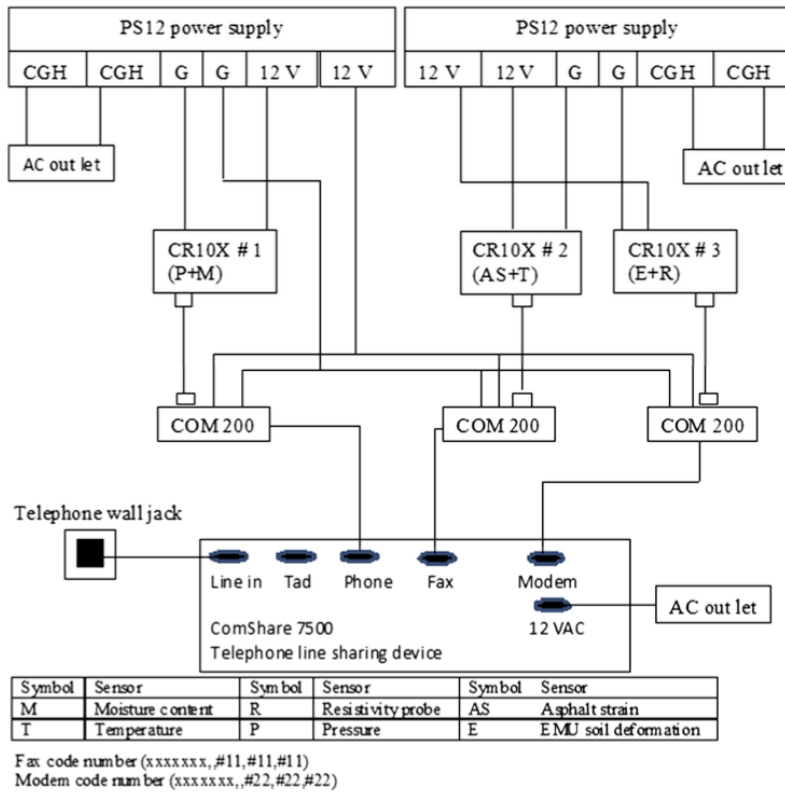


Figure 2-10 Example data acquisition system layout (Maadani et al, 2015)



Figure 2-11 Example data acquisition system layout (Dong et al., 2017)



Figure 2-12 Data acquisition and control system panel

The main duties of data acquisition software are raw data processing and visualization. A complete data acquisition, analysis, and penetration system must need appropriate software. Typical software manufacturers include ROMDAS, Omega, and Karol-Warner, among others. However, the software evolves faster and varies more comparing to the hardware, but the basic principles of the software selection and developments follow such rules:

- Data processing efficiency
- Comprehensive yet detailed representation of raw data
- User-friendly interface for clear interpretations
- Takes full advantage of the Data Acquisition Processor (DAP) specifications in the Graphical User Interface (GUI) environment (Mohammad et al, 1994).

Example Instrumented Sections

To improve current and future pavement instrumentation practices, the review of past instrumented field sections is necessary as it helps identify underlying issues. Two example projects were briefly discussed below.

Started in 1998 and ended in late 1999, Virginia Department of Transportation (VDOT) conducted a pioneering smart pavement instrumentation project. The test section has a length of 3.2km, a width of 100m, and several different depths. The monitoring sensors included (Figure 2.15): pressure cells, strain gauges, thermocouples for temperature recording, TDR probes for soil moisture recording, and resistivity probes for frost depth detecting. The data acquisition system collects and processes both static environment data and dynamic stress and strain data. Pavement response data were later collected with a testing truck of controlled loading tire pressure and controlled speeds over a one-year period. In the end, finite element models were applied to verify the pavement response results. The final results showed that the effective bonding conditions at the interfaces between road layers may be necessary to be taken account into for accurate performance predictions (Barriera et al, 2020). However, the project did not include the long-term daily traffic loadings, but only used the experimental truck with controlled

volume and weight. The lack of arbitrariness without actual traffic conditions may result in overfitting issues in pavement response analysis models.

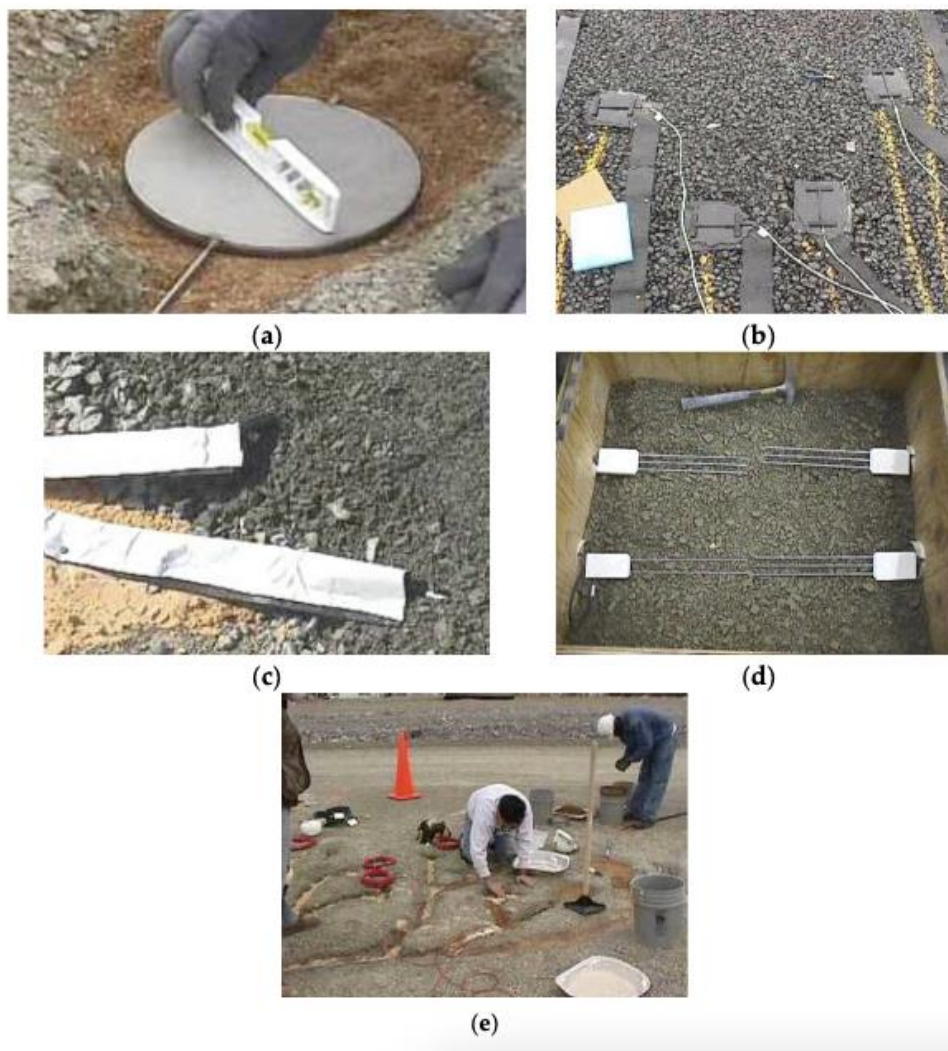


Figure 2-13 Sensor overview and installation for pavement instrumentation.

(a) Pressure cells, (b) H-shaped asphalt strain gauges, (c) thermocouples, (d) TDR probes, and (e) vibrating wire strain gauges (Al-Qadi et al, 2004)

In 2011, the state of Virginia conducted another in-situ pavement monitoring project with improved instrumentation practices on the State Route of 114 (Figure 2.16). Both controlled

traffic and actual traffic were applied. In addition, post-construction M&R activities were taken into account. The objectives of this study included traffic classification, inverse calculation for weigh-in-motion in addition to the pavement structural health monitoring. Sensory system that was similar to the previous one in 1998 were used including strain gauges, pressure cells, thermocouples, and soil moisture probes. Instrumentation layout was carefully designed (Figure 2.17) in order to collect multiple types of data at a time. The vehicle wandering was estimated beforehand. Five horizontal strain gauges were placed in transverse direction to accommodate different wheel paths. Sensor positioning is the key to the accurate inverse calculation of pavement mechanical conditions with applied loads (Barriera et al, 2020).

FEA modelling in ABAQUS was applied to check the proper functioning of the sensors after installation by verifying the inverse calculation of asphalt dynamic modulus and prediction distresses. As a result, traffic volume and speed were able to be estimated using back-calculated AC modulus and vehicle weight from weigh-in-motion scales. Also, Mechanistic-Empirical Pavement Design Guide (MEPDG) method was used to predict fatigue cracking and rutting.

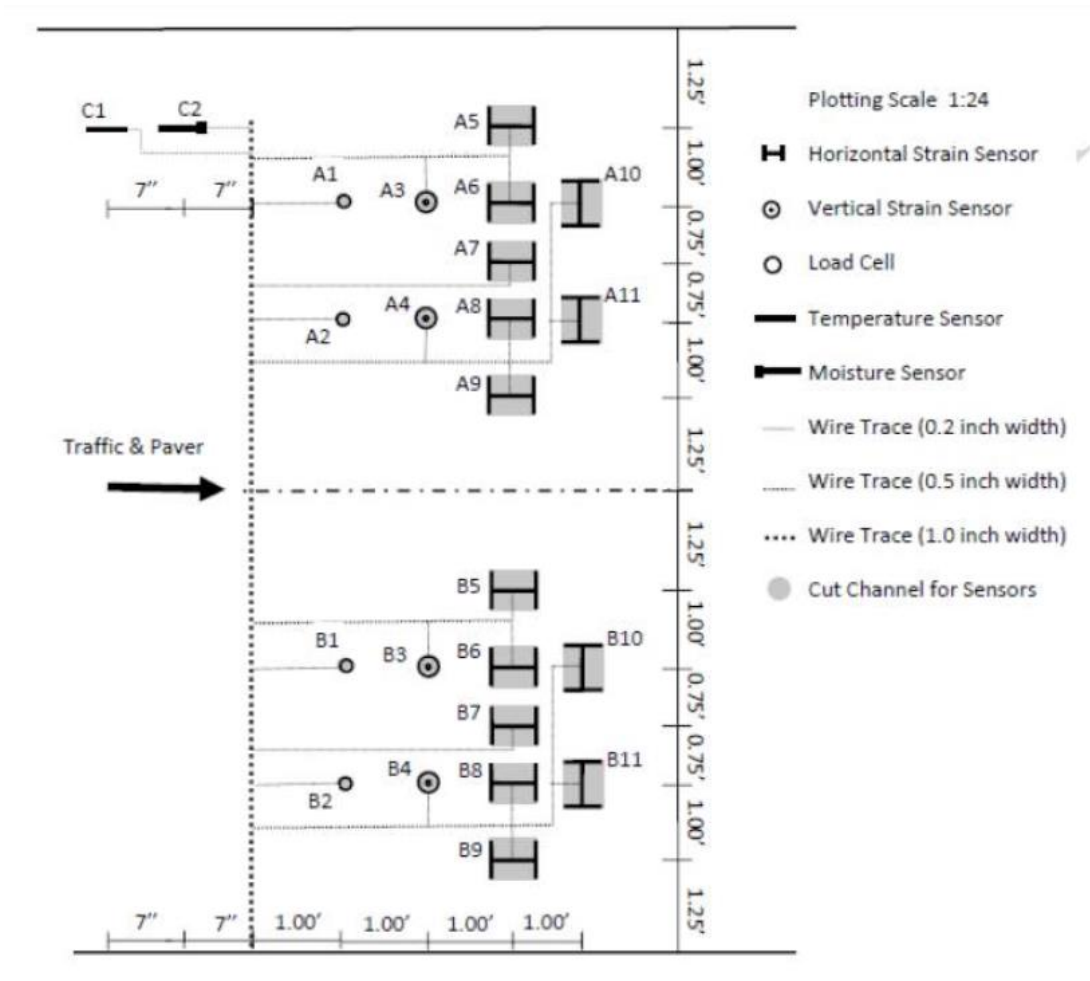


Figure 2-14 Layout of the sensors in the second Smart Pavement Project in Virginia in 2011

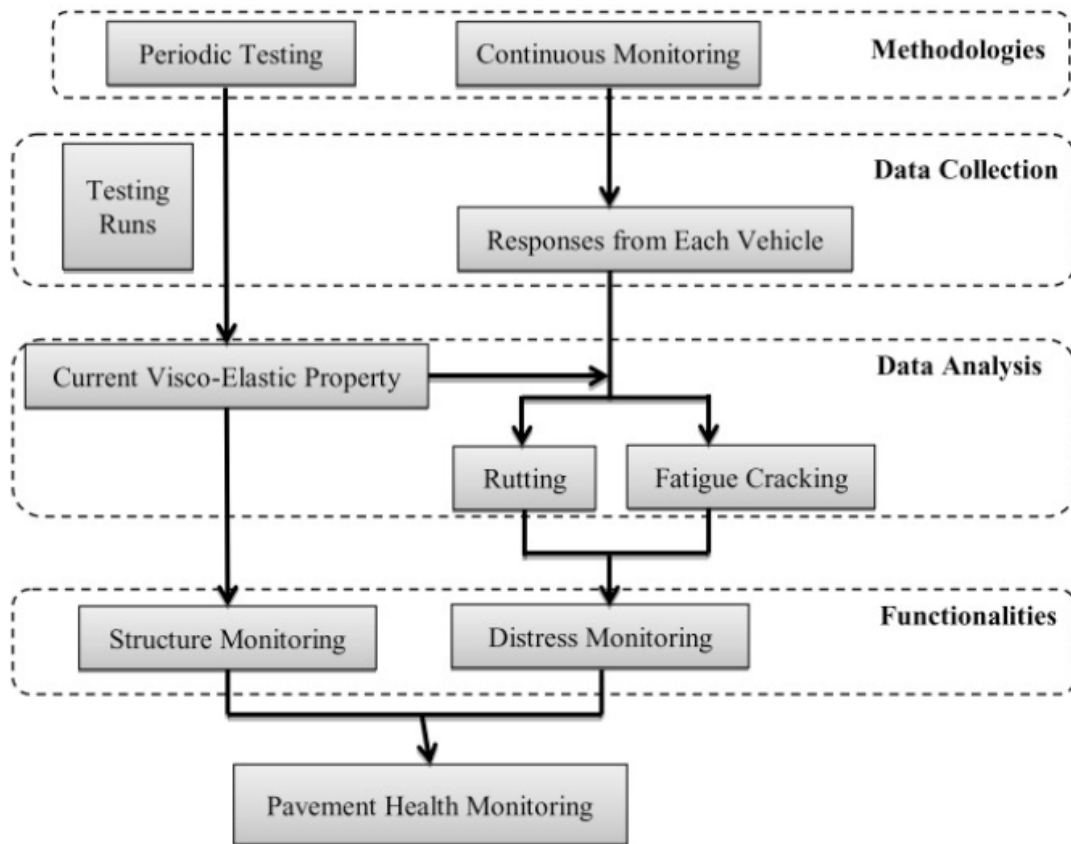


Figure 2-15 Pavement monitoring system outlook of the second Smart Pavement Project in Virginia in 2011 (Wang et al., 2012)

Modern Instrumentation Trends and Innovative Technologies

In the past a few decades, pavement instrumentation relies more on the static measurements where there is a lack of long-term continuous data collection. However, modern data analysis methods such as AI require more consistent, continuous, and dynamic data in order to investigate the underlying pattern. Therefore, a long-term Structural Health Monitoring (SHM) system should be implemented to provide real-time and continuous monitoring of pavement response and structural condition. In addition, modern SHM with wireless technologies ease the data

collection yet increase the data quantity and improve data quality without frequent site visits. A properly implemented SHM also lowers the life cycle cost. (Ansari, 2007).

SHM typically consists of sets of wireless and/or wired sensors that are capable of capturing the simultaneous structural response to the loadings and material and climate conditions within the pavement structural. Due to its high sensitivity, versatility, and superior durability, Optical Fiber Sensing (OFS) has been a leading branch of the wireless sensing systems (Dong, 2017). Current OFS tracks changes in temperature, strain, and other parameters by detecting the induced wavelength and frequency of light travel (Figure 2.18 and 2.19). This multi-functional sensor allows to reduce the need of other devices that may lower the total equipment cost.

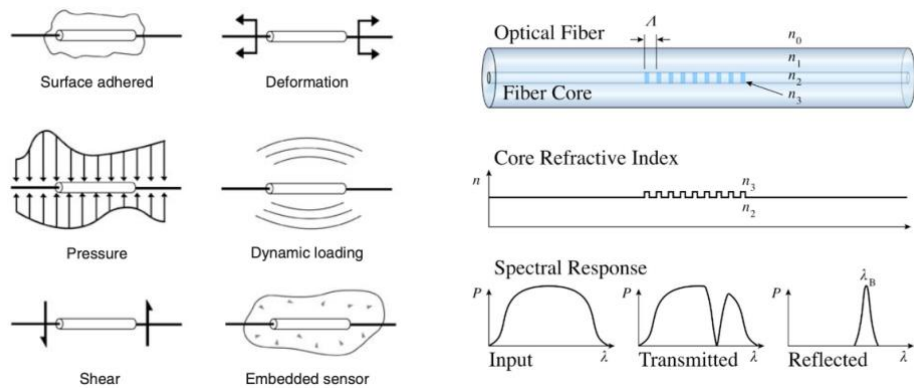


Figure 2-16 Optical fiber sensor configurations and functioning (Ansari, 2007)



Figure 2-17 A typical fiber optic sensor for embedment in concrete (Left); Embedded fiber optic sensors during concreting operations (Right). (Ansari, 2007)

Summary of Findings and General Considerations

Pavement response monitoring is crucial to the structural health maintaining and an essential part of modern pavement management system. In-situ instrumentation is the foundation to such monitoring. Based on the current pavement instrumentation literature review, the sensory system can be organized into two major categories: structural monitoring and environmental monitoring. Also, depending on the length of the data collection period, they can be divided into short-term or long-term, dynamic, and static groups. In order to have comprehensive pavement response data, all monitoring groups need to collect data simultaneously. This paper summarizes the previous pavement performance monitoring practices and the use of essential data collection equipment. The review has identified the types of data that need to be collect strain, stress, soil moisture, pavement temperature, and frost penetration depth. Most commonly used data collection devices are also listed: H-shaped AC strain gauge, soil pressure cell, temperature thermocouple, soil resistivity probe, time-domain reflectometry moisture sensor, and data acquisition hardware set. Furthermore, two example instrumentation projects in Virginia were discussed.

For the strain gauge selection, whether using a full-bridge gauge, or a half-and-quarter bridge counterpart which would need additional signal conditioning and/or more sophisticated Data Acquisition systems, should be carefully considered with the costs and performance. The operation temperature range of pressure cells should be greater than the in-situ temperature range to minimize the hydraulic oil thermal expansion/contraction. Field calibration of pressure cells is required and is often validated by non-destructive testing such as FWD (Tabatabaee and Sebaaly, 1990). As for horizontal and vertical instrumentation layout design, adequate spacing should be maintain between sensors to avoid interferences and to control the number of equipment and the cost. When installing the soil resistivity probes for frost depth monitoring, to ensure the result accuracy, the copper rings on the probes that conducts electric pauses must have proper contact

with soil particles over their entire surface area (Al-Qadi, 2004). In addition, data acquisition system, including the hardware parts and the data processing software, plays a key role in instrumentation projects. The system should be carefully designed and customized to fully accommodate sensor outputs.

Traditional instrumentation methods need frequent field visits. However, recent innovations in instrumentation focus on wireless technologies and internet of things (IoT), which provide long-term and real-time pavement structural health monitoring with remote accesses. Having more quantitative understanding and monitoring of pavement conditions would benefit life cycle cost optimization.

Although many previous instrumentation practices were review, specific instrumentation system designs are still site-specific. Maadani et al. (2015) suggested a few key considerations for instrumentation design:

- The measurement range and output type of sensors
- Sensors' functioning mechanism must be compatible with the data acquisition system
- The life expectancy of sensors
- Other limitations related to the magnetic surrounding environment.
- Manufacturer's specifications such as output and capacity must be carefully examined in the selection process and inspected during installation.

Chapter 3

Data Analysis and Machine Learning Modelling

3.1 Introduction

In the past few years, a considerable number of studies had performed predictive modelling for pavement data analysis using modern AI/ML method. Based on the literature review from Chapter 2, high prediction accuracy has been the main focus from the previous studies and ANN was the most commonly used algorithm allowing their models to achieve an average R^2 of 0.90. However, in the field of pavement management, the M&R decision-makings should not solely depend on accuracy but the proper understanding of prediction logic and reasoning of the algorithm can be informative.

Tree-based algorithms including Decision Tree (DT), however, have not been frequently investigated from the review studies. Although promising results can be seen from the literature review, DT still needs to be investigated to improve accuracy and interpretability of the existing model predicting pavement performance.

Based on the systematic review results, and with a large number of historical records on LTPP database, IRI has been the primary prediction variable used in the previous studies. In terms of pavement engineering, IRI index generalizes pavement surface conditions but does not inform specific distress. LTPP databased is the largest pavement database in North American and was the most extensively used databased among the literature review studies. Therefore, in this study, LTPP database was selected as the main data source due to its wide-range data types, and IRI was selected as the main output variable due to its meaning and vast amount of records. As for the algorithms, decision tree and random forest were selected due to their great visualization capability and adaptability to noisy data. Many of these studies have proven promising results using the state-of-art data analysis techniques, but there is lack of transparency and interpretation of the LTPP data processing among those studies. Data quality and quantity are one of the essentials to achieve the high prediction accuracy regardless the types of prediction methods or

algorithms. Hence, in this study, the focus was not only the implementation of machine learning approach and the modelling methodologies, but the detailed data processing procedures combined with pavement engineering concepts were explained with traceable sources and directories on LTPP database. As LTPP is a large complex database, demonstrating the data selection and processing allows future researchers to reproduce/replicate datasets that can be used for prediction model advancements. More specifically, by identifying underlying issues in LTPP, these procedures also help the users to retrieve more consistent and complete datasets. In addition, this chapter selected and explained the data that are strongly related to pavement roughness and distress based on empirical pavement engineering knowledge.

Overall, a carefully prepared dataset retrieved from LTPP was used for IRI predictions based on a DT model and a Random Forest (RF) model. Then, the IRI prediction process and results were discussed and decision tree(s) were visualized to interpret the prediction process. To further improve the prediction accuracy and model generalization capability, model tuning and hyperparameter optimization were also covered in this section.

3.1.1 Pavement Databases

Database is considered as a core part of the modern PMS which provides necessary quantitative and qualitative information regarding decision-makings at different levels of PMS (Haas et al., 2015). A comprehensive database is required to serve as a basis for the following pavement performance data analysis. Typically, several types of data are being recorded and stored in the PMS database: construction and M&R history, pavement quality measures (distresses, roughness, skid resistance, and structural evaluation), and other special design and research data (Haas et al., 1994). The major function of PMS database is that the stored data can be further utilized and processed to performance various types of analysis and thus control the decision-makings of M&R activities. To provide a solid foundation of different types of performance prediction models, a significant amount of data with long-term yet systematic recording scheme are needed. Many State DOTs and municipalities started to value the importance of pavement

data analysis and management by constructing their own pavement databases in a few decades ago. The quality and amount of data is crucial to the data analysis. Comparing to region and municipal PMS databases, LTPP is a unique blend of pavement-related data from many agencies in different climate zones and with various scales of pavement network. The development robust and versatile pavement performance prediction models demand high-quality data. In terms of the field of AI and ML, model training and prediction accuracy typically represent a positive relationship with data quality and quantity. Hence, in this study, LTPP was selected as the primary database for the following machine learning data analysis.

Long-Term Pavement Performance (LTPP) Database

Long-Term Pavement Performance (LTPP) database, initiated by Strategic Highway Research Program (SHRP) in early to mid-1980s as collaboration of the U.S. Federal Highway Administration (FHWA), Transportation Research Board (TRB) and American Association of State Highway and Transportation Officials (AASHTO), is the largest pavement database in North America (FHWA, 2019). LTPP databases intends to incorporate a wide range of data that are related to pavement infrastructure. One of the initial objectives of the LTPP program was to help build better performance prediction models for pavement design and management. The principal categories of data included on LTPP are pavement structure and construction, climate, traffic, performance and distress, and material (Figure 3.1) Over millions of records were stored from 2581 pavement sections from 62 States/Provinces across the U.S and Canada. Most of data on LTPP were stored beginning in 1989 which provides a 20 to 30 years of data coverage period. Figure 3.2 illustrates the processes of LTPP data collection, storage and analysis. LTPP is a relational database which consists of separate yet related tables of data (FHWA, 2019). The database is implemented in Oracle 12 format. LTPP's Ancillary Information Management System (AIMS) collects, converts and organizes raw data into formal categories as known as Pavement Performance Database (PPDB) to ease the data selection. User can easily access the database and generate the request of data download in various methods: Microsoft Excel, SQL, and Microsoft Access (FHWA, 2019).

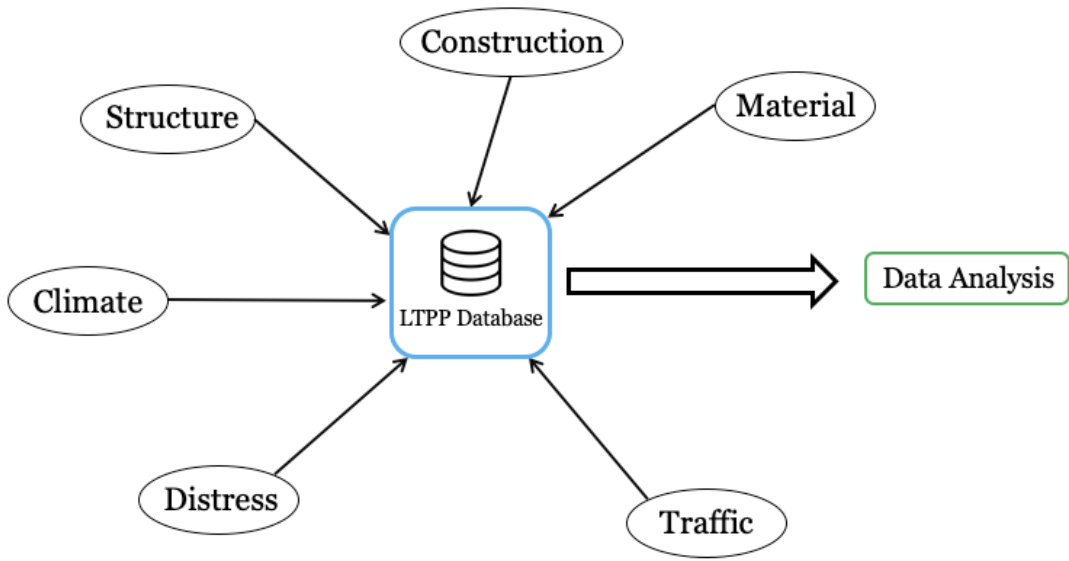


Figure 3-1 Types of data included on LTPP

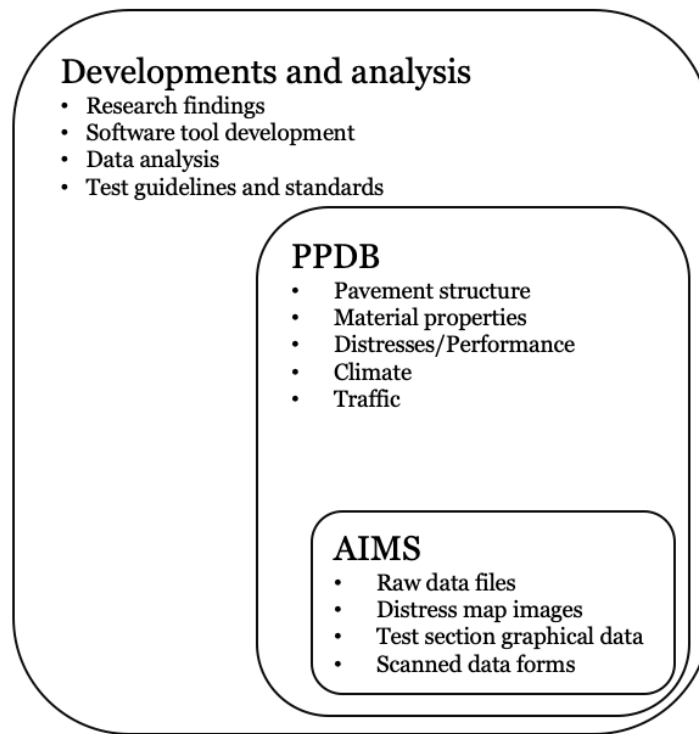


Figure 3-2 LTPP database structure

3.1.2 International Roughness Index

There are many indices that are used to define and evaluate the pavement condition, behavior, distress, and response. Some common indices are International Roughness Index (IRI), Present Serviceability Index (PSI), and Riding Comfort Index (RCI), etc. Pavement Condition Index (PCI) and Surface Distress Index (SDI) are often used to summarize the surface distresses. In PMS, these indices can be modelled to assist in the initial design and M&R decision-makings. In this study, IRI will be used as the major pavement deterioration indicator due to its data availability on LTPP and high popularity in literature review studies.

The international roughness index (IRI), initially developed in 1980s to represent pavement surface conditions in a quantitative method, has been widely used in many transportation agencies worldwide. The calculation of the index is based on a moving quarter-car vehicle math model that quantifies the total vertical vehicle body movement due to the uneven pavement

surface with distresses within 1 kilometer of travelling distance. The typical vehicle operation speed is 80 km/hr (MDOT, 2017). The metric unit of IRI is in meters per kilometer (m/km) and empirical unit of IRI is in inches per mile (in/mi). IRI data collection procedures shall conform to ASTM E950 standard. Higher IRI values indicate rougher pavement surfaces with high distress severity and density, whereas lower values indicate smooth riding conditions with better distress ratings. However, IRI does not indicate pavement structural condition and specific distresses.

Typically, IRI is surveyed using mechanical systems where vertical movements are measured based on Distance Measuring Instrument (DMI) and laser equipment installed on automatic road analyzer (ARAN) vehicle for large-scale measurements at high operation speeds or portable laser IRI profiler for small-scale at low speeds.

IRI value class can vary based on different roadway function types and agencies. For example, IRI is categorized into 3 class by The Michigan Department of Transportation (MDOT, 2017):

- Good: $IRI < 95$ in/mi (1.5m/km)
- Fair: 95 in/mi $< IRI < 170$ in/mi (1.5 m/km $< IRI < 2.7$)
- Poor: 170 in/mi $< IRI$ (2.7 m/km $< IRI$)

3.2 Data Preparation

3.2.1 Data Selection

Data are typically retrieved and delivered in a format of Microsoft Excel tables or Microsoft Access files. Using either the web page of the LTPP or SQL codes can direct to and generate the data sets that users want. In this study, a combination of both web page operations (Figure 3.3) and SQL (Figure 3.4) were used to locate and download the desired data tables.

Tabular Selection
Visual Selection

The as-collected LTPP data units are displayed. InfoPave provides the ability to convert data units to the SI or US Customary systems.

| | |
|---|--|
| ■ Primary Data Classification | 🔑 Key Field |
| 📄 Primary Data | 📄 Basic Fields |
| ■ Advanced Data Classification | 📄 Advanced Fields |
| 📄 Advanced Data | |

| | |
|--|--|
| + Pavement Structure and Construction | <input type="checkbox"/> Show Advanced Data Classification |
| + Climate | <input type="checkbox"/> Show Advanced Data Classification |
| + Traffic | <input type="checkbox"/> Show Advanced Data Classification |
| - Performance | <input type="checkbox"/> Show Advanced Data Classification |

Collapse All

- Pavement Distress
 - ☐ AC
 - ☐ JPCP
 - ☐ CRCP
- ☐ Surface Characteristics
 - ☑ Longitudinal Profile (IRI)
 - ☑ Section Level IRI
 - ☐ Transverse Profile (Rut)
 - ☐ Texture
- ☐ Backcalculation and Deflection
 - ☐ Backcalculation
 - ☐ Deflection

Add to Selection

Figure 3-3 LTPP data selection using web operations

| Query Properties | | | | | | | | |
|-------------------------------------|---|-----------|--------------------------|-----------|------------|-------------------------------------|----------|-------|
| Output | Expression | Aggregate | Alias | Sort Type | Sort Order | Grouping | Criteria | Or... |
| <input checked="" type="checkbox"/> | MON_HSS_VISIT_NO.STATE_CODE | | STATE CODE | ASC | 1 | <input checked="" type="checkbox"/> | | |
| <input checked="" type="checkbox"/> | MON_HSS_VISIT_NO.SHRP_ID | | LTPP SECTION IDENTIFIER | ASC | 2 | <input checked="" type="checkbox"/> | | |
| <input checked="" type="checkbox"/> | MON_HSS_VISIT_NO.VISIT_DATE | | VISIT DATE | ASC | 3 | <input checked="" type="checkbox"/> | | |
| <input checked="" type="checkbox"/> | Round(Avg(MON_HSS_PROFILE_SECTION.IRI_LEFT_WHEEL_PATH), 2) | | AVG LEFT WHEEL PATH IRI | | | <input type="checkbox"/> | | |
| <input checked="" type="checkbox"/> | Round(Avg(MON_HSS_PROFILE_SECTION.IRI_RIGHT_WHEEL_PATH), 2) | | AVG RIGHT WHEEL PATH IRI | | | <input type="checkbox"/> | | |
| <input type="checkbox"/> | MON_HSS_PROFILE_SECTION.VISIT_NO | | | | | <input checked="" type="checkbox"/> | | |
| <input type="checkbox"/> | | | | | | <input type="checkbox"/> | | |

Refresh

SQL Editor ?

```
Select MON_HSS_VISIT_NO.STATE_CODE As "STATE CODE",
MON_HSS_VISIT_NO.SHRP_ID As "LTPP SECTION IDENTIFIER",
MON_HSS_VISIT_NO.VISIT_DATE As "VISIT DATE",
Round(Avg(MON_HSS_PROFILE_SECTION.IRI_LEFT_WHEEL_PATH),
2) As "AVG LEFT WHEEL PATH IRI",
Round(Avg(MON_HSS_PROFILE_SECTION.IRI_RIGHT_WHEEL_PATH),
2) As "AVG RIGHT WHEEL PATH IRI"
From MON_HSS_PROFILE_SECTION
Inner Join MON_HSS_VISIT_NO On MON_HSS_PROFILE_SECTION.VISIT_NO =
MON_HSS_VISIT_NO.VISIT_NO
Group By MON_HSS_VISIT_NO.STATE_CODE.
```

Clear Preview Data Add to Data Bucket

Figure 3-4 LTPP data selection using SQL

Although LTPP contains a great abundance of pavement-related data where there are 15 modules of data with a total number of more than 600 tables, selecting the meaningful and consistent data for IRI prediction can be complicated and challenge. Based on the results from the literature review and empirical pavement engineering knowledge, there are a wide range of factors can possible contribution to pavement deterioration. The basis of the data selection methodology can be summarized as:

- Step 1: Find out and understand the specific data in search of
- Step 2: Refer to the LTPP user manual to locate the tables that contain the target data using SQL and/or HTML operations
- Step 3: Download the table and check the consistency and quantity of the data
- Step 4: If the data quality and quantity are not satisfactory repeat Step 2

Note: One type of data can be stored on multiple tables. While implementing step 4, discussions with a pavement specialist are required.

In terms of data quality, here it refers to the consistency of the combined data set for machine learning data analysis, where every input and output variable value cannot be left as empty. Since the predicted IRI values are on an annual basis, other data such as AADTT and freeze index of the years when IRI values were recorded need to be available as well. For example, the data quality is undesirable when there are 10 IRI records for each year in a 10-year period but only 5 AADTT records were found.

3.2.2 Data Cleaning and Assembly

When selecting the data tables, they need to be combined and cleaned to prepare a large dataset for modelling purpose. These data tables are not interconnected and contain the data from different LTPP test sections in different geographical locations. To join and combine the separate data tables, relational fields are used as linking keys (Table 3.1). The diagram below illustrates the example relationships between interrelated tables by connecting their related fields (Figure 3.5). This example shows a combination of three categories of data tables: annual temperature data (CLM_VMS_TEMP_ANNUAL), traffic data (TRF_TREND), and construction histories (INV_AGE) for all available test sections on LTPP (Figure 3.6). The tables can only be combined when all relational field values are matched (i.e., same State/Province, same test section, and same year/date).

Table 3-1 LTPP data relational fields

| Relational Fields | Description | Example |
|--------------------------|---|---------------------------------------|
| STATE_CODE | An identifier for State/Province. Composed of two-digit numerical value. | 42 (Pennsylvania) |
| SHRP_ID | An identifier for a single test section or a group of test sections. Composed of alphanumeric characters. | 42-1614 (State College, Pennsylvania) |

| | | |
|-----------------|--|--|
| CONSTRUCTION_NO | A cumulative count of construction and M&R events for each test section. | 1 (Original construction) 2 (Original construction and one following M&R event) |
| YEAR/DATE | The year or the date that the data entry has been recorded | 1998 Jan/1/1998 |

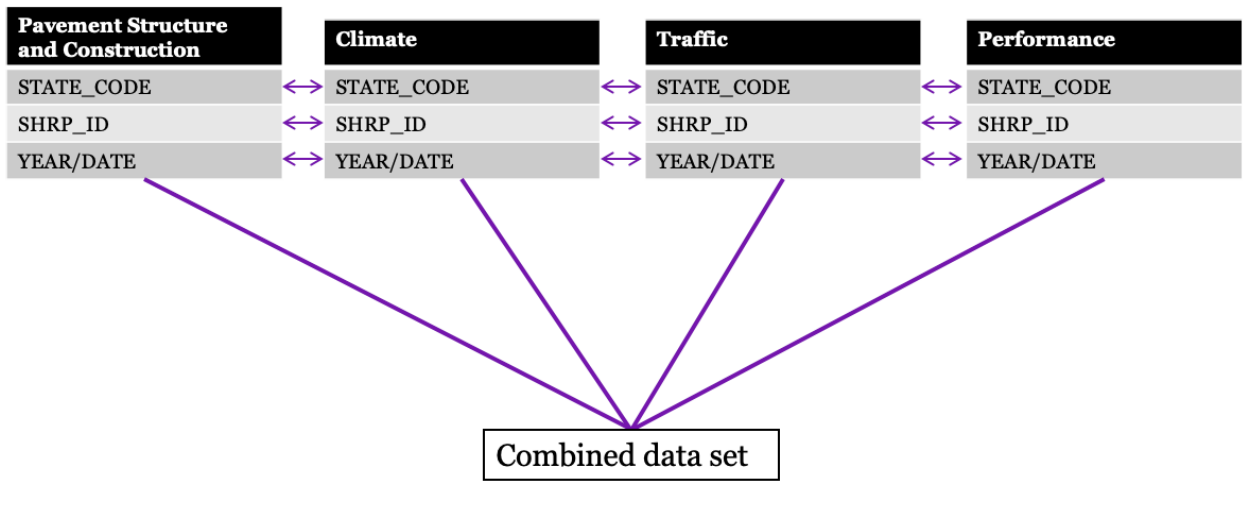


Figure 3-5 LTPP data entity relationship example illustration

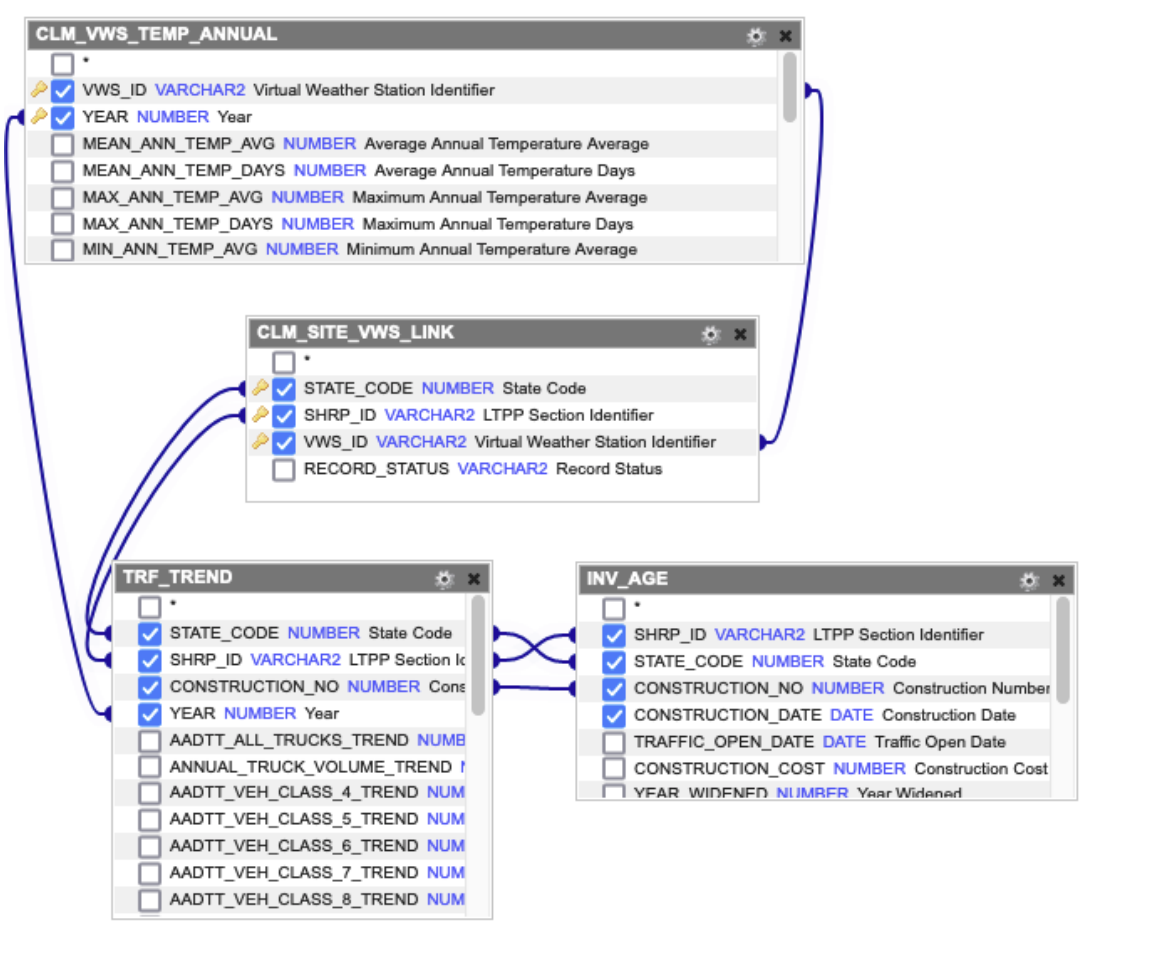


Figure 3-6 Detailed LTPP data entity relationship between AADTT, pavement age and annual temperature

In the field of modern data analysis, AI/ML model prediction accuracy is a reflection of data size and data consistency. Model training is learning process for algorithms. Similar to human intelligence, well-developed knowledge and experience can help a person’s decision-makings and reactions when an unknown situation is introduced. To conclude such, sufficient amount of training data may be beneficial to the test accuracy. Therefore, having a relatively large data size has been always a major objective throughout the data collection and cleaning process. In

addition, along with other aspects to consider, the overall objectives of the LTPP data processing were summarized as:

Data types that:

- Have a large amount of records
- Are widely recorded and available for the majority of the test sections
- Are well-recorded with consistently collection frequency (e.g., no missing data in a specific year)
- Are meaningful to pavement performance/deterioration
- Are consistent with the results from literature review
- Are universal and feasibly obtainable for various States/Provinces/Agencies
- Have low complexity

3.2.3 Challenges

Data consistency has large impacts on model prediction accuracy. Noisy data can limit the algorithms to reach the optimum performance. Although LTPP consists of huge amount of pavement-related data, it started storing data more than 30 years ago where there was a lack of future vision of data usage for advanced data analysis. Select valuable, meaningful yet consistent data from LTPP was quite challenging. In other words, datasets on LTPP are often too inconsistent for ML data analysis because it was not intentionally designed for such analysis in decades ago. For many researchers, LTPP data analysis has always been an uncharted territory with continuous exploration of data interpretation and solutions to the data noise.

In this study, the major steps and challenges of the data cleaning were:

- Match the records that had different collection frequencies and schedules
- Discover the methods to represent and absorb IRI fluctuations due to M&R
- Redefine the initial IRI values
- Select the data tables have the best data qualities and quantities
- Create new data based on existing data when it is necessary

Data Inconsistency and Missing Data

To match a type of data to another, 2 to 3 types of relational fields were used: location reference (STATE_CODE and SHRP_ID), time reference (YEAR, MONTH, or DATE), and construction events (CONSTRUCTION_NO). Each test section only correlates to one location reference and but within a certain time period, the number and the collection time of records can be different. For example, annual average daily truck traffic (AADTT) data are recorded on an annual basis meaning 1 value for each year in each test section. However, pavement condition survey can occur multiple time in a year or in a month; as a result, there could be more than 1 IRI record in a year for a specific test section which illustrate an example of data inconsistency on LTPP. Table 3.2 shows an example of combined AADTT and mean IRI data for test section 1617 in Pennsylvania. Seen from the table, IRI recording started in 1989 and ended in 2004, however, AADTT records were only found between 1998 and 2004. In addition, there were years that both AADTT and IRI records were not found (1996, 2000, and 2001). Such inconsistency may drastically reduce the available data size and thus affect the modeling performance. Thus, without acquiring missing data from other sources, data from different test sections and States/Provinces were combined into a single data set to maximize the data size.

Table 3-2 An example showing data inconsistency on LTPP

| STATE_CODE | SHRP_ID | CONSTRUCTION_NO | VISIT_DATE | Mean IRI | YEAR | AADTT | Note |
|------------|---------|-----------------|------------|----------|------|-------|------------------------------------|
| 42 | 1617 | 1 | 12-02-1989 | 2.25 | 1989 | N/A | Missing AADTT records |
| 42 | 1617 | 1 | 05-15-1990 | 2.28 | 1990 | N/A | Missing AADTT records |
| 42 | 1617 | 2 | 10-09-1991 | 0.83 | 1991 | N/A | Missing AADTT records |
| 42 | 1617 | 2 | 10-15-1992 | 0.81 | 1992 | N/A | Missing AADTT records |
| 42 | 1617 | 2 | 10-15-1993 | 0.85 | 1993 | N/A | Missing AADTT records |
| 42 | 1617 | 2 | 09-13-1994 | 0.84 | 1994 | N/A | Missing AADTT records |
| 42 | 1617 | 2 | 11-10-1995 | 0.86 | 1995 | N/A | Missing AADTT records |
| 42 | 1617 | 2 | N/A | N/A | 1996 | N/A | Missing Both AADTT and IRI records |
| 42 | 1617 | 2 | 11-11-1997 | 0.87 | 1997 | N/A | Missing AADTT records |
| 42 | 1617 | 2 | 08-04-1998 | 0.9 | 1998 | 3680 | |
| 42 | 1617 | 2 | 10-13-1999 | 0.91 | 1999 | 4078 | |
| 42 | 1617 | 2 | N/A | N/A | 2000 | N/A | Missing Both AADTT and IRI records |
| 42 | 1617 | 2 | N/A | N/A | 2001 | N/A | Missing Both AADTT and IRI records |
| 42 | 1617 | 2 | 06-01-2002 | 0.91 | 2002 | 4200 | |
| 42 | 1617 | 2 | 12-04-2002 | 0.91 | 2002 | 4200 | More than 1 measurement per year |
| 42 | 1617 | 2 | 11-08-2004 | 0.93 | 2004 | 4299 | |

Climate Zoning

Although combining the data could enlarge the data size, it was unclear that if there are potential differences between different locations. Based on pavement engineering knowledge, bituminous materials are sensitive to temperature change and have dynamic modulus under different environment settings. Subgrade soil properties are also affected by temperature and moisture. Some previous performance predictive modelling studies (Hossain et al., 2018; Zhang et al., 2017; Piryonesi and El-Dirby., 2021) have segmented data sets based on the climate regions (Figure 3.7). Hence, for this study, climate zoning was introduced to mitigate the potential data noise caused by geographical difference. Climate zoning was first recorded as a type of categorical data along with other continuous numerical data such as AADT and initial IRI. In order to process this combined data set, climate zoning data was digitized using binary classification while other numerical data remain unchanged (Table 3.3).



Figure 3-7 Climate regions on LTPP for pavement test sections (Zhang et al, 2017)

Table 3-3 Digitized climate zoning for LTPP data

| Climate Type | Climate Type 1 | Climate Type 2 | Climate Type 3 | Climate Type 4 |
|-----------------|-------------------|-------------------|-------------------|-------------------|
| Wet, Non-Freeze | 1 | 0 | 0 | 0 |
| Wet, Freeze | 0 | 1 | 0 | 0 |
| Dry, Non-Freeze | 0 | 0 | 1 | 0 |
| Dry, Freeze | 0 | 0 | 0 | 1 |

Table Selection Dilemma

On LTPP, one type of data can be stored on multiple tables. For example, on table 3.4, in terms of traffic data, annual average daily traffic (AADT), annual average daily truck traffic (AADTT), and equivalent single axle load (ESAL) can all be found in both TRF_TREND and TRF_MON_EST_ESAL tables. In TRF_TREND table, data are composed of statistically computed and estimated traffic value, whereas TRF_MON_EST_ESAL table includes annual estimated values from actual test section measurements and monitoring. Based on pavement engineering judgement, using TRF_MON_EST_ESAL may provide more realistic and accurate data, but its records are relatively inconsistent, and the total data size are much less than that of TRF_TREND table. In addition, AADT was not included on TRF_TREND table but on the other. However, heavy vehicles are the major contributors to pavement distress. Pavement design methods such as AASHTO 1993 and AASHTOWare ME are only considering truck traffic (AADTT and ESAL). Thus, AADT can be and were excluded. In terms of machine learning data analysis, data size and quantity matter significantly. Therefore, TRF_MON_EST_ESAL table was replaced by TRF_TREND table.

Table 3-4 Traffic data table comparison

| Data types | Table: TRF_TREND | Table: TRF_MON_EST_ESAL |
|-------------------------|---------------------------------------|--------------------------------|
| AADT | N/A | Inconsistent amount of records |
| AADTT | Good amount of records | Inconsistent amount of records |
| ESAL | Good amount of records | Inconsistent amount of records |
| Recording scheme | Computed & Estimated Value | Monitored Values |

Initial IRI and M&R History Representation

By definition, the first initial IRI value of a test section refers to the measurement immediately after the initial construction and traffic opening. However, a significant number of test section pavements were initially constructed prior to 1989 and before LTPP started to collect surface distress data. This means the first initial IRI values for those test section cannot be found on LTPP database but may be stored on some local project-level PMS databases. In this study, for each test section, the first IRI value recorded on LTPP after 1989 is regarded as the first initial IRI since the original construction.

IRI value increases along with pavement deterioration which is typically a positive function of time. However, post-construction maintenance and rehabilitation (M&R) activities may result in the sudden decrease of IRI value (Figure 3.8). Major M&R events such as milling, HMA overlay and reconstruction can result in a large IRI value drop yet may have only few times during the service life; minor M&R activities such as crack sealing and pothole patching have higher frequencies and often cause small fluctuations. As a result, the use of a single initial IRI value for each test site cannot adapt to the cycles of IRI value change due to the major improvements. To incorporate these IRI value drops, once a major improvement has occurred, the initial IRI is updated from the previous initial IRI value. The time intervals between the current year and the year of initial construction or latest improvement are also calculated as the age since previous

construction or improvement. Furthermore, the number of M&R constructions after 1989 were counted as a cumulative value as CONSTRUCTION_NO. Overall, by having this set of procedure that includes multiple up-to-date initial IRI values, age since last construction, and the number of improvements, the construction history can be numerically represented and localized on the timeframe for each section which provide great adaptability to pavement condition improvements. Also, IRI values were averaged into a single value if there were more than 1 records found per year. Table 3.5 shows an example of the initial IRI and M&R history representation.

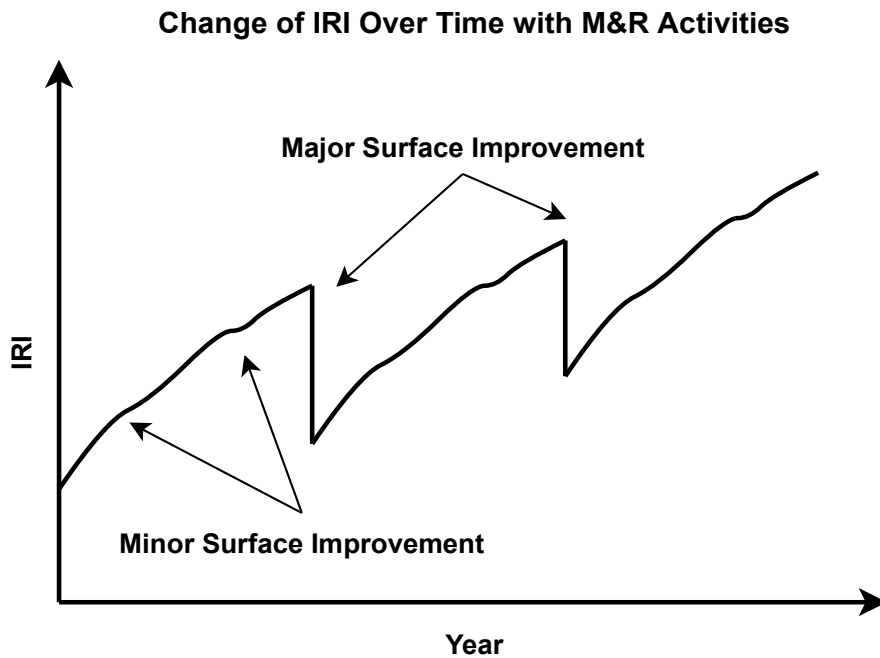


Figure 3-8 Change of IRI over time with M&R activities

Table 3-5 Example of defining initial IRI (MRI0), age since last M&R (AGE0), and the number of constructions (CONSTRUCTION_NO)

| STATE_CODE | SHRP_ID | CONSTRUCTION_NO | Mean IRI (MRI) | YEAR | Initial MRI (MRI0) | AGE0 |
|------------|---------|-----------------|----------------|------|--------------------|------|
| 42 | 1617 | 1 | 2.25 | 1989 | 2.25 | 0 |
| 42 | 1617 | 1 | 2.28 | 1990 | 2.25 | 1 |
| 42 | 1617 | 2 | 0.83 | 1991 | 0.83 | 0 |
| 42 | 1617 | 2 | 0.81 | 1992 | 0.83 | 1 |
| 42 | 1617 | 2 | 0.85 | 1993 | 0.83 | 2 |
| 42 | 1617 | 2 | 0.84 | 1994 | 0.83 | 3 |
| 42 | 1617 | 2 | 0.86 | 1995 | 0.83 | 4 |
| 42 | 1617 | 2 | 0.87 | 1997 | 0.83 | 6 |
| 42 | 1617 | 2 | 0.9 | 1998 | 0.83 | 7 |
| 42 | 1617 | 2 | 0.91 | 1999 | 0.83 | 8 |
| 42 | 1617 | 2 | 0.91 | 2002 | 0.83 | 11 |
| 42 | 1617 | 2 | 0.93 | 2004 | 0.83 | 13 |

3.2.4 Final Input Data Selection

In the end, a total number of 17,147 rows of data were gathered at the end of the data mining process from LTPP. The tables below show the data groups for pavement structure and construction (Table 3.6), climate (Table 3.7), traffic (Table 3.8), and performance (Table 3.9) respectively.

Pavement structure and construction

Table 3-6 Final data for pavement structure and construction

| Data name | Description | Source table on LTPP |
|--------------------|--|----------------------|
| CONSTRUCTION_NO | Cumulative number of construction event | TST_05B |
| ORG_AGE | Age since original construction | PROJECT_HIST_AGE |
| AGE0 | ΔT (years) since latest construction event | EXPERIMENT_SECTION |
| Total_AC_thickness | Total surface asphalt layer thickness | TST_05B |

Climate

Table 3-7 Final data for climate

| Data name | Description | Source table on LTPP |
|------------------|--|-----------------------------|
| Climate_Zone | Climate zones on LTPP: dry/wet and freeze/non-freeze | MERRA_GRID_SECTION |
| TEMP_MEAN_AVG | Average of the daily mean air temperatures 2 meters above the MERRA centroid | MERRA_TEMP_YEAR |
| FREEZE_INDEX | Freeze index | MERRA_TEMP_YEAR |
| FREEZR_THAW | Total number of freeze-thaw days in the year | MERRA_TEMP_YEAR |
| PRECIPITATION | Total precipitation in the year | MERRA_PRECIP_YEAR |
| REL_HUM_AVG_AVG | Average relative humidity | MERRA_HUMID_YEAR |

Traffic

Table 3-8 Final data for traffic

| Data name | Description | Source table on LTPP |
|-------------------------|--|-----------------------------|
| AADTT | Annual Average Daily Truck Traffic for all trucks | TRF_TREND |
| ANNUAL_TRUCK_VOLUME | Annual estimate of trucks in LTPP lane | TRF_TREND |
| AADTT_VEH_CLASS_9_TREND | Annual estimate of class 9 trucks in LTPP lane | TRF_TREND |
| ANNUAL_ESAL_TREND | Annual estimated ESAL for class 4-13 trucks in LTPP lane | TRF_TREND |

Performance

Table 3-9 Final data for pavement performance

| Data name | Description | Source table on LTPP |
|------------------|---|-----------------------------|
| MRI | Averaged Annual Mean International Roughness Index (IRI) | MON_HSS_PROFILE_SECTION |
| MRI0 | Initial MRI value within 1 year after the latest construction event | MON_HSS_PROFILE_SECTION |

3.3 Decision Tree and Random Forest Modelling

Based on the results for the literature review, although the majority of studies using LTPP data used supervised ANN as their primary algorithm type which had resulted in promising accuracies, the decision-making processes of those studies were not able to be interpreted. ANN does provide relatively high prediction accuracy, but it sacrifices the ability to explain the model training, interpreting and predicting processes. Nevertheless, decision tree (DT) algorithms allow the predicting and decision-making process to be explainable yet without a significant decrease in prediction accuracy. Hence, in this section, single DT models and Random Forest (RF) models for comparison were constructed to conduct the predictive modelling of the prepared LTPP data. The models were built on Python 3.8 language with various libraries including Sci-Kit Learn, Pandas and Numpy for data preparation, model training and evaluating, and Matplotlib and Plotly for result visualization. The initial DT and RF models have both shown the existence of overfitting issues. Thus, hyperparameter optimizations were conducted after the initial modelling to prune the decision tree(s) and mitigate the overfitting. Final prediction results were discussed, and the decision tree(s) were visualized.

3.3.1 Background

Classification and Regression Trees

The concept of classification and regression trees (CART) was first introduced by Leo Breiman in 1980s. CART is a type of non-parametric supervised learning approach providing classification and regression of the pre-defined data. CART is indeed suitable for this study since the data set retrieved from LTPP consist of pre-defined and labelled variables. It is also one of the most popular and practical algorithms for inductive inference (Mitchell, 1997). The primary objective of CART is not to develop specific prediction equations but was to approximate target functions with discrete values (Mitchell, 1997). Due to the basis of such, decision trees process greater ability to handle noisy data than logistic and linear regressions do.

Based on the variable type of output predictor (the dependent variable), CART is divided into two primary categories:

- Classification decision trees for the output variable that is categorical
- Regression decision trees for the output variable that is continuous

Classification decision trees are used when the output variable is categorical, which are not numerically continuous. It classifies the final prediction outcome into discrete classes. For example, the classification prediction results can be just divided into positive and negative answers, which are not numerically related. On the other hand, when the target output variable type is continuous rather than discrete classifications, the regression trees were deployed to predict the specific value of the output variable. In this study, since the dependent variable IRI is a type of continuous variable with specific values, the regression method was selected and implemented. Figure 3.9 and 3.10 below show examples of classification tree and regression tree, respectively.

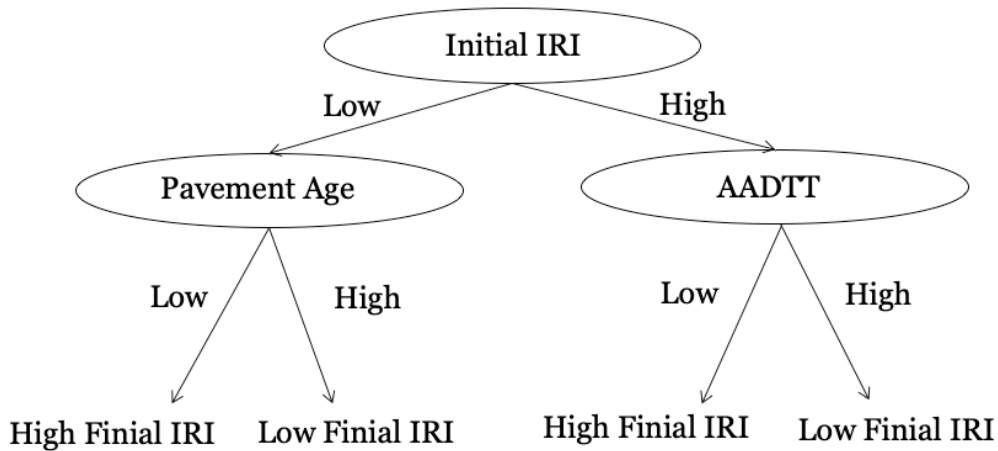


Figure 3-9 Illustration of Decision Tree classification

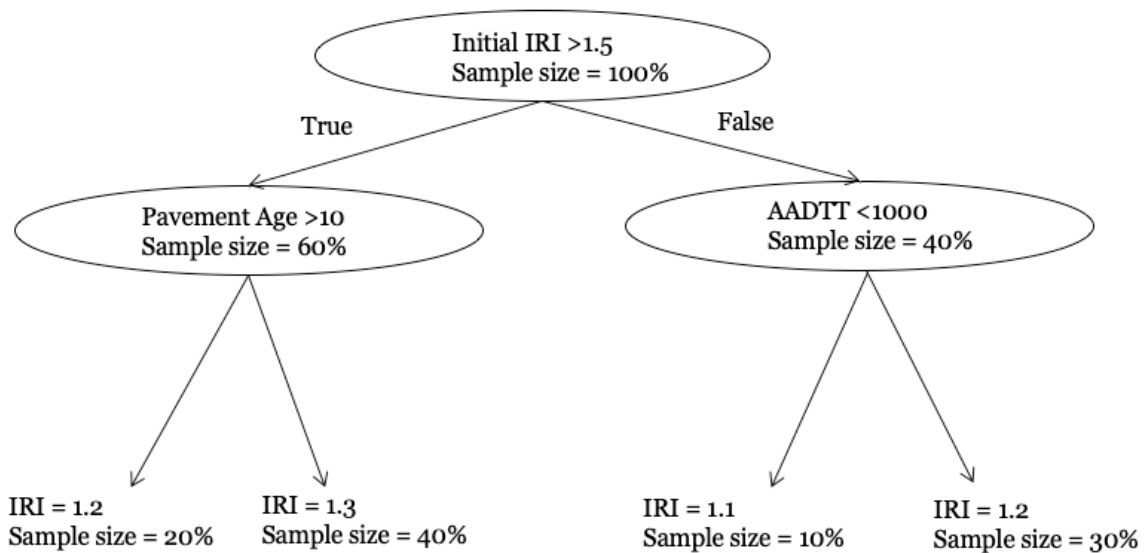


Figure 3-10 Illustration of Decision Tree regression

CART splits the data along the tree from the root node and descends to leaf nodes. Root node is the base of the tree where the dataset is complete, and the leaf node is where the splitting process terminates. A splitting criterion was assigned at each node to further split the samples. The basis of CART is repetitive binary classification splitting the parent node into two child nodes. During the splitting process, along with the increase of tree growth and depth, the dataset is partitioned

into smaller subsets stepwise as the number of samples on each node decreases and the decision rules and the complexity of the tree increase How tree algorithm functions is further summarized in the following steps (Breiman, 1984):

1. Finding each feature’s best split that maximizes the splitting criterion
2. Finding each node’s best split that maximizes the splitting criterion
3. Using the best split to split the node
4. Repeat all three steps above until terminating criterion is satisfied

There are a few types of splitting criterion and the criterion used in classification trees and regression trees are different. Classification trees use Gini’s index whereas the regression trees implemented in this study used squared error. In this study, at each node, the splitting decision was made in order to achieve least squared error which is equivalent to L2 loss function (Equation 3.1).

$$L2 \text{ Loss Function (Least Squared Error)} = \sum_{i=1}^n (y_{true} - y_{predicted})^2 \quad (3.1)$$

Although decision tree algorithm provides great visualization ability to the decision-making process, it still suffers from a few limitations including overfitting. Table 3.10 below summarizes the major advantages and limitations.

Table 3-10 Advantages and limitations of decision tree algorithm

| Advantages | Limitations |
|--|--|
| <ul style="list-style-type: none"> • Superior decision-making visualization and interpreting abilities • Dependent (output) variable can be both categorical and numerical data • Able to handle noisy data | <ul style="list-style-type: none"> • Prone to overfitting with overly grown trees • Hyperparameter tuning can be complicated • Instable when small data variations occurred |

Random Forest

Random forest algorithm an ensemble learning method that is composed of a set of decision trees instead of a single decision tree. It is a further development based on CART which is still a non-parametric supervised learning and uses labelled data (Breiman, 2001). As a descendant of decision tree, depending on the data type, random forest was divided into two types: classification for categorical output variable and regression for continuous variable. Random forest algorithm creates bootstrapped sample datasets derived from the original dataset. Meanwhile, this bootstrapping process incorporates feature randomness by randomly generating subsets of data samples. By training decision trees with random subsets of data, the correlations between the trees within the forest are minimized. Composed a number of decision trees, random forest is a more effective tool to tackle overfitting comparing to a single decision tree (Breiman, 2001). Output evaluation methods of random forest differs from that of decision tree. Random forest classification that is based on categorical output variable is evaluated based on a majority voting, whereas random forest regression averages the output prediction from each of the single trees. Figure 3.11 below illustrates the basic structure of a random forest model.

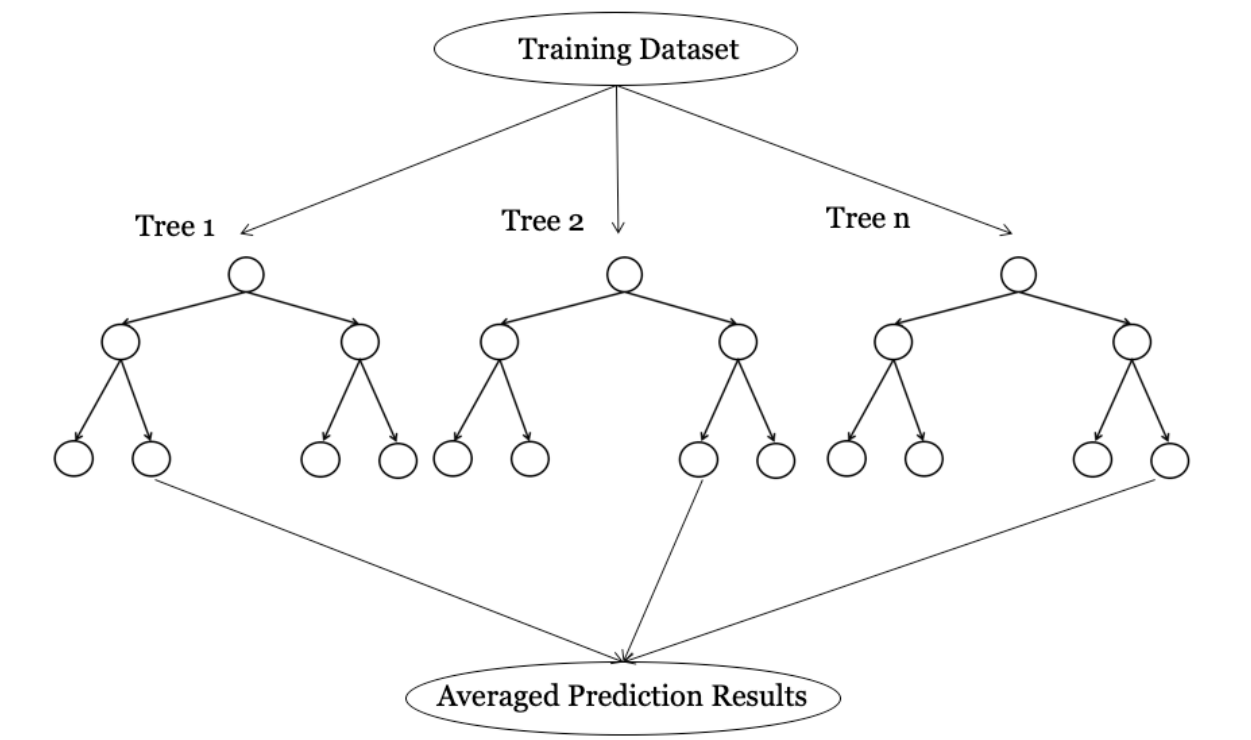


Figure 3-11 Illustration of a Random Forest model

Although random forest is an advancement of single decision tree, overfitting still existing in random forest models which is one of the major disadvantages of the algorithm. Table 3.11 below summarizes the advantages and limitations of random forest.

Table 3-11 Advantages and limitations of random forest algorithm

| Advantages | Limitations |
|---|---|
| <ul style="list-style-type: none"> • Less overfitting comparing to decision tree • Still provides good visualization ability • Flexible to handle noisy data | <ul style="list-style-type: none"> • Still likely to overfit when the trees are complex • High computational cost when the forest is complex • May require large date sets |

| | |
|---|--|
| <ul style="list-style-type: none"> Feasible to evaluate feature importance | |
|---|--|

3.3.2 Model Training and Evaluation

Decision Tree Model

To build the decision tree model in this study, DecisionTreeRegressor algorithm developed by Sci-kit Learn library was implemented in Python 3.8 environment. The entire dataset consisting of 17,147 observations was divided into two groups: 80% (13,717) for model training and 20% (3,430) for model testing. All groups of data set have 15 input variables and 1 output variable.

In the initial default decision tree models, hyperparameters (Table 3.12) were untuned where the tree was allowed to fully grow with complexity without constraints. In addition to the testing, a 10-fold cross-validation (CV) was performed on the training dataset by using the trained model. Since there was only one training dataset and one testing dataset, model overfitting might exist. Hence the objective of CV is to repeatedly estimate the model prediction accuracy on unintroduced data to investigate the potential overfitting. In the CV process, the testing data were excluded, and the training data set was further divided by the number of folds (k), which was 10 in this case.

The coefficient of determination (R^2) and mean square error (MSE) were used to evaluate the model performance. Equation 3.2 and 3.3 shows the calculation methods of R^2 and MSE respectively. Table 3.13 below is the result summary of model training, testing and 10-fold CV.

$$R^2 = 1 - \frac{\sum_{i=1}^n (y_i - \hat{y}_i)^2}{\sum_{i=1}^n (y_i - \bar{y}_i)^2} \quad (3.2)$$

$$MSE = \frac{1}{n} \sum_{i=1}^n (y_i - \hat{y}_i)^2 \quad (3.3)$$

y_i = observed target value

\hat{y}_i = predicted value,

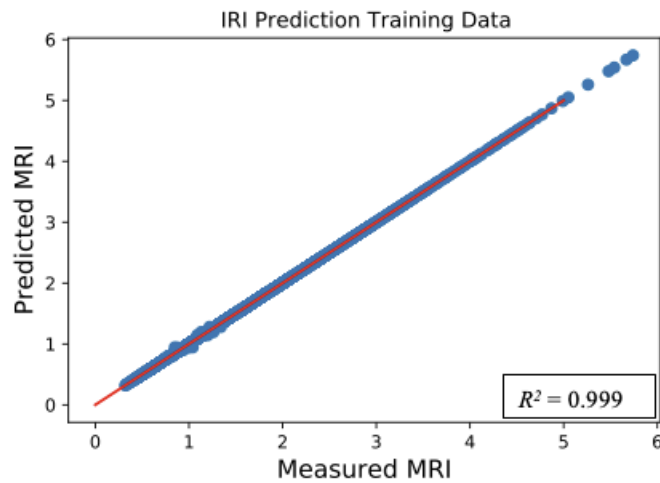
\bar{y}_i = mean observed value.

Table 3-12 Initial decision tree model parameters

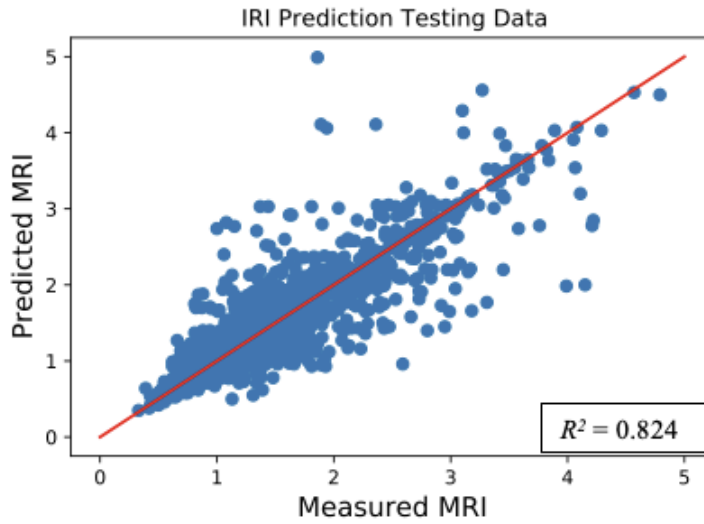
| Parameter | Value |
|---|-------|
| Tree depth | 35 |
| The number of leaves | 9903 |
| Minimum number of samples on each leaf node | 1 |
| Minimum number of samples on each split | 2 |
| Total number of features | 18 |

Table 3-13 Prediction result summary from the initial decision tree model

| Set | Average R^2 | Average MSE |
|------------------|---------------|---------------|
| Training | 0.999 | 3.82e-6 |
| Testing | 0.824 | 0.0567 |
| Cross-validation | 0.833 | 0.057 |



(a)



(b)

Figure 3-12 Initial decision tree training (a) and testing (b) results

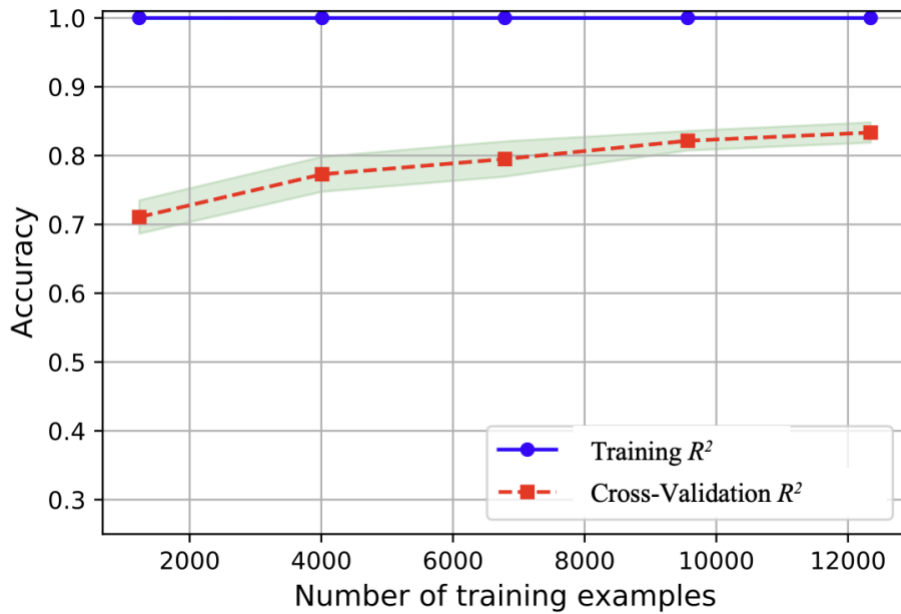


Figure 3-13 Learning curve of training data

Figure 3.12 and 3.13 show the training accuracy (3.12 a), testing accuracy (3.12 b) and the learning curve of the initial decision tree model. In addition, the entire decision had large

complexity, so only a part of the visualized decision tree was displayed on figure 3.14 below. In the end, these results indicate that the initial decision tree overfitted:

- A large gap between training accuracy and testing accuracy
- Training accuracy constantly maintained at close to 1.0
- The number of samples on the terminal leaf node was very low (around 1~2)

Therefore, a decision tree pruning process was required to improve the overfitting.

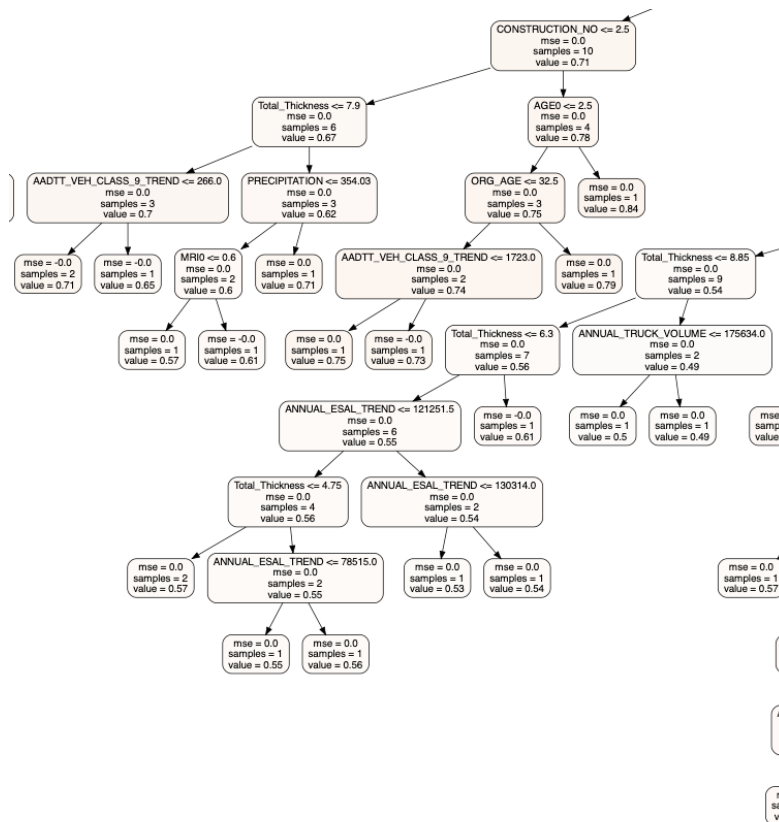


Figure 3-14 Visualization of a part of the initial decision tree

Random Forest Model

Similar to the decision tree model, the random forest model was developed using RandomForestRegressor from sci-kit learn library (Pedregosa et al., 2011). The same dataset consisting of 80% training data and 20% testing data was used applied for this random forest model. Unlike the single tree model, a random forest model may consist up to hundreds of trees which is more complex. Hence, the number of trees needs to be considered when constructing the model in terms of such aspects:

- Computational cost
- Visualization feasibility
- Prediction accuracy
- Overfitting

In the initial random forest model, while the numbers of the trees are pre-defined, there were no other hyperparameter constraints meaning the trees were allowed to grow for the optimum prediction accuracy. Figure 3.15 below shows the relationship between the number of trees and training, testing and cross-validation accuracies. The accuracies started to converge when the number of trees was reaching around 5 to 10, and eventually maintained at around 0.91 as the number of trees rise to more than 20 (Figure 3.15). Both test and cross-validation accuracies were higher than 0.875 when the number of trees was more than 3. In addition, fewer trees would allow better decision-making visualization and potentially help reduce the overfitting issues. As a result of such early convergence of the accuracies, the number of trees shall be limited to 5 for the further optimization of the model.

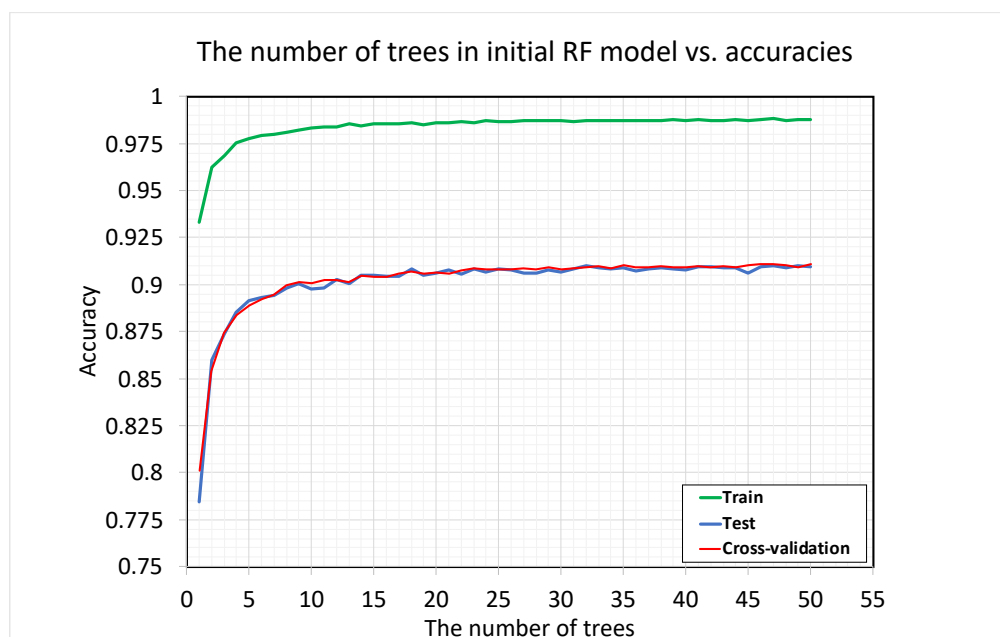


Figure 3-15 The number of trees in initial random forest model vs. accuracies

3.3.3 Model Pruning and Hyperparameter Optimization

Decision Tree Pruning

In the initial decision tree model, overfitting was observed as the training accuracy was more than 15% higher than testing accuracy that was close to 1.0. Overfitting indicates the tree is overly grown. There are two approaches to prevent the tree from overfitting: pre-pruning and post-pruning (Bramer, 2013). Pre-pruning is used to limit the tree growth by pre-defining the hyperparameters before the construction of the tree, whereas post-pruning is used to remove the branches and leaves after the tree has been developed. Although pre-pruning may save the computational costs and is more efficient than post-pruning, post-pruning often provides better accuracy by customizing the developed model (Fürnkranz, 1994). Thus, a cost complexity pruning process was conducted to optimize the complexity of the tree and avoid the overfitting.

Minimal Cost-Complexity Pruning (CCP) algorithm is developed based on $\alpha \geq 0$, which is the complexity parameter (Breiman, 1984). Minimal CCP method is based on the principle of finding the lowest cost-complexity by minimizing the value from a combination of the number of

terminal nodes, complexity parameter alpha, and the misclassification rate. The equation used to define the cost-complexity is defined as such (Equation 3.4):

$$R_\alpha(T) = R(T) + \alpha |\tilde{T}| \quad (3.4)$$

Where $R_\alpha(T)$ is a linear combination of the cost of the tree and its complexity, $R(T)$ is total misclassification rate of the terminal leaf nodes, α (alpha) is the complexity parameter, and $|\tilde{T}|$ is the number of terminal leaf nodes (Breiman, 1984).

The results of the CCP process were illustrated on figure 3.16 below. Higher alpha values indicate larger number of nodes pruned. The testing accuracy reached to around 83% to 84% where the training accuracy fluctuated between 85% and 91%. The peak testing accuracy peaked at 84.2% when the alpha value was 0.000188. As the value of alpha increased, the number of nodes and the depth of the tree decreased (Figure 3.17). This would result in an overall decrease of tree complexity and improve the overfitting problems.

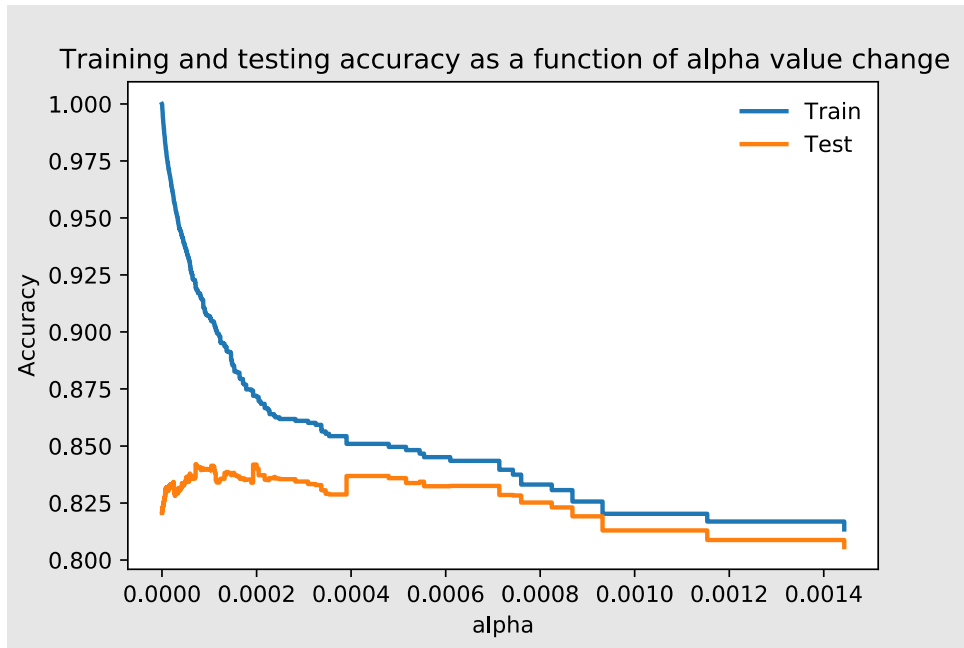


Figure 3-16 Training and testing accuracy as a function of alpha value

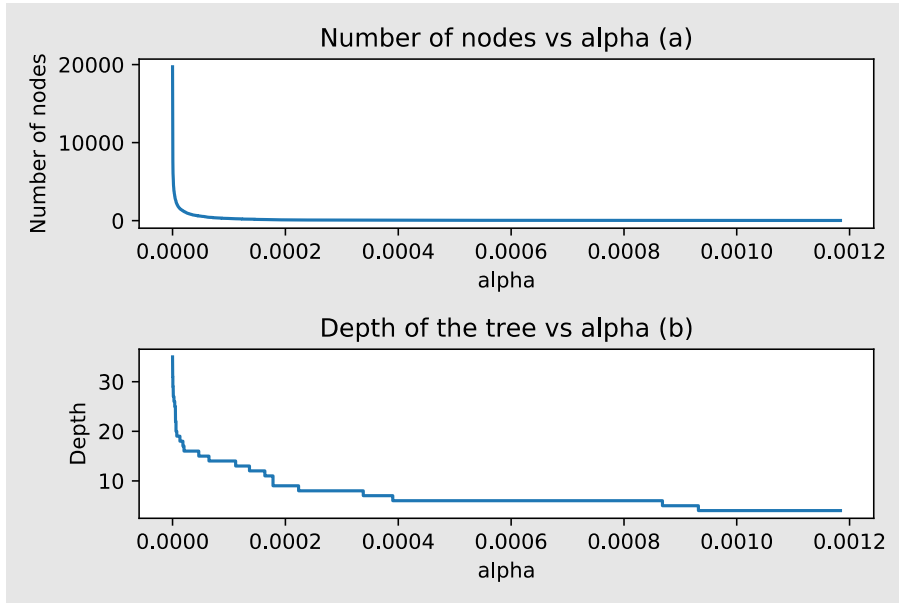


Figure 3-17 The number of nodes (a) and the depth of the tree (b) as a function of alpha value

Based on the results from the post-pruning process, an example of the pruned model was shown below with its train, test and cross-validation accuracy (Table 3.14) and the tree visualization (Figure 3.19). The pruned parameters were shown on table 3.15 and the training and testing results were also shown on figure 3.18. In this pruned model, the cost-complexity alpha value was pre-defined as 0.000188. Both testing and cross-validation accuracies increased by 1% to 2% while there was a drop of 8% in training accuracy. The complexity of the tree also significantly decreased as the total number of leaves reduced from 9903 to 57 and the depth decreased from 35 to 9. As a result, not only the punning process improved the prediction accuracy, it also enhanced tree’s generalization capability to adapt to other unknown datasets.

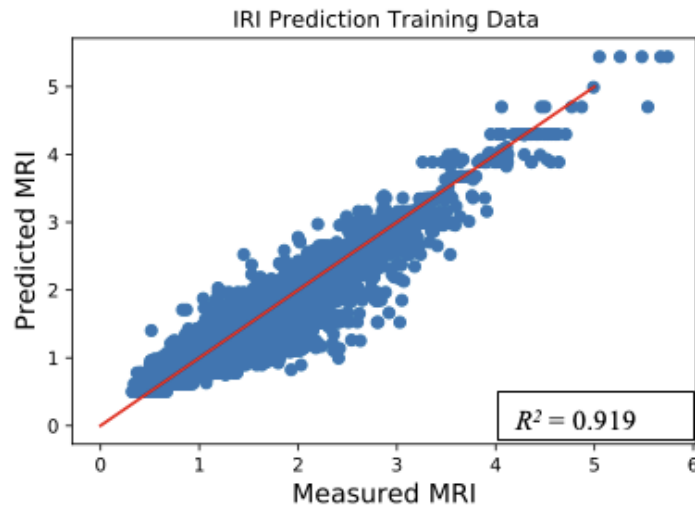
Table 3-14 Prediction result summary from the pruned decision tree model

| Set | Average R^2 | Average MSE |
|----------|---------------|---------------|
| Training | 0.919 | 0.0275 |
| Testing | 0.842 | 0.0511 |

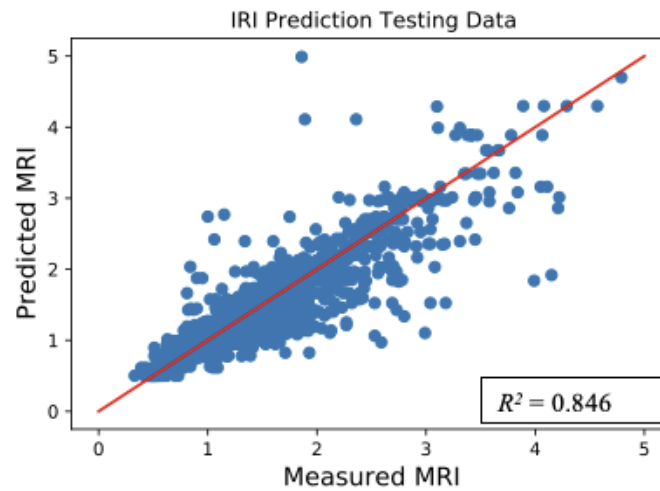
| | | |
|------------------|-------|--------|
| Cross-validation | 0.846 | 0.0523 |
|------------------|-------|--------|

Table 3-15 Pruned tree model parameters

| Parameter | Value |
|---|--------------|
| Tree depth | 9 |
| The number of leaves | 57 |
| Minimum number of samples on each leaf node | 1 |
| Minimum number of samples on each split | 2 |
| Total number of features | 18 |



(a)



(b)

Figure 3-18 Pruned decision tree training (a) and testing (b) results

In conclusion, the final decision tree model was able to achieve satisfactory test and cross-validation accuracies of 83 to 85% after the pruning process depending on the specific parameter alpha, and its generalization capability has been improved while maintaining the great prediction

process visualization ability. Figure 3.19 shows a part of the pruned decision tree that informs the decision-making process.

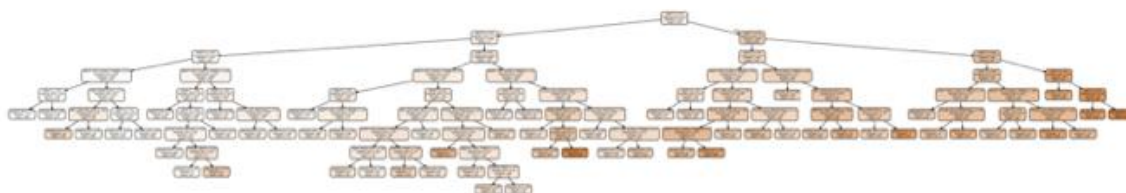


Figure 3-19 Visualization of the full pruned decision tree

Random Forest Hyperparameter Optimization

Comparing to a single decision tree model, a random forest model has greater model complexity as it consists of multiple randomized trees. Potential overfitting issues in RF can be possibly mitigated by the unique features in the model (Breiman, 2001):

- Each individual tree was trained by using bootstrapped sample
- The correlations between the trees are minimized and those randomized trees have strong independency

However, overfitting could still happen if the individual trees are allowed to grow without any limits. Single DT post-pruning results in optimized alpha values that are re-applied into the training model to generate new outputs. On the other hand, for RF model, trees are randomly generated in each training process meaning post-pruning is based on the previous trees and re-applying the tuned alpha values will not fit the tree in the next training process. Therefore, pre-pruning that regulates the hyperparameters at the beginning of the training process were used to mitigate the overfitting problem, i.e., limit the growth of the trees.

Grid search technique was deployed to find the optimum combination of hyperparameters that improve the prediction accuracies yet leverages overfitting. Each hyperparameter is pre-defined with a range of values and each value in the range will be applied into the model training process. The number of values for each hyperparameter and multiply it by the total number of hyperparameters is equal to the total number of combinations for the grid search input. There are few hyperparameters limiting the tree growth and the overall complexity of the forest which can mitigate the overfitting problems:

- Maximum tree depth
- Minimum number of samples on each leaf node
- Maximum number of features considered for splitting a node
- Number of trees in the forest

In this case, the trial hyperparameters are summarized on table 3.16 below. Although the accuracies started to converge based on figure 3.15 in section 3.4.3.2, the number of trees was limited to 5 in order to prioritize the visualization feasibility yet without a major sacrifice in prediction accuracy.

Table 3-16 Hyperparameters for the RF grid search

| Hyperparameters | Values |
|--|-------------------------------|
| Number of trees | 1, 2, 3, 4, 5 |
| Max tree depth | 5, 10, 15, 20, 25, 30, 35, 40 |
| Min number of samples on each leaf node | 10, 20, 30, 40, 50 |
| Max number of features considered for splitting a node | 6, 8, 10, 12, 14, 16, 18 |

The grid search results were interpreted on multi-dimensional plots. Figure 3.20 shows the example results when the number of trees is 3. Typically, high number of samples on each leaf, high tree depth and high number of features may result in overfitting. As a result, the tuning

result visualization on figure 3.20 helps balance the hyperparameter selection and the prediction accuracy. For example, the cross-validation accuracy reached 0.859 when there were no maximum limits of the number of features, the maximum tree depth was 10, and the minimum number of samples on each leaf was 36 (Figure 3.21 and Table 3.17).

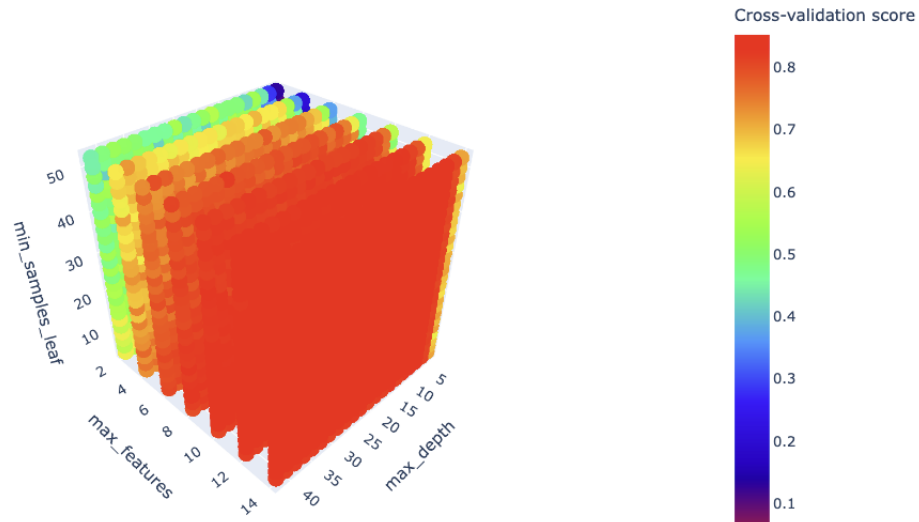


Figure 3-20 Visualization of hyperparameter tuning results when the num of trees is 3

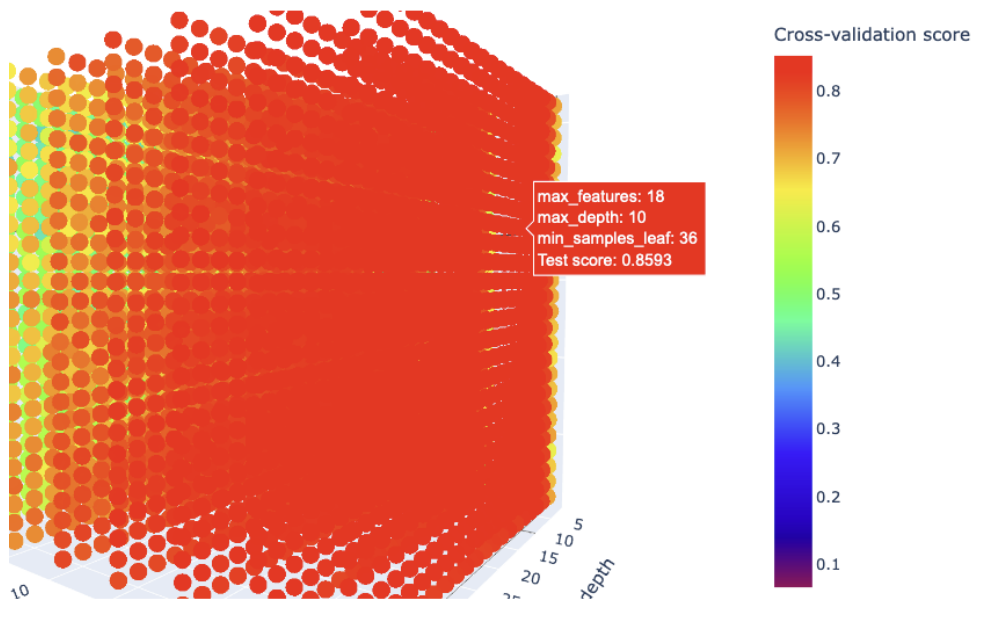


Figure 3-21 Hyperparameter selection based on accuracy scores

Table 3-17 RF grid search results

| Hyperparameters | Values |
|--|--|
| Number of trees | 3 |
| Max tree depth | 10 |
| Min number of samples on each leaf node | 36 |
| Max number of features considered for splitting a node | 18 (original total number of features) |
| Train accuracy | 0.858 |
| Test accuracy | 0.874 |
| 10-fold Cross-validation accuracy | 0.859 |

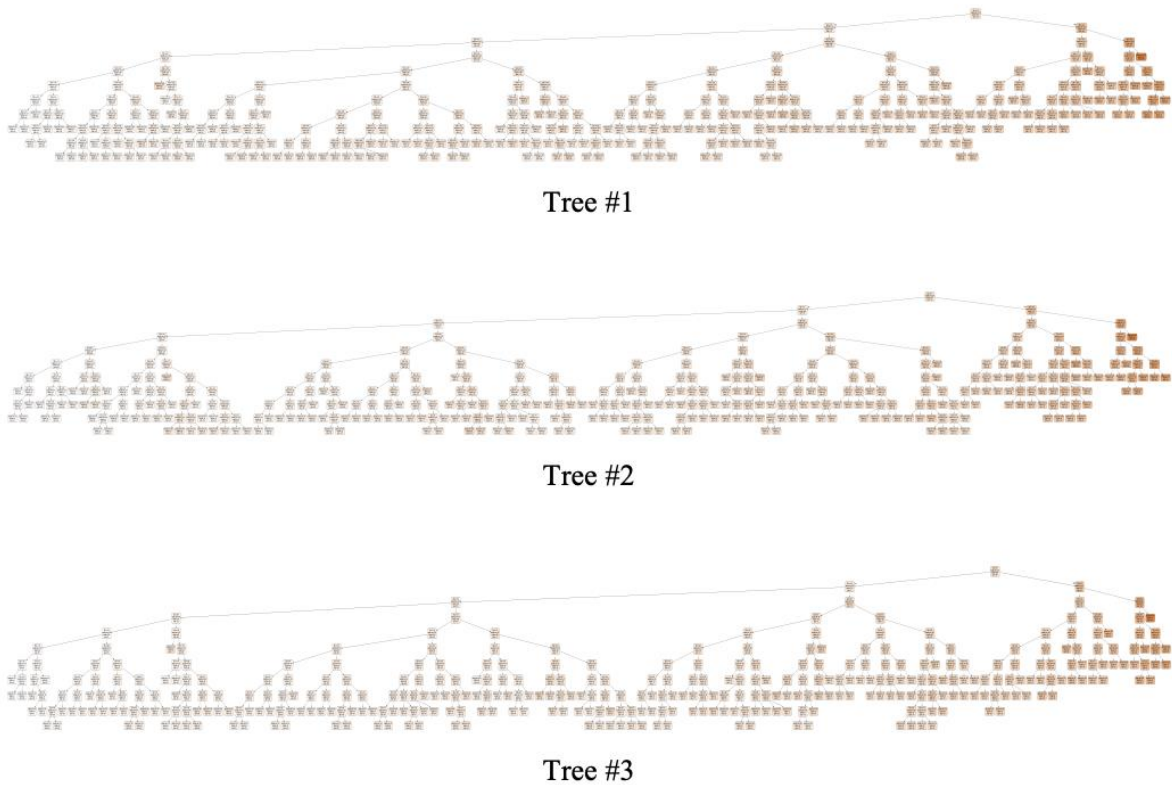


Figure 3-22 Optimized RF model with a total number of 3 trees

However, comparing to the pruned single tree model (CV accuracy = 0.846) , although the tuned RF model could provide slight better accuracies, the trade-off was the visualization feasibility. Figure 3.22 below shows the three trees in the pruned RF model. The trees are still too complex to be accurately interpreted.

3.4 Discussion and Conclusion

At the end of the data processing stage, 15 input variables and 1 output variables were selected from LTPP database. The final total data size was 17,147. Based the systematic literature review, there were only 2 studies that had more that 15,000 data points (Gone et al, 2019; Piryonesi and El-Dirby, 2021). However, both of those studies had used not just LTPP but additional databases from local municipalities and State/Provincial DOTs. The data sizes of the rest of studies were typically below 5,000. This indicates that data size in study is much above the average data size.

Although the final data size is quite considerable, data quality is still not optimum and needs improvements. For example, for a test section from year 1995 to 2005, there are years (e.g., 2001 and 2004) that AADTT or IRI records could be missing.

Conclusions were drawn from the single decision tree modelling and random forest modelling:

- Pruned single tree model was able to achieve a prediction (cross-validation) accuracy of 84.6%.
- After the pruning process, the complexity of the single tree model decreased, and visualization of the tree was enhanced allowing the decision-making process to be interpreted.
- Although the pruned RF model could provide slight better accuracies, the interpretation of trees is not as clear as the pruned DT model.

Both DT model and RF models resulted in a good IRI prediction accuracy yet maintained a clear visualization of the prediction process. Performance of these algorithms collected in the future (similar to other machine learning algorithms) can be improved if with having data with high quality and consistency. A set of data collection scheme regulating the data collection frequency and scheduling shall be established prior to the data collection. A few suggestions for data collection based on this work are:

- AADTT and AADT should be recorded annually and monthly in each year and in each month with no missing records in a period of time.
- Temperature and moisture data should be collected for multiple times in a day (preferably hourly) to reflect day-and-night temperature fluctuations and freeze-thaws.
- Initial IRI profiling should be made prior to the traffic opening date.
- Surface condition surveys including IRI profiling and distress surveys should be conducted regularly between consistent periods of time (i.e., every 8 months or 12 months). Once the first interval has been defined, it should not be changed for future

surveys (e.g., when the second IRI profiling is 12 months after the initial profiling, the following ones should all be held 12 months apart).

- Mechanistic pavement response should be dynamically monitored that the data are collected and stored upon each repetition of the vehicle loading in all hours of a day.
- After the initial construction, each later M&R activity should be explicitly documented for its type, construction duration, material used, and thickness for milling and/or overlay.
- After each M&R, surface condition surveys should be conducted again prior to opening to traffic. If it is a major M&R such as full-depth milling and overlay, the M&R event should be regarded as an initial construction that starts a new set of data collection time intervals (e.g., if last IRI profiling was conducted in January and the major M&R happened in March, the next IRI profiling should be conducted in March in next year when the survey time interval is every 12 months).

Further discussions between data analysis experts and experience pavement engineers shall be held to define the specific data collection regulations and database management. Detailed data collection plans should be made prior to the data collect.

Chapter 4

Design and Finite Element Modelling of Pilot Section

4.1 Overview

In the instrumented pavement section, to understand the pavement response due to vehicle loading, asphalt strain gauges and pressure cells are embedded in the pavement structure as physical tools to capture the dynamic stresses and strains. In addition to physical instrumentation, robust quantitative modeling such as finite element analysis (FEA) of the test section is also capable of demonstrating the pavement response due to traffic loading. FEA modeling can serve as a validation tool to compare the actual data stress and strain collected from physical sensors. When full-scale instrumentation of the pavement section is conducted, pavement response data collected from strain gauges and pressure cells are collected. However, the impact of those embedded artefact on pavement structure and pavement response under traffic loading are not clear. Those sensors could potentially affect the strain and stress distributions as their material properties are different from pavement material. Prior to the FEA modeling process, a review of the instrumented test section was also conducted in order to provide the necessary information of roadway geometry, pavement structure, material used and subgrade conditions. At the end, the goal of this modelling process is to discover such effects and provide possible suggestions to the layout design of strain gauges and pressure cells.

4.2 Geometry and Pavement Structure Design Review

The proposed location of pilot section is in Courtland Ave West, Kitchener, ON which belongs the Region of Waterloo. The specific pavement segment is situated in between Hayward Ave (STA. 10+351.98) and Highway 7 & 8 on-ramp (STA. 10+013.00). The total pavement length is 338.98m. Due to the unsatisfactory existing pavement condition with unacceptable levels of distresses including pothole, alligator cracking, transverse cracking, the whole roadway structure was re-designed and would be re-constructed. The reconstruction plan includes both surface pavement structure and the drainage systems underneath the pavement layers. The roadway function class is urban arterial, and the speed limit is 50 km/h (City of Kitchener, 2019). The

estimated peak AADT count in year 2031 in this segment is below 2,000 vehicles and at an average of 1,500 to 1,700 with an annual growth rate of 1.5%. The number of designed lanes in each traffic direction is 2. The subgrade condition has been classified as silty clay to clayey silt with an approximate resilient modulus of 30 MPa (Fraser, 2019). The thickness of the subgrade was considered as infinite. Conforming to OPSS 3090 standard, the frost penetration depth of the pavement segment is 1.2 m. Given the penetration depth ratio is 0.6, the minimum designed pavement structural thickness is 720mm. Table 4.1 below shows the design pavement structural and material of the reconstruction project. In this case, the total designed pavement thickness is 745mm which is acceptable for the frost penetration criterion.

Table 4-1 Pavement structural and material design of the test section

| Pavement Layer | Material | Thickness (mm) |
|-----------------------|---------------------------|-----------------------|
| Surface AC | SP 12.5 FC2 | 50 |
| Surface AC | SP 19 | 145 |
| Base | Granular A | 150 |
| Subbase | Granular B | 400 |
| Subgrade | Silty clay to clayey silt | Infinite |

4.3 Instrumentation Layout Design

The initial instrumentation layout design was illustrated on figure 4.1 and 4.2. The set of instrumentation sensors include asphalt strain gauge, soil pressure cell, temperature thermocouple and moisture probes. Adequate spacing between each sensor was assigned to avoid the measurement interference issues. Horizontal strain gauges were placed in both longitudinal direction and transverse direction to monitoring the strain at each direction. Since axle width can vary depending on the vehicle type and wheel paths do not always stay on a constant track, the spacings between the strain gauges and pressure cells along the transverse direction are 2.5m and 1.8m respectively. These varying spacings help capture the peak stress and stress better. In terms of the vertical layout design, since pavement temperature is related to depth, temperature

thermocouples are installed in both asphalt layers and base layers. In addition, soil moisture level depends on the material drainage property, therefore, two soil moisture probes are placed in Granular B layer and Subgrade layer. Soil pressure cells are placed 150mm below the top of the Granular B layer to measure the vertical stress due to vehicle loading.

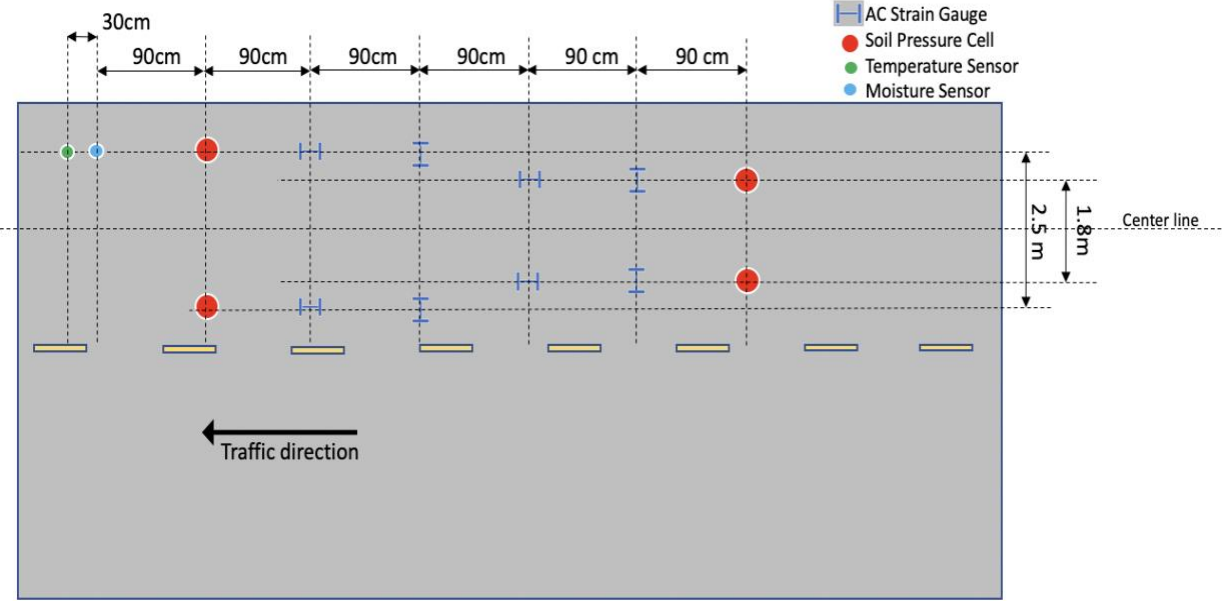


Figure 4-1 Pilot section instrumentation layout design (top view)

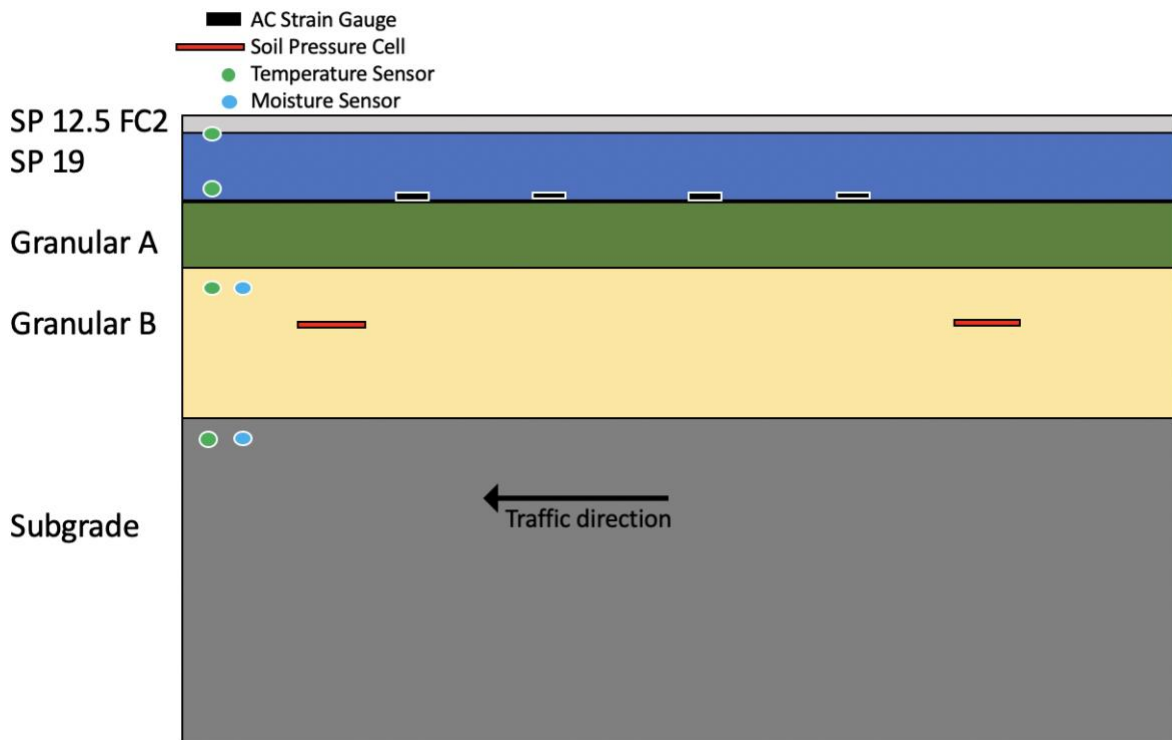


Figure 4-2 Pilot section instrumentation layout design (cross-section view)

4.4 Finite Element Modelling

4.4.1 Model Geometry

To determine the part geometry for ABAQUS modelling, the following part details need to be identified:

- Vehicle axle and wheel type, spacing and tire pressure
- Tire contact area
- Total pavement structure geometry
- The geometries of asphalt strain gauge and soil pressure cell

Tire Pressure and Axle Configuration

The representative vehicle type has been selected as FHWA class 9 truck since it typically accounts for the highest truck volume percentage. The combination of tandem axle and dual wheel was selected. Based on the Ontario AASHTOWare ME Default Parameter Manual (MTO, 2019), the default tire pressure, the default average dual tire spacing and the default axle spacing have been selected as 827.4KPa (approximately 0.83MPa), 305mm and 1.45m, respectively (Table 4.2 and 4.3).

Table 4-2 AASHTOWare Pavement ME Design Defaults Axle Configuration

| Axle Configuration | Default Values |
|---------------------------|-----------------------|
| Average axle width (m) | 2.59 |
| Dual tire spacing (mm) | 305 |
| Tire pressure (kPa) | 827.4 |

Table 4-3 Ontario Typical Defaults for Axle Spacing

| Axle type | Average axle spacing within axle group, m |
|------------------|--|
| Tandem | 1.45 |
| Tridem | 1.68 |
| Quad | 1.32 |

Tire Contact Area

Tire contact area can vary depending on the vehicle loading and tire pressure and there are no default values provided by the Ontario AASHTOWare ME Default Parameter Manual.

Therefore, in this section, tire contact area was estimated based on the theories developed by Huang (2004). Technically, the actual shape of the tire contact area on top of the AC layer is approximately elliptical or circular (Huang, 2004). However, in order to simplify the calculation of the contact area for pavement loading analysis, the shape can be converted from to elliptical or circular to rectangular while the total areas are equivalent (Huang, 2004). The length of the actual contact area is L and the width is 0.6L (Huang, 2004). After the shape conversion, the

length of the rectangle can be represented as $0.8712L$ and width remains the same, which is $0.6L$ (Huang, 2004). As a result, the length to width ratio of the rectangle can be derived as 1.452. Figure 4.3 illustrates actual shape and converted rectangular shape and equation 4.1 shows the area calculation for both shapes.

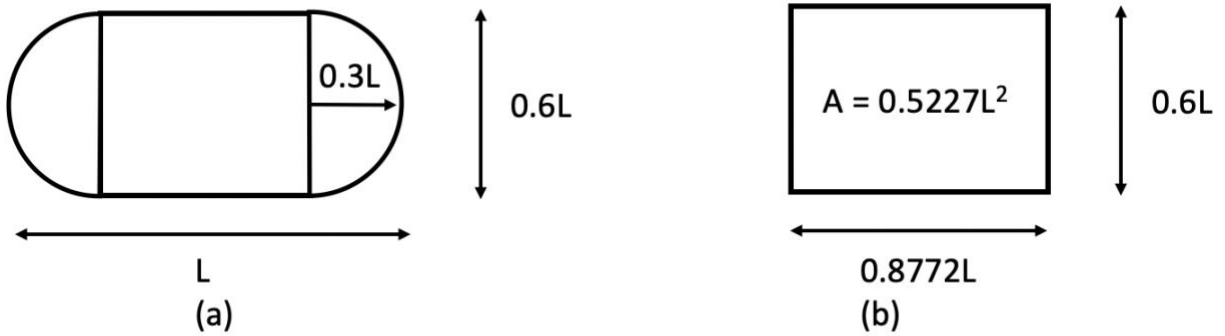


Figure 4-3 Actual tire contact area (a) and rectangular tire contact area (b)

$$Area = \pi 0.3L^2 + (0.4L)(0.6L) = 0.5227L^2 \quad (4.1)$$

Table 4.4 below shows the measure tire pressure, vehicle loading and tire contact area from an experiment conducted by Nega (2017). Based on such combination of the values, given the default tire pressure is 0.83MPa and the length to width ratio of 1.452, the length and width of the rectangular area were estimated as 290mm and 200mm respectively (Figure 4.4). Specific partitioned pavement structure geometry based on the tire contact area is illustrated on figure 4.5 below.

Table 4-4 Measured tire pressure, wheel loading, contact area, and mean contact pressure (Nega, 2017)

| Tire Pressure (kPa) | Wheel Loading (kN) | | | Contact Area (m ²) | | Mean Contact Pressure (kPa) | | |
|---------------------|--------------------|--------|------|--------------------------------|-------|-----------------------------|--------|------|
| | Front | Middle | Rear | Front | Rear | Front | Middle | Rear |
| 350 | 28.4 | 21.6 | 22.6 | 0.059 | 0.045 | 484 | 476 | 498 |
| 490 | 28.4 | 21.6 | 22.6 | 0.050 | 0.042 | 571 | 516 | 539 |
| 630 | 28.4 | 21.6 | 22.6 | 0.044 | 0.039 | 648 | 552 | 578 |
| 700 | 28.4 | 21.6 | 22.6 | 0.040 | 0.038 | 715 | 573 | 599 |
| 350 | 31.6 | 34.4 | 35.2 | 0.067 | 0.067 | 474 | 510 | 522 |
| 490 | 31.6 | 34.4 | 35.2 | 0.055 | 0.062 | 578 | 555 | 568 |
| 630 | 31.6 | 34.4 | 35.2 | 0.048 | 0.056 | 661 | 610 | 624 |
| 700 | 31.6 | 34.4 | 35.2 | 0.044 | 0.051 | 720 | 677 | 693 |
| 350 | 31.6 | 44.6 | 46.1 | 0.067 | 0.085 | 475 | 524 | 518 |
| 490 | 31.6 | 44.6 | 46.1 | 0.055 | 0.077 | 580 | 578 | 572 |
| 630 | 31.6 | 44.6 | 46.1 | 0.048 | 0.070 | 663 | 636 | 629 |
| 700 | 31.6 | 44.6 | 46.1 | 0.044 | 0.063 | 722 | 708 | 699 |

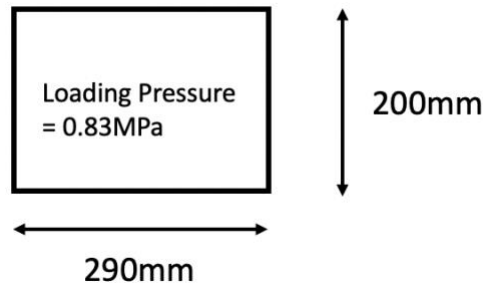


Figure 4-4 Tire loading pressure and dimension used for ABAQUS input

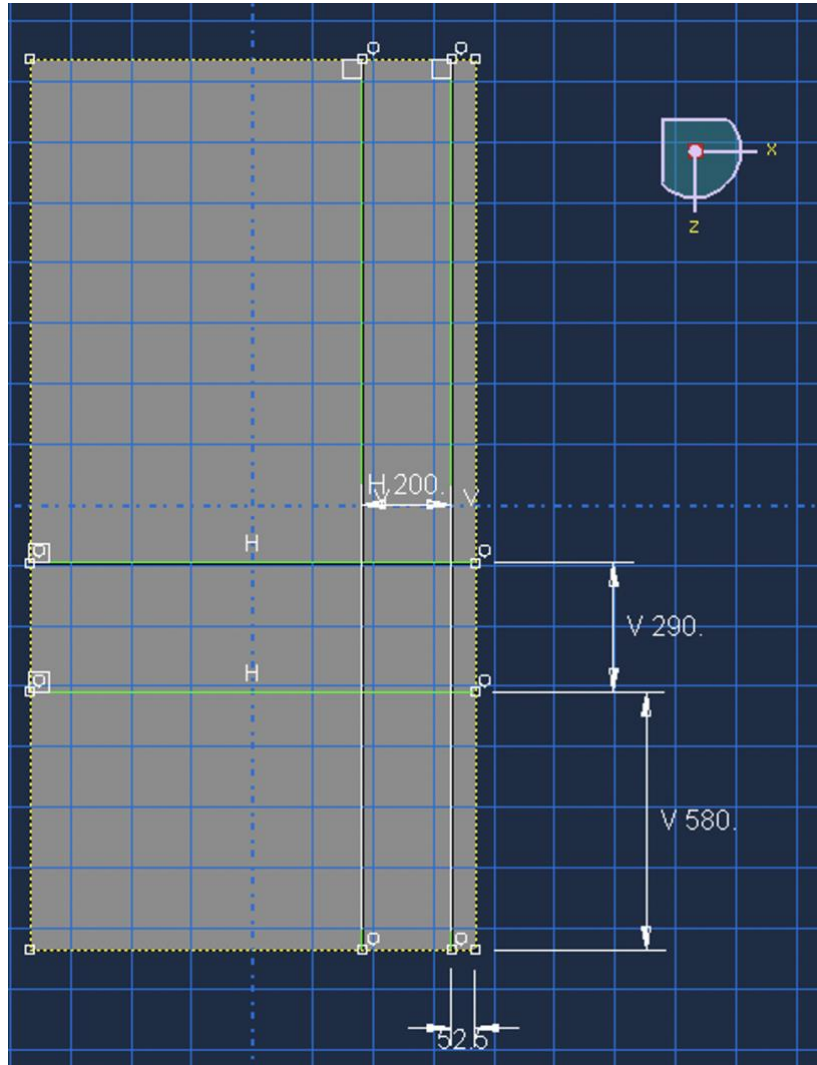


Figure 4-5 Pavement layer surface partitioning geometry with respect to tire loading. (Unit: mm)

Asphalt Strain Gauge and Pressure Geometries

In order to include asphalt strain gauge and pressure cell in the FEM pavement structure model, their geometry shall be determined first. The asphalt strain gauge and the soil pressure cell used in this case are: PAST-II AC by Dynatest (Figure 4.6) and RST Total Earth Pressure Load Cells (TEPLC) 9” (Figure 4.8), respectively. The dimensions of the instrumentation sensors are shown on figure 4.7 and 4.9 below.

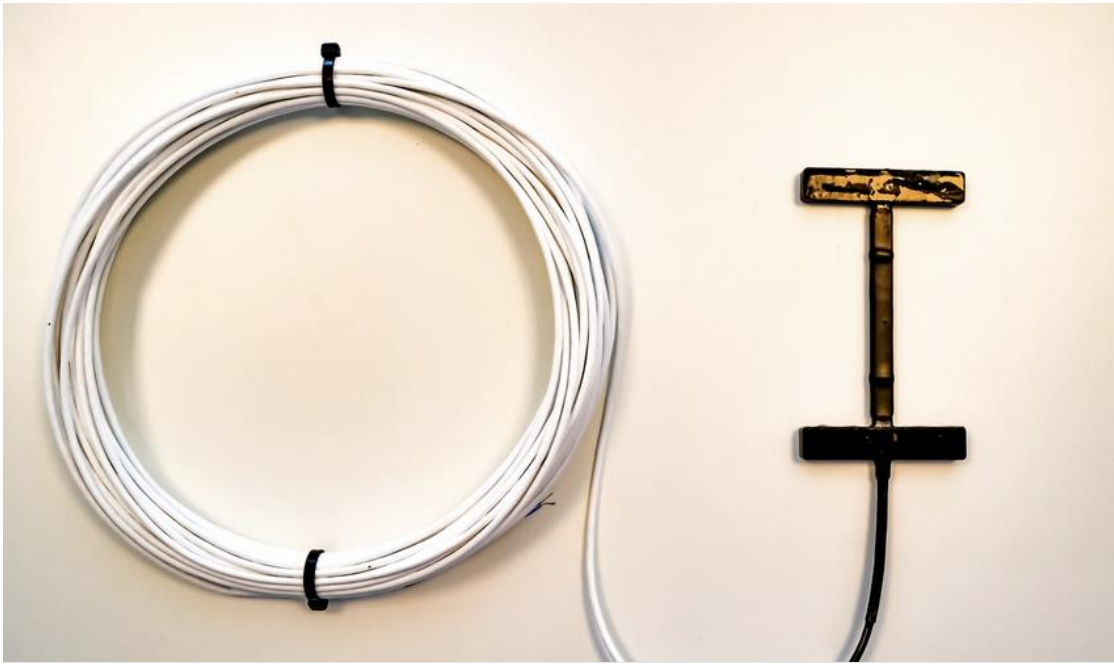


Figure 4-6 Dynatest PAST-II AC strain gauge (Dynatest, 2022)

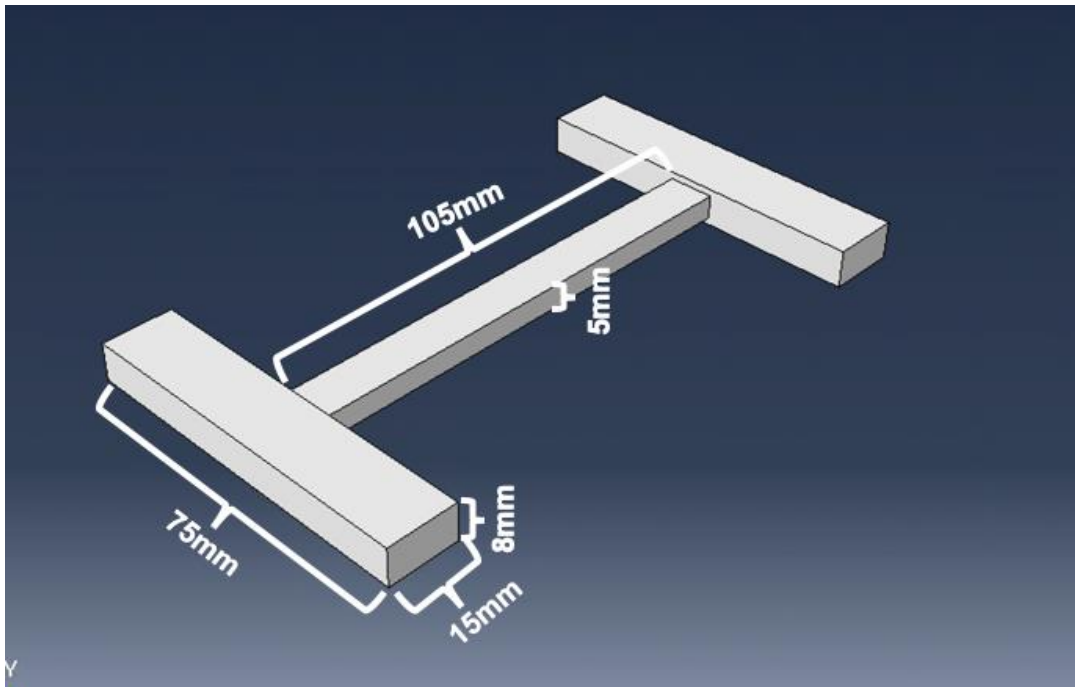


Figure 4-7 The Dimension of Dynatest PAST-II AC strain gauge used in ABAQUS

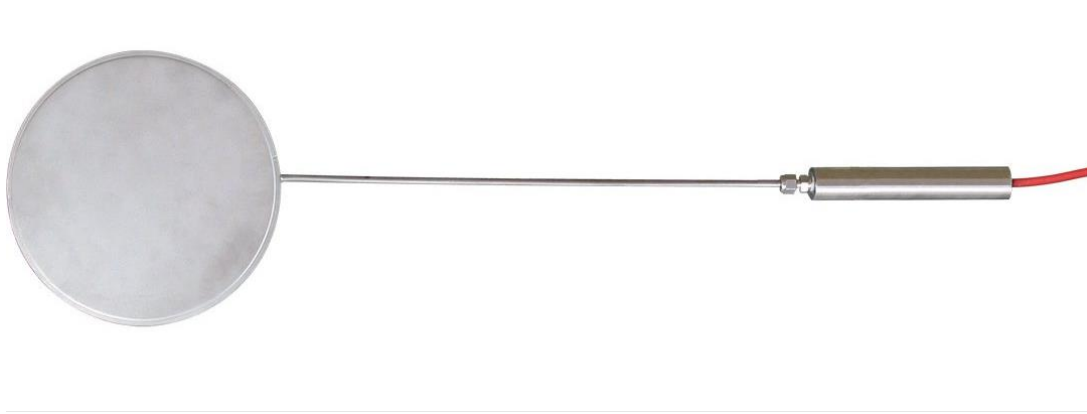


Figure 4-8 RST Total Earth Pressure Load Cells 9"

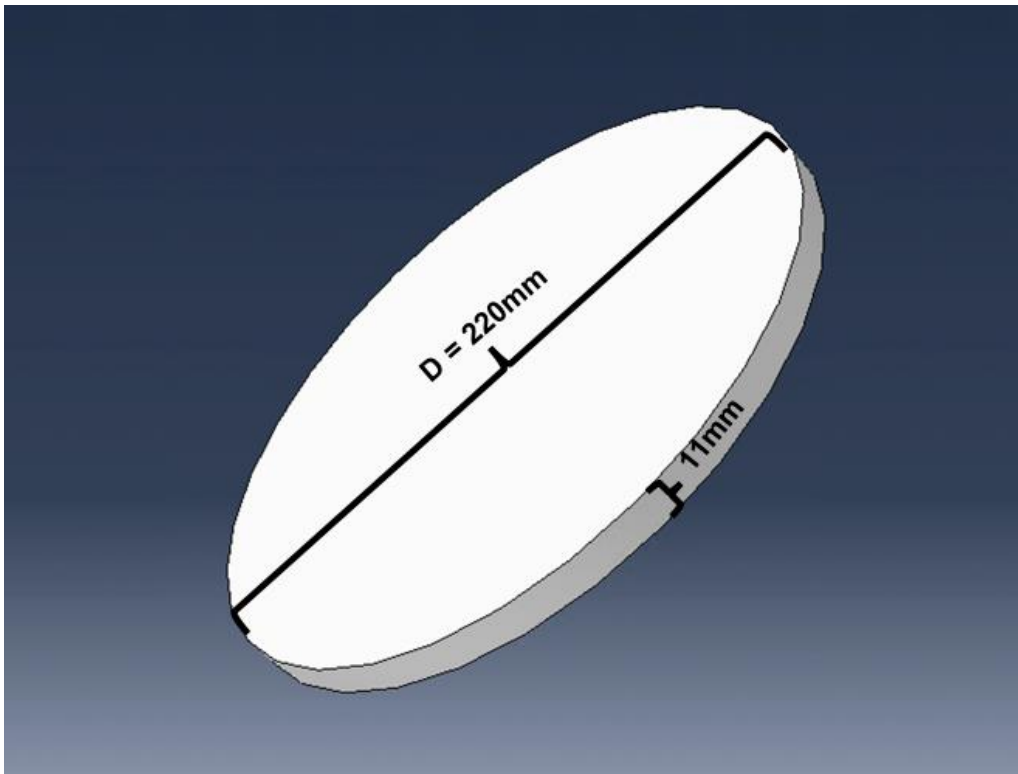


Figure 4-9 The dimension RST Total Earth Pressure Load Cells 9" used in ABAQUS

Total pavement structure geometry

The number of pavement layers and the thickness of each has been identified from the section review on table 4.1. As for the subgrade, a representative thickness of 0.8m was used in the model. In order to minimize the computational cost, $\frac{1}{4}$ axisymmetry was used. In this model, the length is 2.0m, the width is 1.0m and the total representative thickness is 1.545m (Figure 4.10).

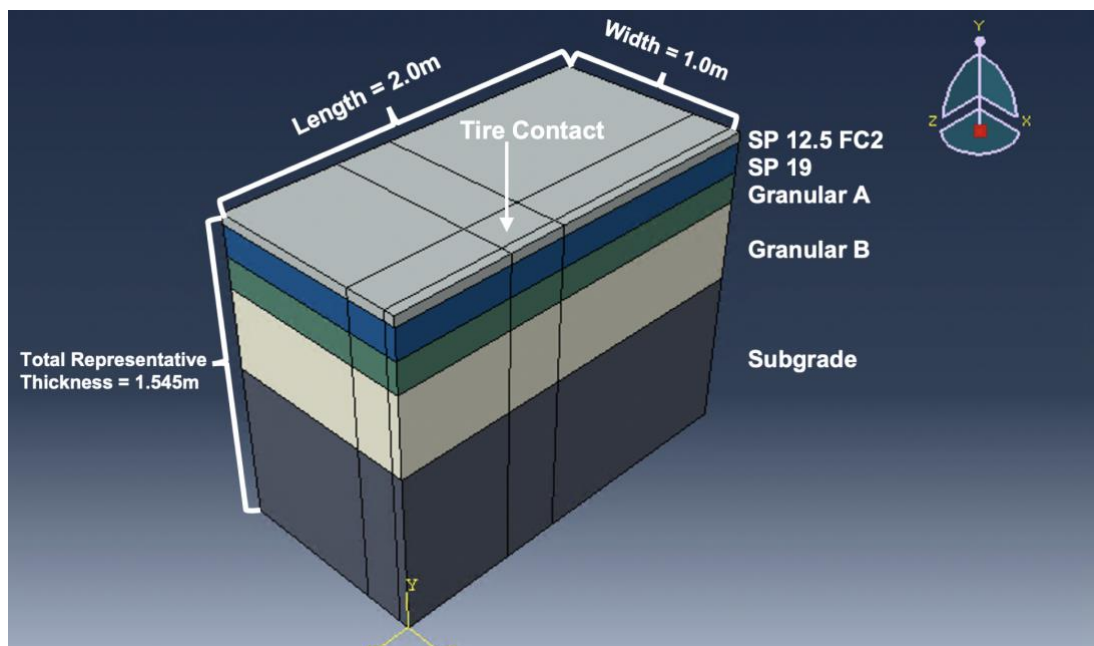


Figure 4-10 Pavement structure geometry without instrumentation sensors

For the horizontal sensor alignment, the sensors were chosen to be vertically aligned with the peak stress and strain areas. The initial finite element model without instrumentation suggested that the peak stress and strain occurred not directed under the tire contact area but in between the dual tires. Details about the uninstrumented model were discussed in section 4.4.6. As a result, in the instrumented model, both pressure cell and strain gauge were vertically centered in between the dual tire spacing area (Figure 4.11 and 4.12). In terms of the vertical instrumentation layout, asphalt strain gauge was buried at the bottom of the SP 19 layer and soil pressure cell is located 150mm below the Granular B layer (Figure 4.13).

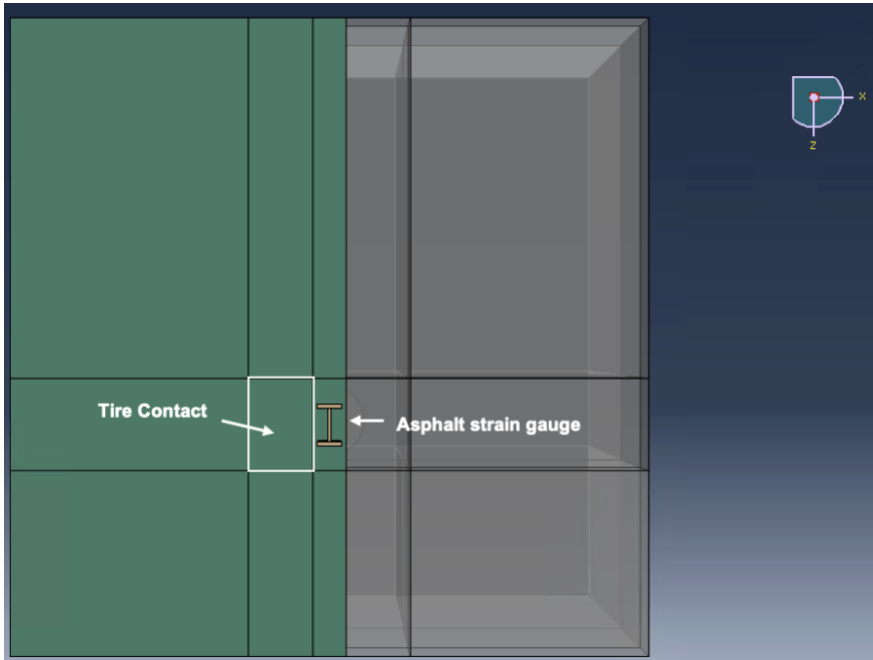


Figure 4-11 Horizontal layout design of asphalt strain gauge

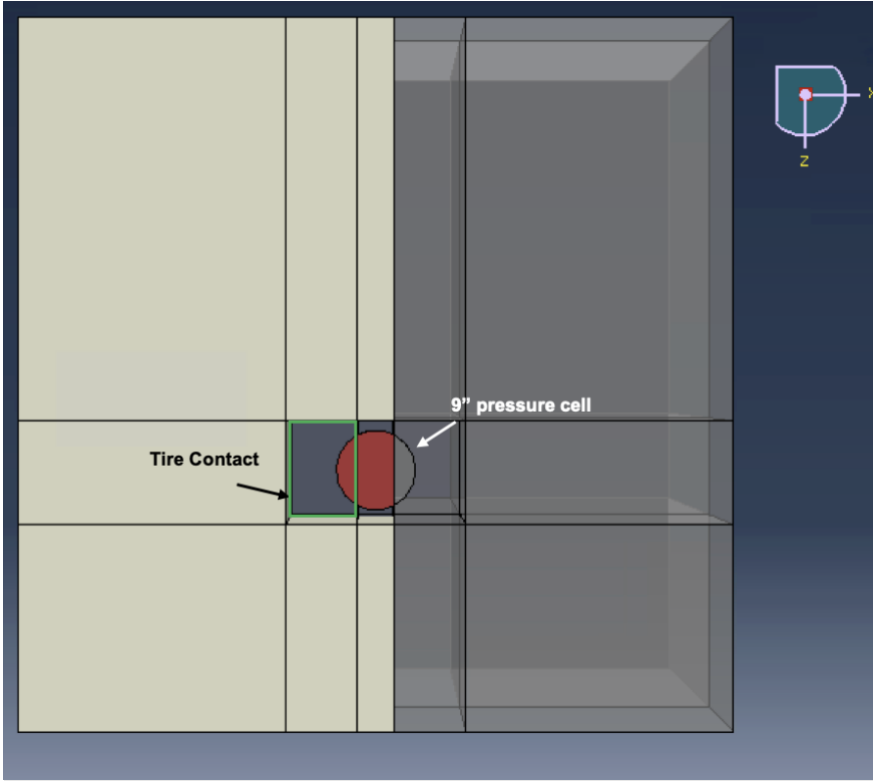


Figure 4-12 Horizontal layout design of pressure cell

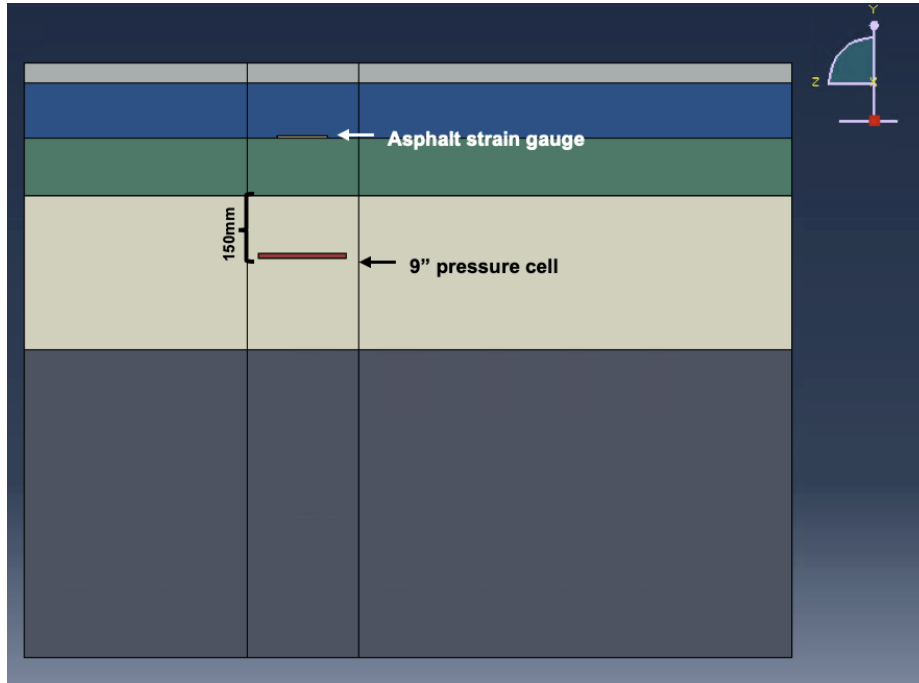


Figure 4-13 Vertical layout design of strain gauge and pressure cell

4.4.2 Material Property

After the geometry of the pavements has been defined, the material properties are the next to be characterized in ABAQUS analysis. In the proposed FE model, the pavement section consists of 5 layers and 2 types of sensors: asphalt strain gauge and soil pressure cell. Based on the construction plan of the test section, the use of material for each pavement layer has been specified. Thus, a total of 7 material sections with 7 types of materials were included in this model (Table 4.5). Material properties for each layer were selected as default values from the Ontario's Default Parameters for AASHTOWare Pavement ME Design Manual (the Pavement ME manual) (MTO, 2019).

Table 4-5 Material property summary

| Part | Material | Young's Modulus (MPa) | Mass Density (kg/m³) | Poisson's Ratio |
|--|--|------------------------------|--|------------------------|
| Asphalt Concrete | SP 12.5 FC2 | 5095.7 | 2530 | 0.35 |
| Asphalt Concrete | SP 19 | 5621.2 | 2460 | 0.35 |
| Granular Base | Granular A | 250 | 2048.3 | 0.35 |
| Granular Subbase | Granular B-II | 200 | 2013.7 | 0.35 |
| Subgrade | Classification ML/MI, Category 6 | 30 | 1940 | 0.325 |
| Dynatest PAST-II AC (asphalt strain gauge) | Mostly Epoxy | 2200 MPa | 1100 | 0.3 |
| RST 9" Total Earth Pressure Load Cell | Stainless Steel | 193 GPa | 8000 | 0.27 |

Asphalt Material Property

First surface layer is a surface AC course that its material is specified as SP 12.5 FC 2, which has mass density of 2530 kg/m³ since the project location is situated in west region of Ontario (Table 4.6). The binder course consists of SP 19 material with a mass density of 2460 kg/m³ (Table 4.6). Asphalt is a type of viscoelastic material that its resilient modulus can vary under different loading conditions frequency and temperature settings. Typically, the dynamic modulus of the

asphalt material is a list of values that can be determined as a function of both loading frequency and temperature. In this study, the temperature was selected at 21 °C to represent the non-freeze pavement conditions. On the other hand, the dynamic loading frequency is related to the vehicle travelling speed (Huang, 2004). Huang (2004) has suggested that a vehicle speed of 64km/h corresponds to haversine loading wave pulse time = 0.028s. Then, the loading time can be further derived into the frequency for asphalt dynamic modulus tests on equation 4.2 (Huang, 2004). In this case, give an approximate loading wave pulse time = 0.03s (when vehicle speed = 50km/h < 64km/h), the frequency can be calculated as $f = 5\text{Hz}$. In addition, Shell (1978) also suggested that a vehicle speed of 50km/h to 64km/h corresponds to a frequency of 8Hz. As a result, the frequency for the asphalt mix modulus has been identified as 5Hz from the Ontario AASHTOWare ME Default Parameter Manual (Appendix IV). Then, given both of the loading frequency and the temperature, the target asphalt mix modulus values were identified on table 4.7.

$$t = \frac{1}{2\pi f} \quad (4.2)$$

t = loading time

f = frequency

Table 4-6 Ontario Superpave properties (MTO, 2019)

| Asphalt Layers | | SP 12.5 | SP 19.0 | SP 25.0 | SMA 12.5 |
|--|-----------------------------|--|----------|----------|------------|
| Thickness (mm) | | Project specific | | | |
| Mixture Volumetric | | | | | |
| Unit Weight (kg/m ³) | | See Note 1 | 2460 | 2469 | See Note 1 |
| Effective Binder Content - by Volume (%) | | 11.8 | 11.2 | 10.4 | 14.6 |
| Air Voids (%) ^{Note 2} | | 7.0 | | | |
| Poisson's Ratio ^{Note 3} | | 0.35 for existing HMA (select calculated for new HMA) | | | |
| Mechanical Properties | | | | | |
| Dynamic Modulus | | "Input level: 3" selected | | | |
| Aggregate Gradation | % Passing the 19 mm Sieve | 100 % | 96.9 % | 89.1 % | 100.0 % |
| | % Passing the 9.5 mm Sieve | 83.2 % | 72.5 % | 63.3 % | 73.1 % |
| | % Passing the 4.75 mm Sieve | 54 % | 52.8 % | 49.3 % | 29.7 % |
| | % Passing the 75 µm Sieve | 4 % | 3.9 % | 3.8 % | 9.3 % |
| G Star Predictive Model | | "Use viscosity based model (nationally calibrated)" selected | | | |
| Reference Temperature | | 21.1 °C | | | |
| Asphalt Binder ^{Note 4} | | PG 64-28 | PG 58-28 | PG 58-28 | PG 70-28 |
| Indirect Tensile Strength – 10 deg.C (MPa) | | Calculated | | | |
| Creep Compliance (1/GPa) | | "Input level: 3" selected | | | |
| Thermal | | | | | |
| Thermal Conductivity (watt/meter-Kelvin) | | 1.16 | | | |
| Heat Capacity (joule/kg-Kelvin) | | 963 | | | |
| Thermal Contraction | | Calculated | | | |

Note 1: For SP 12.5, the unit weight is 2,460 kg/m³. For SP 12.5FC1, FC2 and SMA 12.5, unit weight varies from different regions: Central and North regions – 2,520 kg/m³; East region – 2,390 kg/m³; West region – 2,530 kg/m³

Table 4-7 Modulus of asphalt mixes used in this study

| Asphalt Mix | Mix Code | Modulus (MPa) | Temperature (°C) | Frequency (Hz) |
|-------------|----------|---------------|------------------|----------------|
| SP 12.5 FC2 | 3 | 5095.7 | 21 | 5 |
| SP 19 | 16 | 5621.2 | 21 | 5 |

Base, Subbase and Subgrade Material Properties

Granular A is used as the primary base material and Granular B Type II is used to construct the subbase (Appendix). According to a previous geotechnical site investigation report at 321 Courtland Ave nearby the pilot section, the subgrade soils often consist of a large fraction of silty and clayey material providing moderate to low resilient modulus (Fraser, 2019). Hence, based on table 4.8 (MTO, 2019), subgrade soil is categorized as type 6 ML and is used for the material property input with a resilient modulus of 30 MPa. The materials for all layers were considered at linear elastic.

Table 4-8 Ontario subgrade moduli and soil classification

| Brief Description | Category No. | MTO Classification (MTO, 1980) | Drainage Characteristics | Susceptibility at Frost Action | M _R (MPa) Good | M _R (MPa) Fair | M _R (MPa) Poor |
|---|--------------|--------------------------------|-------------------------------|--------------------------------|---------------------------|---------------------------|---------------------------|
| Rock, rock fill, shattered rock, boulders/cobbles | 1 | Boulders/cobbles | Excellent | None | 90 | 80 | 70 |
| Well graded gravels and sands suitable as granular borrow | 2 | GW, SW | Excellent | Negligible | 80 | 70 | 50 |
| Poorly graded gravels and sands | 3 | GP, SP | Excellent to fair | Negligible to slight | 70 | 50 | 35 |
| Silty gravels and sands | 4 | GM, SM | Fair to semi-impervious | Slight to moderate | 50 | 35 | 30 |
| Clayey gravels and sands | 5 | GC, SC | Practically impervious | Negligible to slight | 40 | 30 | 25 |
| Silts and sandy silts | 6 | ML, MI | Typically poor | Severe | 30 | 25 | 18 |
| Low plasticity clays and compressible silts | 7 | CL, MH | Practically impervious | Slight to severe | 35 | 20 | 15 |
| Medium to high plasticity clays | 8 | CI; CH | Semi-impervious to impervious | Negligible to severe | 30 | 20 | 15 |

Instrumentation Sensor Material Properties

In addition to the geotechnical properties of the pavement layers, the material properties of asphalt strain gauge and soil pressure cell were also identified. In this study, Dynatest PAST-II AC strain gauge is embedded on the bottom of the AC layers to monitor the strain under traffic loading. The strain gauge is primarily made of epoxy material providing a modulus of about 2200 MPa (Table 4.9)/ It was considered a uniform piece of solid epoxy for ABAQUS modelling. RST Total Earth Pressure Load Cells (TEPLC) 9” was used to monitor the subbase and subgrade pressures. TEPLC is primarily made of stainless steel. Therefore, a uniform and solid 304 stainless steel plate with a modulus of 193GPa (Harvey, 1982) was selected to represent TEPLC in ABAQUS.

Table 4-9 Dynatest PAST-II AC strain gauge material property

| Specifications | |
|--------------------|---|
| Type | PAST II (For AC or PCC) |
| Range | Up to 1500 μ strain |
| Configuration | Single strain gage (1/4 bridge) |
| Cell material | Epoxy–Fiberglass |
| Coating | Epoxy–Silicone–PFT–Titanium |
| Resistance | 120 Ω \pm 1.0 %; GF=2.0 |
| Voltage | Up to 12V (full bridge) |
| Temperature | -30° to 150°C -22° to 300°F |
| Σ E-modulus | \approx 2200 MPa \approx 320 ksi |
| Cross section | \approx 0.5 sq. cm \approx 0.078 sq. in |
| Cell Force | 0.110 N/ μ strain \approx 0.024 lbf/ μ strain |
| Fatigue life | Theoretically up to 10 ⁸ cycles |
| Service life | Typically > 36 months |

4.4.3 Boundary Conditions, Loading, Interaction, and Final Models

In this study, to investigate the potential relationships between asphalt strain gauge, pressure cell and pavement structure, four static implicit finite element models were constructed in ABAQUS to simulate different scenarios (Figure 4.14):

- Model 1: No instrumentation sensors
- Model 2: Includes pressure cell only, no strain gauge
- Model 3: Includes strain gauge only, no pressure cell
- Model 4: Includes both pressure cell and strain gauge

All four models were constructed based on 1/4 axisymmetry along x-axis and y-axis to minimize the computational cost. The axisymmetric surfaces were assigned with symmetry boundary condition where $U1=UR2=UR3=0$ for the x-axis symmetric surface and $U3=UR1=UR2=0$ for the z-axis symmetric surface (Figure 4.15). The bottom was assigned with displacement boundary condition where the $U1=U2=U3=0$. The tire loading was defined as uniform pressure with a magnitude of 0.83MPa. To ensure the slipping between each layer is minimum, tangential

behavior and rough contact condition were assigned for each interface allowing the infinite friction.

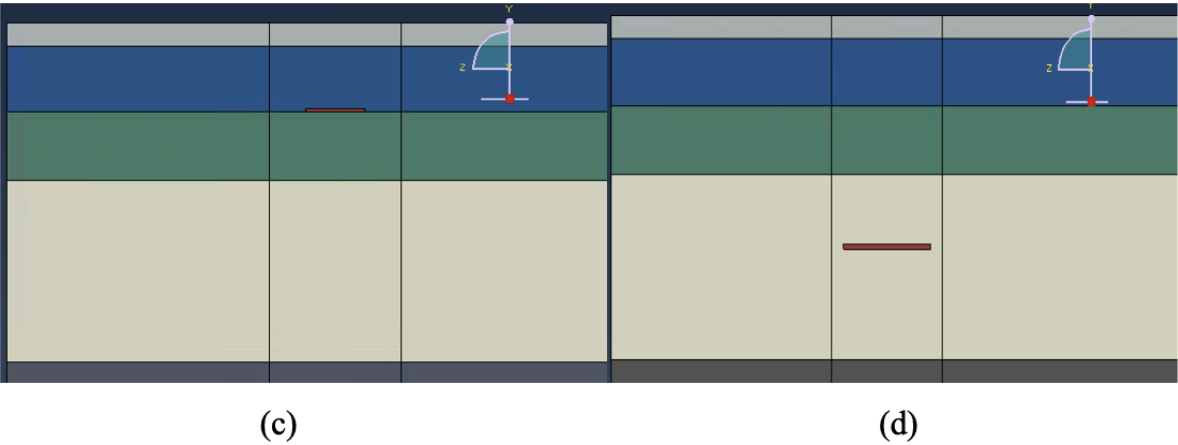
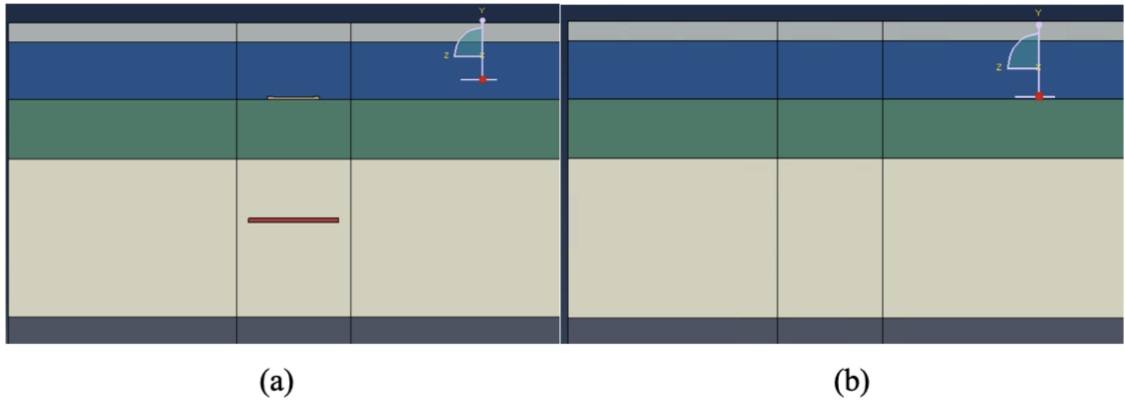


Figure 4-14 Instrumented and non-instrumented models: (a) Both strain gauge and pressure cell, (b) no sensors, (c) only strain gauge, and (d) only pressure cell

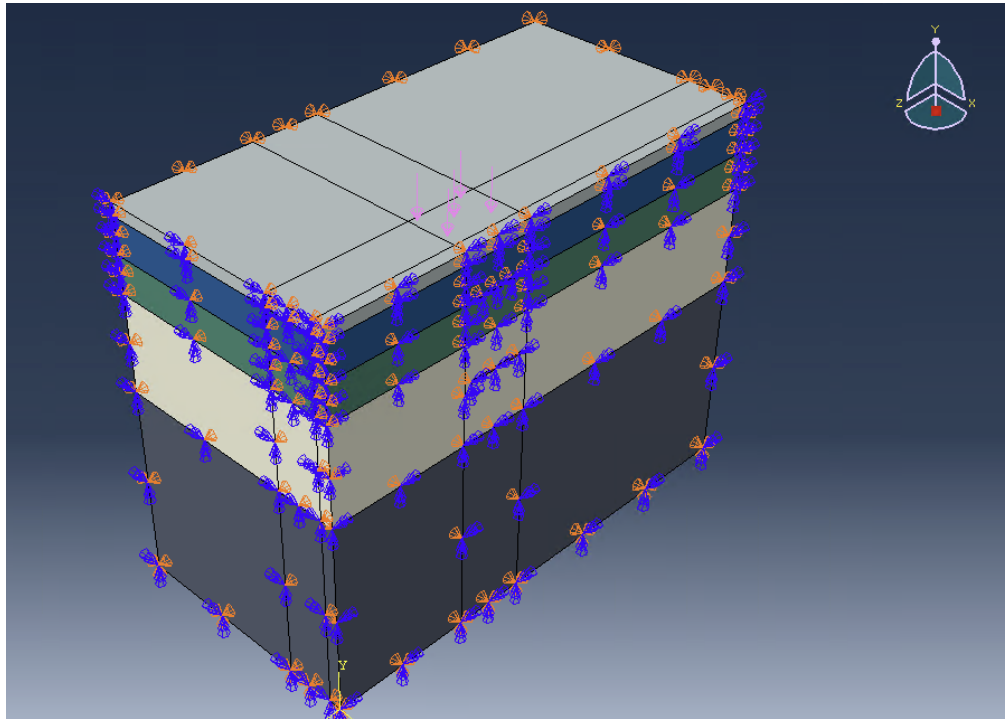


Figure 4-15 Boundary conditions and loading of the model

4.4.5 Meshing Techniques and Mesh Independence

Considering the unique shape of the instrumentation sensors, the mesh type used for all models were consistent which was 10-node tetrahedral (C3D10). However, meshing size can be difficult to control near the instrumentation sensor area. Typically, stress and strain would change along with the change of mesh size if it were mesh dependent. Therefore, in order to generate consistent stress and strain outputs that are not significantly affected by mesh size, independent meshing was used for all parts of the models so that the final results do not depend on the level of mesh convergence. Also, all four models have been defined with same global mesh size and same local mesh size in their regions that do not include the sensors. The regions that include the sensors may not have the consistent mesh size and pattern as it was automatically generated by

computer. Also, the mesh size was further refined for the tire loading area and installed sensor area (Figure 4.16).

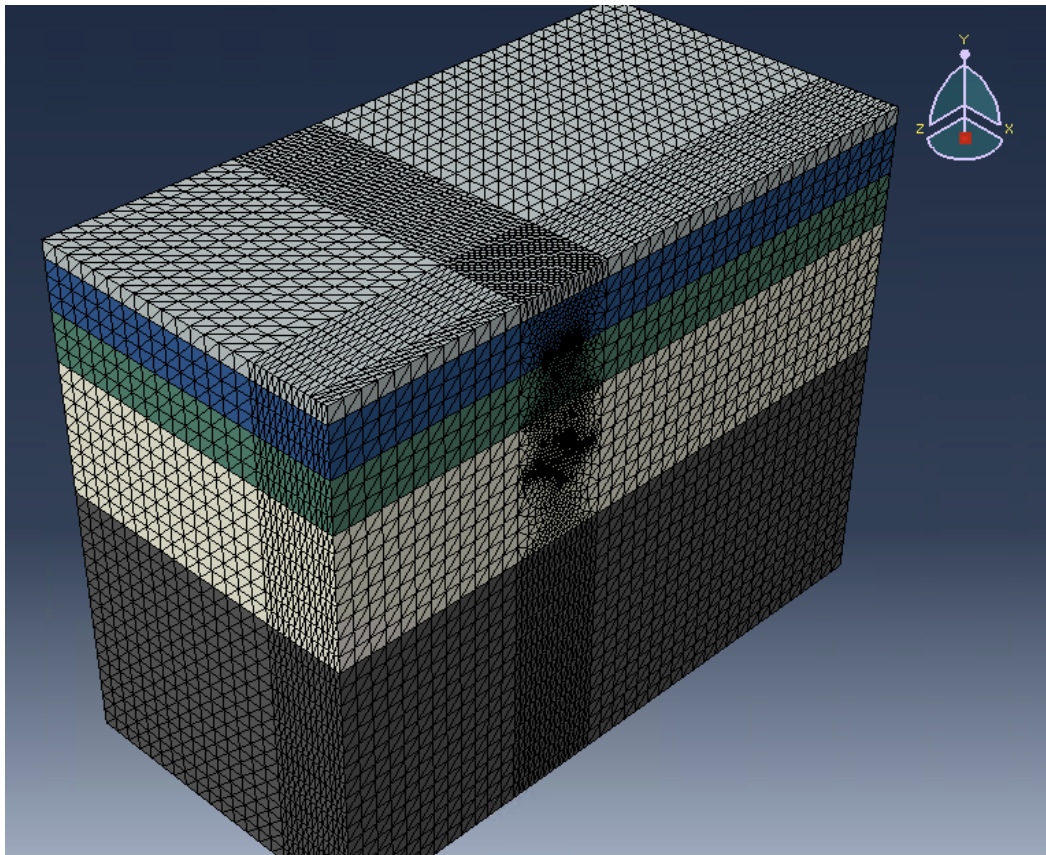


Figure 4-16 Mesh for the instrumented model

4.4.6 Result Discussion

The stress and strain output results will be discussed and compared for all four models to quantify the effect of instrumentation objects embedded in the pavement structure. As the initial step, the uninstrumented model was generated first to investigate the stress and strain concentration regions in asphalt and base layers. Then, the visualization result of the uninstrumented model suggested that the peak value regions were not direct located underneath the tire loading area but were located more toward to the area under the spacing between the dual tires (Figure 4.17). Hence, the analysis reference locations were selected from not only the area

directly under the tire loading and but the area under the dual tire spacing. In the end, nodal values of stress, stress and pressure outputs from 4 models were selected from a total of 6 reference areas in each model (Figure 4.18).

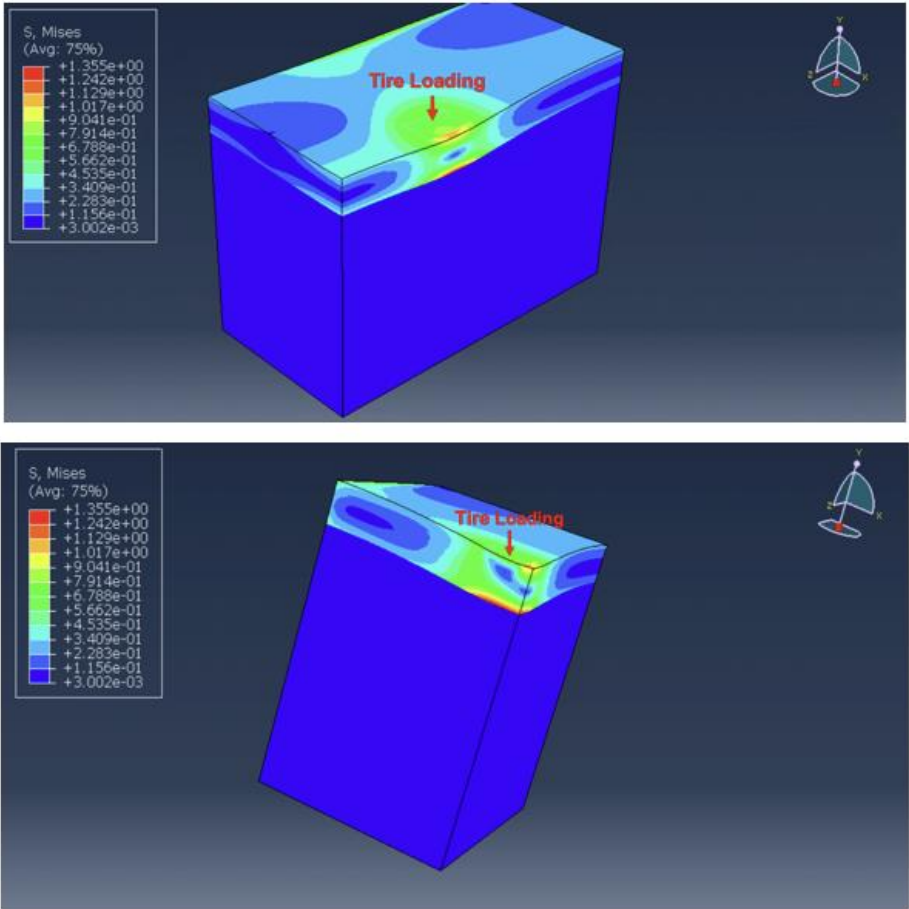


Figure 4-17 Von Mises stress distribution of the uninstrumented model

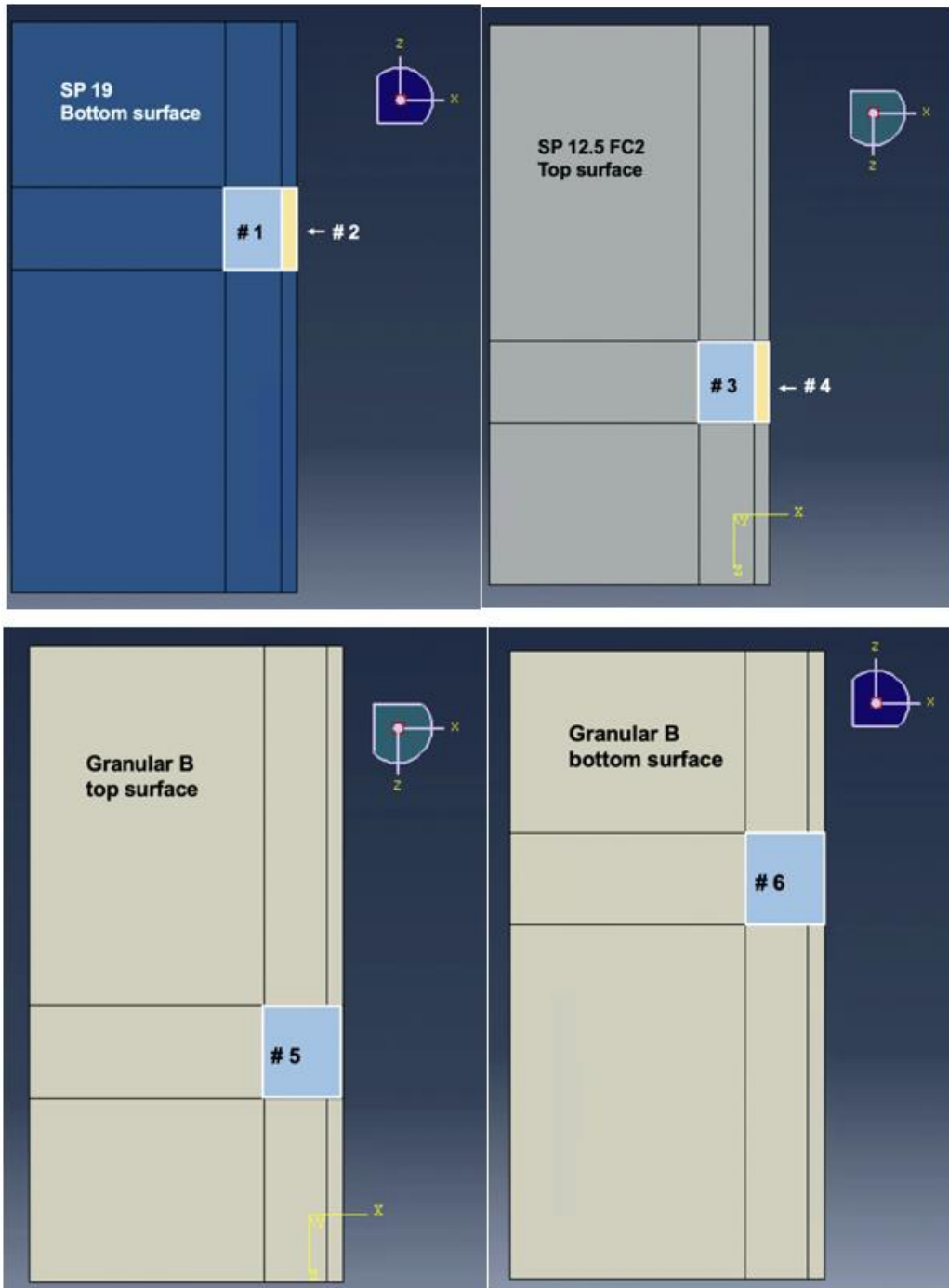


Figure 4-18 Referencing areas for the ABAQUS output results

Table 4-10 Average peak Von Mises stress and tensile strain

| Reference area (nodes location) | No instrumentation | Only strain gauge | Only pressure cell | Both pressure and strain gauge |
|--|---|---|---|---|
| #1 - At the bottom of SP 19 layer directly under the tire loading area | Smises = 1.355 E11 = 1.28e-04 E33 = 1.68e-04 | Smises = 1.32 E11 = 0.000125 E33 = 0.000168 | Smises = 1.35 E11 = 1.28e-04 E33 = 1.67e-04 | Smises = 1.32 E11 = 0.000126 E33 = 0.00017 |
| #2 - At the bottom of SP 19 layer under the dual tire spacing area | Smises = 1.27 E11 = 1e-04 E33 = 1.75e-04 | Smises = 1.58 E11 = 0.000182 E33 = 0.00022 | Smises = 1.26 E11 = 1e-04 E33 = 1.75e-04 | Smises = 1.56 E11 = 1.83e-04 E33 = 2.23e-04 |
| # 3 - On the top surface of SP 12.5 FC2 layer in the tire loading area | Smises = 0.8 Min E11 = - 0.00015 Min E33 = - 0.000162 | Smises = 0.8 Min E11 = - 0.00015 Min E33 = - 0.000164 | Smises = 0.8 Min E11 = - 0.00015 Min E33 = - 0.000163 | Smises = 0.83 Min E11 = - 0.00015 Min E33 = - 0.00016 |
| # 4 - On the top surface of SP 12.5 FC2 layer between the | Smises = 1.13 Min E11 = -9.8e-05 | Smises = 1.13 Min E11 = -9.4e-05 | Smises = 1.13 Min E11 = -9.8e-05 | Smises = 1.13 Min E11 = -9e-05 |

| | | | | |
|-------------------|-------------------------|-------------------------|-------------------------|------------------------|
| dual tire spacing | Min E33 = - 0.000169 | Min E33 = - 0.000169 | Min E33 = - 0.000168 | Min E33 = - 0.00017 |
|-------------------|-------------------------|-------------------------|-------------------------|------------------------|

Table 4-11 Average peak Von Mises stress and vertical pressure

| Reference area (nodes location) | No instrumentation | Only strain gauge | Only pressure cell | Both pressure and strain gauge |
|---|---------------------------------------|---------------------------------|-----------------------------------|---|
| # 5 - On top surface of Granular B | Smises = 7.44e- 02 S22 = -0.077 | Smises = 0.0744 S22 = -0.077 | Smises = 0.077 S22 = -0.082 | Smises = 0.0778 S22 = -0.082 |
| # 6 - On bottom surface of Granular B | Smises = 0.046 S22 = -0.031 | Smises = 0.046 S22 = -0.031 | Smises = 0.048 S22 = -0.032 | Smises = 0.048 S22 = -0.032 |

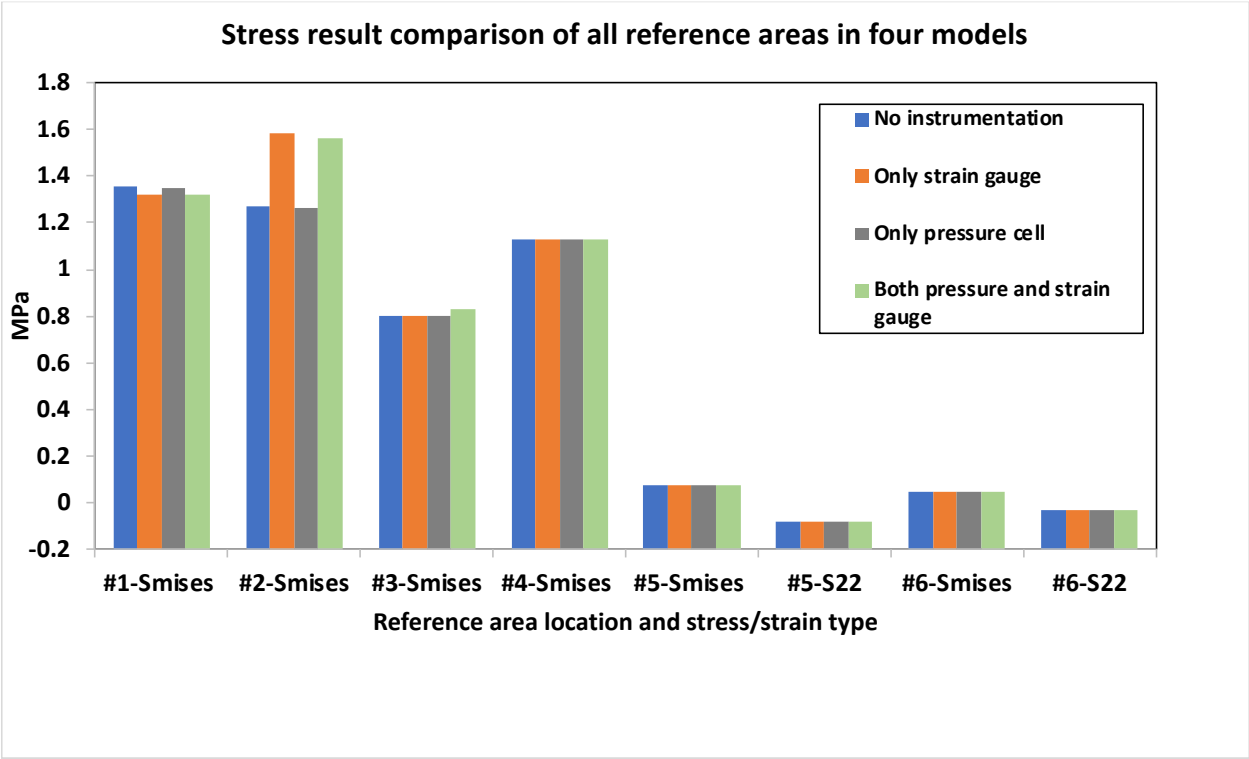


Figure 4-19 Stress results comparison of all reference areas in four models

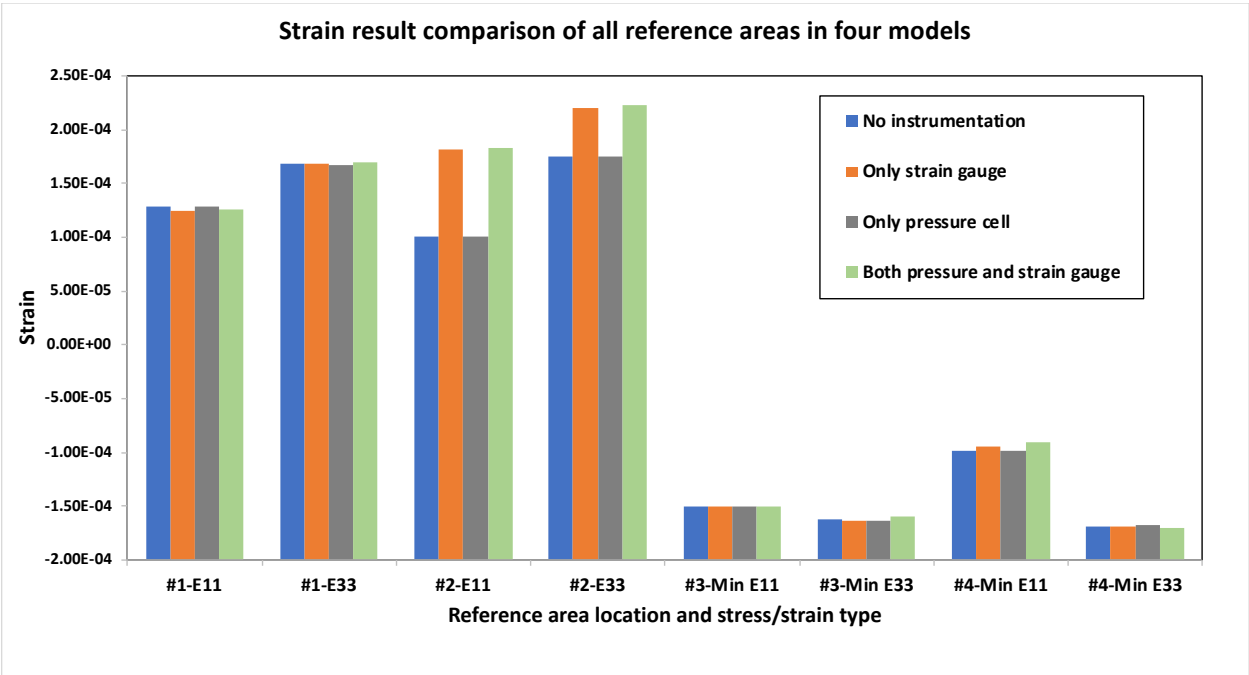
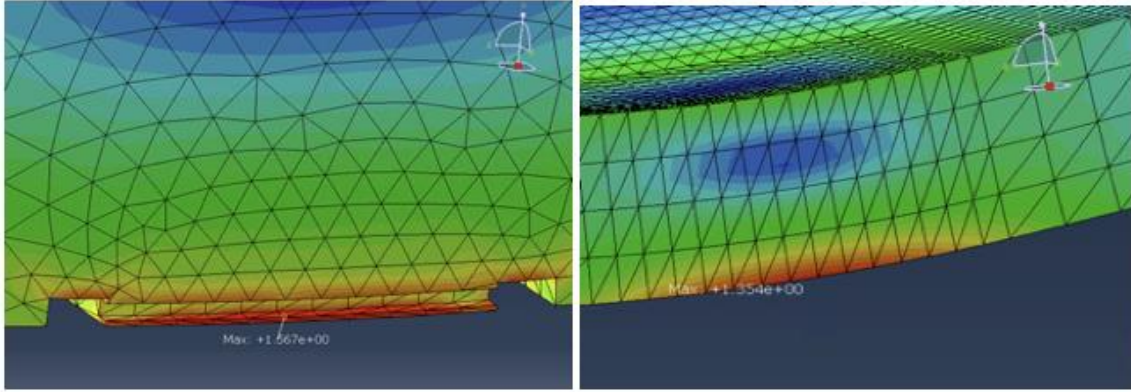
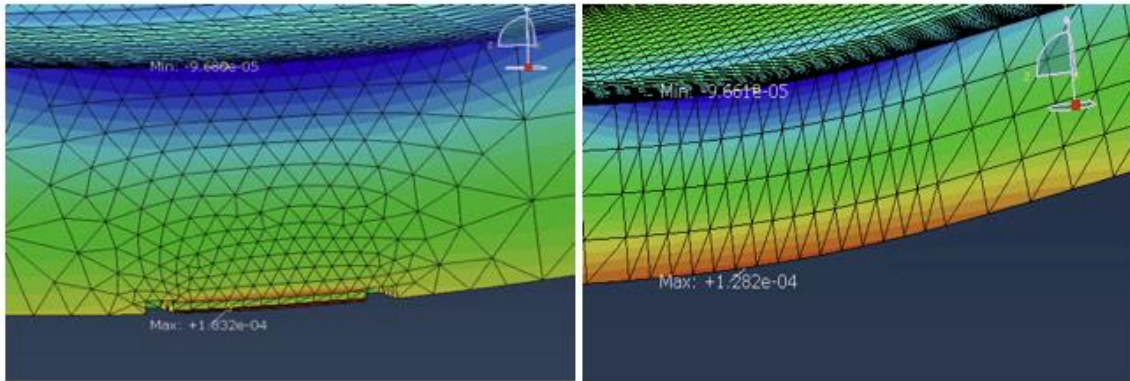


Figure 4-20 Strain results comparison of all reference areas in four models

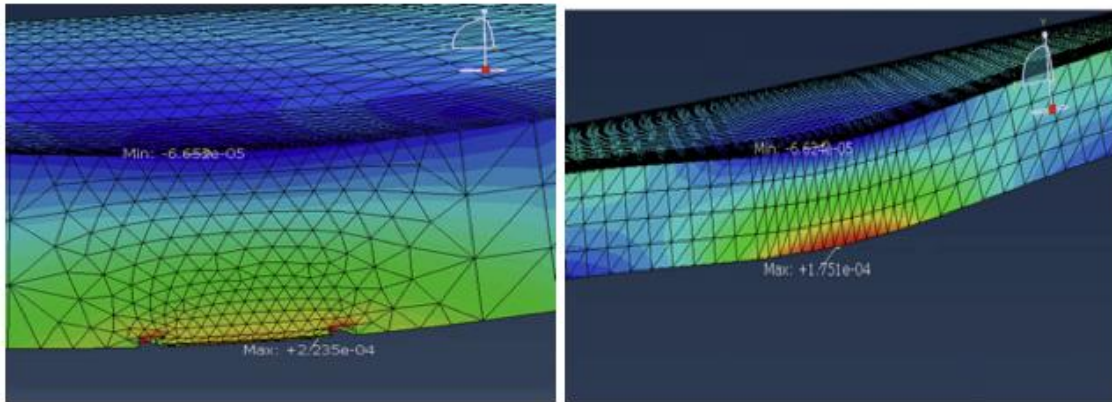
Based on the result comparison on figure 4.19 and 4.20, all four models have presented consistent stress responses to the tire loading in reference area 1, 3, 4, 5, 6 except for area 2. In area 2, which is at the bottom of the SP 19 layer and in between the dual tire spacing, the models that included strain gauge have triggered higher Von Mises stress (S Mises) and vertical stress (S22) in the asphalt material surrounds the strain gauge (Figure 4.21 a and b). Von Mises stress is a criterion to determine if the material will yield or fracture which generalizes the material behavior. In addition, the horizontal strains along X (E11) and Z (E33) directions were analyzed and compared (Figure 4.22 c, d, e, and f). Again, area 2 showed higher values of E11 and E33 than other areas. This because that the resilient modulus of asphalt strain gauge (2200MPa) is significantly lower than SP 19 (>5000MPa), and a very thin layer of SP 19 below the strain gauge was segregated from the original SP 19 structure (Figure 4.22) where the peak stress and strain values occurred. Overall, the surrounding areas of strain gauge in SP 19 layer have experience higher stress and horizontal strain under static tire loading.



(a) Both strain gauge and pressure and strain gauge (b) Only pressure cell no strain gauge
 Max Von Mises stress = 1.567 MPa Max Von Mises stress = 1.354 MPa



(c) Both strain gauge and pressure and strain gauge (d) Only pressure cell no strain gauge
 Max E11 = 1.832e-04 Max E11 = 1.282e-04



(e) Both strain gauge and pressure and strain gauge (f) Only pressure cell no strain gauge
 Max E33 = 2.235e-04 Max E33 = 1.751e-04

Figure 4-21 Stress and strain comparison between the models with and without strain gauge

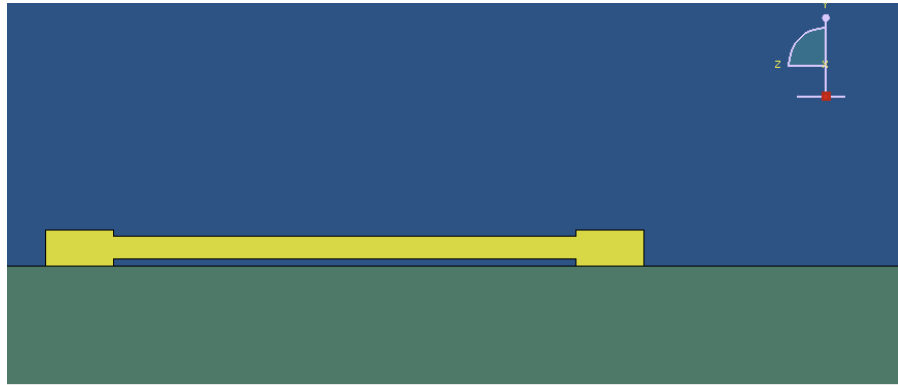


Figure 4-22 Specific location of the strain gauge (yellow) at the bottom of the SP 19 layer (blue) and above the Granular A layer (green)

4.5 Conclusion

Pavement instrumentation involves a series of sensors to monitor the pavement structural health and dynamic responses under traffic loading. The basis of the pavement instrumentation and structural health monitoring is to analyze the data that are collected from the embedded sensors. However, there are limited understandings of the interactions between the foreign objects (sensors) and the pavement structure. How and what the instrumentation sensors would affect the stress and strain distributions within the pavement structure is unclear. In order to investigate the effect of instrumentation sensors embedded within the pavement structure, static finite element analysis was conducted to quantitatively analysis pavement responses.

In addition, prior to the FEA modelling, a brief review of the instrumentation site construction plan was conducted to provide the necessary geometry and material inputs for the ABAQUS model. The proposed flexible pavement design includes 4 layers with a total thickness of 745mm:

- Surface course: 50 mm of SP 12.5 FC2
- Binder course: 145 mm of SP 19
- Base: 150mm of Granular A
- Subbase: 400mm of Granular B

Based on the details provides from the site design plan, a set of four static implicit finite element models were constructed in ABAQUS:

- Includes both strain gauge and pressure cell
- Includes only strain gauge
- Includes only pressure cell
- Original pavement structure without sensors

The pavement response results were analyzed and compared in terms of Von Mises stress (S Mises), vertical stress (S_{22}), and horizontal strains (E_{11} and E_{33}). A total of 6 reference locations were kept consistent throughout the 4 models to provide precise comparison. These locations are on top of the SP 12.5 surface, at the bottom surface of the SP 19, and the surfaces on top and bottom of the Granular B.

After the comparison and analysis of the stress and strain values from the different models, several conclusions were drawn:

- The peak Von Mises stress is located directly under the tire loading area at the bottom of the SP 19 layer
- The peak horizontal strain (E_{33}) along the vehicle travel direction was located under the area in between the dual tire spacings at the bottom of the SP 19 layer.
- The peak horizontal strain (E_{11}) in the transverse direction is located in the tire loading areas at the bottom of the SP 19 layer.
- Peak horizontal strains (E_{11} and E_{33}) appeared in the areas that surround the strain gauges. This happened when the modulus of the strain gauge was lower than the asphalt material. In addition, the unique shape of the strain gauge has segmented SP 19 into smaller sections thus reduced the asphalt material's ability to distribute the load.
- Although the pressure cell is composed of high strength steel material (193 GPa), modelling results have shown its negligible effect to stress and strain measurements in the upper AC layers when the pressure cell embedded in the Granular B layer and

150mm below layer's top surface. This suggests that when the strain gauge and pressure cell are vertically aligned together, the depth of the pressure cell shall be enough to prevent the potential impact on the strain gauge located above. The specific vertical distance requirement may depend on the material properties of the pavement layers. Preferably, to avoid such potential interference, a horizontal distance between pressure cell and strain gauge should be maintained at least 3 ft.

At the end, despite there may be slight difference between actual pavement responses and the readings recorded by instrumentation sensors, embedded sensors are still able to provide accurate strain and stress measurements in an effective way. Instrumentation sensors are the key components of the pavement structural health monitoring. Instrumentation layout design and installing shall be carefully conducted based on a thorough site review to avoid the potential interference.

Chapter 5

Conclusions and Future Work

5.1 Summary of Findings and Conclusions

Based on the analysis and discussion results from Chapter 2, 3, and 4 of this research, the following findings and conclusions were drawn:

- Recent methodologies of machine learning applications in pavement performance prediction have been identified:
- Based on literature review, ANN algorithm has been predominantly used to achieve high prediction accuracy, which was the focus of most previous studies. However, the interpretation of prediction process has not yet been the focus of previous studies, which is in fact crucial to pavement M&R decision-making.
- Using the input parameters suggested from literature review, a decision tree model, and a random forest model for IRI prediction were constructed. After algorithm optimization and pruning, both models achieved promising results.
- Both DT and RF models presented clear visualization of decision trees. Although the RF model had slightly higher accuracy, it consists of multiple trees with high structural complexity which can be difficult to understand and analyze. On the other hand, the single tree from DT model has better interpretability, allowing for concise understanding of prediction process.
- Data quantity and quality significantly affect model prediction accuracy. Based on data inconsistency issue on current pavement database, general rules for future data collection schemes are summarized:
 - The collection frequency and interval for all types of data must be carefully considered and planned prior to the official opening to traffic.
 - Corresponding update of collection frequency and interval should be made to each major M&R event.

- In-situ pavement monitoring must include following types of measurement: AC strain, soil pressure, temperature and moisture at various depths, and frost penetration. Innovative SHM technologies and equipment are beneficial, but the design should also pay attention to avoid device interference.
- Finite element analysis (FEA) was utilized to investigate subsurface structural condition with embedded sensors and under loading:
 - The peak Von Mises stress is located directly under the tire loading area at the bottom of SP 19 layer
 - The peak horizontal strain (E33) along the vehicle travel direction was located under the area in between the dual tire spacings at the bottom of the SP 19 layer.
 - The peak horizontal strain (E11) in the transverse direction is located in the tire loading areas at the bottom of the SP 19 layer.
 - Peak horizontal strains (E11 and E33) appeared in the areas that surround the strain gauges
 - When the pressure cell embedded in the Granular B layer and 150mm below layer's top surface. it showed negligible effect to strain measurements in upper AC layers
- Based on FEA results, when strain gauge and pressure cell are vertically aligned together, to avoid potential device interference, a horizontal distance between pressure cell and strain gauge shall be maintained at least 3 ft. The specific vertical distance requirements may depend on the material properties of the pavement layers. In order to capture the peak horizontal strain, asphalt strain gauges should be place at the bottom of binder course (SP 19). The spacing of strain gauges and pressure cells should be in multiple widths to accommodate different vehicle axle width and different wheel path (e.g, 2.5m-2.6m for trucks and 1.8m-2m for passenger vehicles).

5.2 Research Contributions

In this research, key contributions were made to AI/ML-aided pavement performance data analysis and in-situ pavement monitoring:

- This study has provided a systematic literature review of AI/ML-aided pavement performance prediction studies of which the outcomes help future researchers determine effective predictive modelling strategies efficiently by reducing random errors and biases and highlighting underlying problems. The most commonly used algorithm types, input variables, output predictors, and databases have been identified and evaluated from the review studies.
- Previous AI/ML-aided pavement performance prediction studies have focused on the use of neural networks (ANN) to achieve high results accuracy, but whether more interpretable algorithms such as DT are also able to result in similar level of accuracy while improving interpretability has not been investigated. Based on the IRI prediction models in this study, it has been demonstrated that DT and RF algorithms are capable of achieving promising accuracy while providing clearer decision-making visualization using pavement data.
- Since LTPP is the largest pavement database in North America and highly accessible to public researchers, by explaining the data selection and cleaning processes, this study provides concise instructions of LTPP data preparation allowing future researchers to reproduce/replicate the datasets from LTPP for model advancements.
- Based on the common data inconsistency problems on LTPP database, this study has initiated the regulation planning of mechanistic data collection and formulated criteria for optimizing condition data collection. High data quality and quantity help prediction models to maximize the performance.

- How asphalt strain gauge and soil pressure cell affect the pavement structure under loading has been discovered via finite element approach. The interaction between strain gauge and pressure cell has also been identified based on FEA modelling allowing the sensor layout design to avoid the interference of stiff pressure cell in strain measurements and reading errors.

5.3 Recommendations for Future Work

Based on the outcome of this thesis, recommendations for future work are summarized:

- Develop machine learning models based on the existing dataset for IRI prediction using other supervised learning approaches including neural networks to better compare different algorithms' performance.
- Compare the accuracy and efficiency all types of algorithms and identify the advantages and limitations of each type of model. Discuss and evaluate their overall practicability and implementation feasibility (i.e., the cost-effectiveness ratio of input data complexity and computational cost to accuracy)
- Develop detailed pavement in-situ pavement monitoring data collection regulations defining specific collection frequencies and periods. Improve the existing conditional survey data collection scheme: may reduce the survey frequency but the scheduling should be carefully consulted with pavement management experts.
- Develop a preliminary prototype of multi-functional wireless sensor that allows for real-time monitoring of asphalt temperature and strength.
- Initial the pilot section construction, determine the location of instrumented area, and adjust the instrumentation layout and device selection based on actual in-situ condition accordingly (e.g., may increase the depth of pressure cell position based on the actual thickness and quality of subbase layers).
- Establish an online cloud repository for data exchange, storage and management.
- Conducting initial conditional data collection and material characterization.

- Once the instrumentation site starts to function, integrate the pre-constructed machine learning frameworks onto the accumulated datasets and further optimize the models.

Letter of Copyright Permissions



Palansky, Thomas <tpalansky@ctlgroup.com>

To: Jianqi Kang



Tue 2022-08-16 17:12

Permission granted with the proper credit (CTLGroup) under the picture.

Regards,
Thomas S. Palansky, PE, Assoc. DBIA™
Vice President, Business Development

Check out our new and enhanced website!
www.ctlgroup.com



CTLGroup
5400 Old Orchard Road
Skokie, IL 60077-1030
Direct: (847) 972-3078
Cell: (708) 473-7400
Fax: (847) 965-6541
tpalansky@ctlgroup.com



In New York, Michigan, and North Carolina, CTLGroup operates through CTL Engineers & Construction Technology Consultants, P.C.

CTLGroup Asphalt Strain Gauges



Al-Qadi, Imad L. <alqadi@illinois.edu>

To: Jianqi Kang



Tue 2022-08-16 17:46



Sure. Best of luck.

Regards,
Imad Al-Qadi

Sent from an iPhone

On Aug 16, 2022, at 11:40 PM, Jianqi Kang <jianqi.kang@uwaterloo.ca> wrote:

Dear Mr. Al-Qadi

My name is Jianqi Kang and I am a graduating student from the University of Waterloo specializing in pavement engineering. My Master's thesis has included some picture of the following article: *The Virginia Smart Road: The impact of pavement instrumentation on understanding pavement performance (2004)*. My thesis topic is *Pavement Performance Prediction Using Machine Learning and Instrumentation in Smart Pavement*. I would like to ask for the citation permission that I could use the picture without any technical modifications in my thesis. Pictures are attached in the Word document. It would be appreciated if you could get back to me soon.

Best,

Jianqi Kang,
MASc Candidate
Centre for Pavement and Transportation Technology (CPATT),
Department of Civil & Environmental Engineering
University of Waterloo

Al-Qadi, I. L., Loulizi, A., Elseifi, M., & Lahouar, S. (2004). The Virginia Smart Road: The impact of pavement instrumentation on understanding pavement performance. *Journal of the Association of Asphalt Paving Technologists*, 73(3), 427-465.

License Details

This Agreement between Mr. Jianqi Kang ("You") and Elsevier ("Elsevier") consists of your license details and the terms and conditions provided by Elsevier and Copyright Clearance Center.

Print

Copy

| | |
|--|---|
| License Number | 5371000306475 |
| License date | Aug 16, 2022 |
| Licensed Content Publisher | Elsevier |
| Licensed Content Publication | Construction and Building Materials |
| Licensed Content Title | Predictive quality of the pavement ME design program for field performance of warm mix asphalt pavements |
| Licensed Content Author | Weiguang Zhang,Shihui Shen,Ahmed Faheem,Prasanta Basak,Shenghua Wu,Louay Mohammad |
| Licensed Content Date | Jan 30, 2017 |
| Licensed Content Volume | 131 |
| Licensed Content Issue | n/a |
| Licensed Content Pages | 11 |
| Type of Use | reuse in a thesis/dissertation |
| Portion | figures/tables/illustrations |
| Number of figures/tables/illustrations | 1 |
| Format | electronic |
| Are you the author of this Elsevier article? | No |
| Will you be translating? | No |
| Title | Pavement Performance Prediction Using Machine Learning and Instrumentation in Smart Pavement. |
| Institution name | University of Waterloo |
| Expected presentation date | Aug 2022 |
| Portions | Figure 2 |
| Requestor Location | Mr. Jianqi Kang 726 Cedar Bend Dr Waterloo, ON N2V 2R2 Canada Attn: Mr. Jianqi Kang GB 494 6272 12 |
| Publisher Tax ID | |
| Total | 0.00 CAD |

Zhang, W., Shen, S., Faheem, A., Basak, P., Wu, S., & Mohammad, L. (2017). Predictive quality of the pavement ME design program for field performance of warm mix asphalt pavements. *Construction and Building Materials*, 131, 400-410.

This is a License Agreement between Jianqi Kang ("User") and Copyright Clearance Center, Inc. ("CCC") on behalf of the Rightsholder identified in the order details below. The license consists of the order details, the Marketplace Order General Terms and Conditions below, and any Rightsholder Terms and Conditions which are included below. All payments must be made in full to CCC in accordance with the Marketplace Order General Terms and Conditions below.

| | | | |
|------------------|-------------|-------------|-------------------------------------|
| Order Date | 16-Aug-2022 | Type of Use | Republish in a thesis/dissertation |
| Order License ID | 1258588-1 | Publisher | American Society of Civil Engineers |
| ISSN | 0887-381X | Portion | Image/photo/illustration |

LICENSED CONTENT

| | | | |
|-------------------|--|------------------|-------------------------------------|
| Publication Title | Journal of Cold Regions Engineering | Country | United States of America |
| Author/Editor | TECHNICAL COUNCIL ON COLD REGIONS ENGINEERING. | Rightsholder | American Society of Civil Engineers |
| Date | 01/01/1987 | Publication Type | Journal |
| Language | English | | |

REQUEST DETAILS

| | | | |
|---|--------------------------|-----------------------------|----------------------------------|
| Portion Type | Image/photo/illustration | Distribution | Canada |
| Number of images / photos / illustrations | 5 | Translation | Original language of publication |
| Format (select all that apply) | Electronic | Copies for the disabled? | No |
| Who will republish the content? | Academic institution | Minor editing privileges? | No |
| Duration of Use | Life of current edition | Incidental promotional use? | No |
| Lifetime Unit Quantity | Up to 499 | Currency | CAD |
| Rights Requested | Main product | | |

NEW WORK DETAILS

| | | | |
|-----------------|--|----------------------------|------------------------|
| Title | Pavement Performance Prediction Using Machine Learning and Instrumentation in Smart Pavement | Institution name | University of Waterloo |
| Instructor name | Hassan Baaj | Expected presentation date | 2022-08-31 |

ADDITIONAL DETAILS

| | | | |
|------------------------|-----|---|-------------|
| Order reference number | N/A | The requesting person / organization to appear on the license | Jianqi Kang |
|------------------------|-----|---|-------------|

REUSE CONTENT DETAILS

| | | | |
|---|--|--|---|
| Title, description or numeric reference of the portion(s) | The pictures of instrumentation devices and installation | Title of the article/chapter the portion is from | Instrumentation for Monitoring Pavement Performance in Cold Regions |
| Editor of portion(s) | N/A | Author of portion(s) | TECHNICAL COUNCIL ON COLD REGIONS ENGINEERING. |
| Volume of serial or monograph | N/A | Issue, if republishing an article from a serial | N/A |
| Page or page range of portion | 8-12 | Publication date of portion | 2014-10-09 |

Maadani, O., Abd El Halim, A. O., & Mostafa, N. (2015). Instrumentation for monitoring pavement performance in cold regions. *Journal of cold regions engineering*, 29(4), 04014017.

References

- Abo-Hashema, M. A. (2013). Modeling pavement temperature prediction using artificial neural networks. *Airfield Highw. Pavement: Sustainable Effic. Pavements - Proc. Airfield Highw. Pavement Conf.*, 490–505.
- Al-Qadi, I. L., Lahouar, S., & Loulizi, A. (2001). In situ measurements of hot-mix asphalt dielectric properties. *NDT & e International*, 34(6), 427-434.
- Al-Qadi, I. L., Loulizi, A., Elseifi, M., & Lahouar, S. (2004). The Virginia Smart Road: The impact of pavement instrumentation on understanding pavement performance. *Journal of the Association of Asphalt Paving Technologists*, 73(3), 427-465.
- Amin, M. S. R., & Amador-Jiménez, L. E. (2015). Pavement management with dynamic traffic and artificial neural network: A case study of Montreal. *Can. J. Civ. Eng.*, 43(3), 241–251.
- Amin, S. R., & Amador-Jiménez, L. E. (2017). Backpropagation Neural Network to estimate pavement performance: dealing with measurement errors. *Road Mater. Pavement Des.*, 18(5), 1218–1238.
- Ansari, F. (2007). Practical implementation of optical fiber sensors in civil structural health monitoring. *Journal of intelligent material systems and structures*, 18(8), 879-889.
- Attoh-Okine, N. O. (2002). Combining use of rough set and artificial neural networks in doveled-pavement-performance modelling - a hybrid approach. *Journal of Transportation Engineering*, 128(3), 270–275.
- Attoh-Okine, N. O., Cooger, K., & Mensah, S. (2009). Multivariate adaptive regression (MARS) and hinged hyperplanes (HHP) for doveled pavement performance modeling. *Constr Build Mater*, 23(9), 3020–3023.
- Barriera, M., Pouget, S., Lebental, B., & Van Rompu, J. (2020). In situ pavement monitoring: A review. *Infrastructures*, 5(2), 18.
- Barua, L., Zou, B., Noruzoliaee, M., & Derrible, S. (2020). A gradient boosting approach to understanding airport runway and taxiway pavement deterioration. *Int. J. Pavement Eng.*

- Basheer, I. A., & Najjar, Y. M. (1996). A neural network-based distress model for Kansas JPCP longitudinal joints. *Intell Eng Syst Artif Neural Networks*, 6, 983–987.
- Bayrak, M. B., Guclu, A., Ceylan, H., & Iowa State University, A. (2005). *Rapid Pavement Backcalculation Technique for Evaluating Flexible Pavement Systems*. 14p-.
- Beltrán, G., & Romo, M. (2014). Assessing artificial neural network performance in estimating the layer properties of pavements. *Ingen. Invest.*, 34(2), 11–16.
- Bianchini, A., & Bandini, P. (2010). Prediction of pavement performance through neuro-fuzzy reasoning. *Comput.-Aided Civ. Infrastruct. Eng.*, 25(1), 39–54.
- Bramer, M. (2013). Ensemble classification. In *Principles of Data Mining* (pp. 209-220). Springer, London.
- Breiman, L. (2001). Random forests. *Machine learning*, 45(1), 5-32.
- Breiman, L., Friedman, J. H., Olshen, R. A., & Stone, C. J. (1984). *Classification and regression trees*. Routledge.
- Burak Goktepe, A., Agar, E., & Hilmi Lav, A. (2006). Role of learning algorithm in neural network-based backcalculation of flexible pavements. *J. Comput. Civ. Eng.*, 20(5), 370–373.
- Ceylan, H., Guclu, A., Tutumluer, E., & Thompson, M. R. (2005). Backcalculation of full-depth asphalt pavement layer moduli considering nonlinear stress-dependent subgrade behavior. *Int. J. Pavement Eng.*, 6(3), 171–182.
- Chandra, S., Sekhar, C. R., Bharti, A. K., & Kangadurai, B. (2013). Relationship between pavement roughness and distress parameters for indian highways. *J. Transp. Eng.*, 139(5), 467–475.
- Chang, J., Chen, S., Chen, D., & Liu, Y. (2008). Rutting Prediction Model Developed by Genetic Programming Method Through Full Scale Accelerated Pavement Testing. *2008 Fourth International Conference on Natural Computation*, 6, 326–330.
- Chen, C., Seo, H. S., Zhao, Y., Chen, B., Kim, J. W., Choi, Y., & Bang, M. (2019). Pavement damage detection system using big data analysis of multiple sensor. *Int. Conf. Smart Infrastruct. Constr., ICSIC : Driv. Data-Inf. Decis.-Mak.*, 559–569

- Choi, J.-H., Adams, T. M., & Bahia, H. U. (2004). Pavement roughness modeling using back-propagation neural networks. *Comput.-Aided Civ. Infrastruct. Eng.*, 19(4), 295–303.
- Choi, S., & Do, M. (2020). Development of the road pavement deterioration model based on the deep learning method. *Electronics (Switzerland)*, 9(1).
- City of Kitchener. (2019). *Complete Streets Kitchener.*, Kitchener, October 2019., https://www.kitchener.ca/en/resourcesGeneral/Documents/DSD_Transport_Complete_Streets_Kitchener_Community_Edition.pdf
- Deng, Y., Luo, X., Zhang, Y., & Lytton, R. L. (2021). Evaluation of flexible pavement deterioration conditions using deflection profiles under moving loads. *Transp. Geotech.*, 26.
- Deng, Y., Luo, X., Zhang, Y., Cai, S., Huang, K., Shi, X., & Lytton, R. L. (2021). Determination of flexible pavement deterioration conditions using Long-Term Pavement Performance database and artificial intelligence-based finite element model updating. *J. Struct. Control Health Monit.*, 28(2).
- Domitrović, J., Dragovan, H., Rukavina, T., & Dimter, S. (2018). Application of an artificial neural network in pavement management system. *Teh. Vjesn.*, 25, 466–473.
- Dong, Y., Shao, Y., Li, X., Li, S., Quan, L., Zhang, W., & Du, J. (2019). Forecasting Pavement Performance with a Feature Fusion LSTM-BPNN Model. *Proceedings of the 28th ACM International Conference on Information and Knowledge Management, Conference Proceedings*, 1953–1962.
- Dong, Z., Ma, X., & Shao, X. (2018). Airport pavement responses obtained from wireless sensing network upon digital signal processing. *International Journal of Pavement Engineering*, 19(5), 381-390.
- Eldin, N. N., & Senouci, A. B. (1995). Pavement condition-rating model using backpropagation neural networks. *Microcomput Civ Eng*, 10(6), 433–441.
- Elshamy, M. M. M., Tiraturyan, A. N., Uglova, E. v., & Zakari, M. (2020). Development of the non-destructive monitoring methods of the pavement conditions via artificial neural networks. *J. Phys. Conf. Ser.*, 1614(1).

- Federal Highway Administration. (2019). *Long-Term Pavement Performance Information Management System User Guide*, Washington, D.C., Federal Highway Administration. FHWA-RD-03-088
- Fraser, T. (2019). 321 Courtland Avenue, Kitchener ON Former Schneider's Plant. *Preliminary Stormwater Management Report.*, Stantec Consulting Ltd.
- Fürnkranz, J., & Widmer, G. (1994). Incremental reduced error pruning. In *Machine Learning Proceedings 1994* (pp. 70-77). Morgan Kaufmann.
- Georgiou, P., Plati, C., & Loizos, A. (2018). Soft Computing Models to Predict Pavement Roughness: A Comparative Study. *Adv. Civ. Eng.*, 2018
- Gong, H., Sun, Y., & Huang, B. (2019). Gradient Boosted Models for Enhancing Fatigue Cracking Prediction in Mechanistic-Empirical Pavement Design Guide. *J Transp Eng Part B Pavements*, 145(2).
- Gong, H., Sun, Y., Hu, W., & Huang, B. (2021). Neural networks for fatigue cracking prediction using outputs from pavement mechanistic-empirical design. *Int. J. Pavement Eng.*, 22(2), 162–172.
- Gong, H., Sun, Y., Hu, W., Polaczyk, P. A., & Huang, B. (2019). Investigating impacts of asphalt mixture properties on pavement performance using LTPP data through random forests. *Constr Build Mater*, 204, 203–212.
- Gong, H., Sun, Y., Mei, Z., & Huang, B. (2018). Improving accuracy of rutting prediction for mechanistic-empirical pavement design guide with deep neural networks. *Constr Build Mater*, 190, 710–718.
- Gong, H., Sun, Y., Shu, X., & Huang, B. (2018). Use of random forests regression for predicting IRI of asphalt pavements. *Construction and Building Materials*, 189, 890-897.
- Gopalakrishnan, K., & Ceylan, H. (2008). Stiffness characterisation of full-scale airfield test pavements using computational intelligence techniques. *IES J. Part A Civ. Struct. Eng.*, 1(4), 280–290.

- Gopalakrishnan, K., Ceylan, H., & Guclu, A. (2009). Airfield pavement deterioration assessment using stress-dependent neural network models. *Struct. Infrastructure Eng.*, 5(6), 487–496.
- Government of Ontario. (2010). *Foundation, Frost Penetration Depths for Southern Ontario* (3090.101). Ontario Provincial Standard Specification.
- Gu, F., Luo, X., Zhang, Y., Chen, Y., Luo, R., & Lytton, R. L. (2018). Prediction of geogrid-reinforced flexible pavement performance using artificial neural network approach. *Road Materials and Pavement Design*, 19(5), 1147-1163.
- Guo, F., Zhao, X., Gregory, J., & Kirchain, R. (2021). A weighted multi-output neural network model for the prediction of rigid pavement deterioration. *Int. J. Pavement Eng.*
- Gupta, A., Kumar, P., & Rastogi, R. (2011). Pavement deterioration and maintenance model for low volume roads. *Int. J. Pavement Res. Technol.*, 4(4), 195–202.
- Haas, R., & Hudson, W. R. (2015). *Pavement asset management*. John Wiley & Sons.
- Haas, R., Hudson, W. R., & Zaniewski, J. P. (1994). *Modern pavement management*.
- Harvey Philip, D. (1982). Engineering Properties of Steels. *Metals Park, OH: American Society for Metals*.
- He, L., Zhu, H., & Gao, Z. (2018). Performance evaluation of asphalt pavement based on bp neural network. *NeuroQuantology*, 16(6), 537–545.
- Heidari, M. J., Najafi, A., & Alavi, S. (2018). Pavement deterioration modeling for forest roads based on logistic regression and artificial neural networks. *Croat. J. For. Eng.*, 39(2), 271–287.
- Hossain, M. I., Gopiseti, L. S. P., & Miah, M. S. (2017). Prediction of international roughness index of flexible pavements from climate and traffic data using artificial neural network modeling. In *Airfield and highway pavements 2017* (pp. 256-267).
- Hossain, M. I., Gopiseti, L. S. P., & Miah, M. S. (2019). International roughness index prediction of flexible pavements using neural networks. *Journal of Transportation Engineering, Part B: Pavements*, 145(1), 04018058.

- Hosseini, S. A., Alhasan, A., & Smadi, O. (2020). Use of deep learning to study modeling deterioration of pavements a case study in Iowa. *Infrastructures*, 5(11), 1–17.
- Huang, Y. H. (2004). *Pavement analysis and design* (Vol. 2, pp. 401-409). Upper Saddle River, NJ: Pearson Prentice Hall.
- Huyan, J., Li, W., Tighe, S., Zhai, J., Xu, Z., & Chen, Y. (2019). Detection of sealed and unsealed cracks with complex backgrounds using deep convolutional neural network. *Automation in Construction*, 107, 102946.
- Jalal, M., Floris, I., & Quadrifoglio, L. (2017). Computer-aided prediction of Pavement Condition Index (PCI) using ANN. *Proc. Int. Conf. Comput. Ind. Eng., CIE*.
- Kalooop, M. R., El-Badawy, S. M., Ahn, J., Sim, H.-B., Hu, J. W., & Abd El-Hakim, R. T. (2020). A hybrid wavelet-optimally-pruned extreme learning machine model for the estimation of international roughness index of rigid pavements. *Int. J. Pavement Eng.*
- Kamboozia, N., Ziari, H., & Behbahani, H. (2018). Artificial neural networks approach to predicting rut depth of asphalt concrete by using of visco-elastic parameters. *Constr Build Mater*, 158, 873–882.
- Karan, M. A., Christison, T. J., Cheetham, A., & Berdahl, G. (1983). Development and implementation of Alberta's pavement information and needs system. *Transportation Research Record*, 938, 11-20.
- Karballaezadeh, N., Danial, M. S., Moazemi, D., Band, S. S., Mosavi, A., & Reuter, U. (2020). Smart structural health monitoring of flexible pavements using machine learning methods. *Coatings*, 10(11), 1–18.
- Kargah-Ostadi, N. (2014). Comparison of machine learning techniques for developing performance prediction models. In *Computing in Civil and Building Engineering (2014)* (pp. 1222-1229).
- Makendran, C., Murugasan, R., & Velmurugan, S. (2015). Performance prediction modelling for flexible pavement on low volume roads using multiple linear regression analysis. *Journal of Applied Mathematics*, 2015.

- Attoh-Okine, N. O. (1999). Analysis of learning rate and momentum term in backpropagation neural network algorithm trained to predict pavement performance. *Advances in engineering software*, 30(4), 291-302.
- Abdelaziz, N., Abd El-Hakim, R. T., El-Badawy, S. M., & Afify, H. A. (2020). International Roughness Index prediction model for flexible pavements. *International Journal of Pavement Engineering*, 21(1), 88-99.
- Radwan, M. M., Abo-Hashema, M. A., Faheem, H. P., & Hashem, M. D. (2019, November). ANN-based fatigue and rutting prediction models versus regression-based models for flexible pavements. In *International Congress and Exhibition" Sustainable Civil Infrastructures"* (pp. 117-133). Springer, Cham.
- Jia, X., Woods, M., Gong, H., Hu, W., Huang, B., & Faraj, B. (2019). Utilization of State Performance Indices to Correlate National Performance Measures for Asphalt Pavements in Tennessee. *Transportation Research Record*, 2673(6), 379-388.
- Hossain, M. I., Gopiseti, L. S. P., & Miah, M. S. (2019). International roughness index prediction of flexible pavements using neural networks. *Journal of Transportation Engineering, Part B: Pavements*, 145(1), 04018058.
- Ziari, H., Sobhani, J., Ayoubinejad, J., & Hartmann, T. (2016). Prediction of IRI in short and long terms for flexible pavements: ANN and GMDH methods. *International journal of pavement engineering*, 17(9), 776-788.
- Ling, M., Chen, Y., Hu, S., Luo, X., & Lytton, R. L. (2019). Enhanced model for thermally induced transverse cracking of asphalt pavements. *Construction and Building Materials*, 206, 130-139.
- Lou, Z., Gunaratne, M., Lu, J. J., & Dietrich, B. (2001). Application of neural network model to forecast short-term pavement crack condition: Florida case study. *Journal of infrastructure systems*, 7(4), 166-171.
- Lucey, J., Fathi, A., & Mazari, M. (2019). Predicting Pavement Roughness as a Performance Indicator Using Historical Data and Artificial Intelligence. In *Airfield and Highway*

- Pavements 2019: Innovation and Sustainability in Highway and Airfield Pavement Technology* (pp. 10-18). Reston, VA: American Society of Civil Engineers.
- Kaya, O., Ceylan, H., Kim, S., Waid, D., & Moore, B. P. (2020). Statistics and artificial intelligence-based pavement performance and remaining service life prediction models for flexible and composite pavement systems. *Transportation Research Record*, 2674(10), 448-460.
- Owusu-Ababio, S. (1998). Effect of neural network topology on flexible pavement cracking prediction. *Computer-Aided Civil and Infrastructure Engineering*, 13(5), 349-355.
- Abo-Hashema, M. A. (2013). Modeling pavement temperature prediction using artificial neural networks. In *Airfield and highway pavement 2013: Sustainable and efficient pavements* (pp. 490-505).
- Roberts, C. A., & Attoh-Okine, N. O. (1998). A comparative analysis of two artificial neural networks using pavement performance prediction. *Computer-Aided Civil and Infrastructure Engineering*, 13(5), 339-348.
- Gopalakrishnan, K., Ceylan, H., & Guclu, A. (2009). Airfield pavement deterioration assessment using stress-dependent neural network models. *Structure and Infrastructure Engineering*, 5(6), 487-496.
- Braban-Ledoux, C., & Sundin, S. (2000). Building a deterioration model for pavement management using artificial neural networks: application to rut depth prediction. *Recherche-Transports-Securite (French)*, (68).
- Guan, Z., Feng, J., Wu, Q., & Zhang, P. (2018). Mechanical analysis of full-scale accelerated pavement loading facility based on multi-body dynamics. *Systems Science & Control Engineering*, 6(1), 528-536.
- Willis, J. R. (2008). A synthesis of practical and appropriate instrumentation use for accelerated pavement testing in the United States. In APT'08. Third International

Conference Centro de Estudios y Experimentación de Obras Públicas (CEDEX)
Transportation Research Board.

- Kargah-Ostadi, N., & Stoffels, S. M. (2015). Framework for development and comprehensive comparison of empirical pavement performance models. *Journal of Transportation Engineering*, 141(8), 04015012.
- Karlaftis, M. G., Loizos, A., & Board, T. R. (2006). *Neural Networks and Nonparametric Statistical Models: Comparative Analysis in Pavement Condition Assessment*. 28p-.
- Kaur, D., & Chou, E. (1999). Applying neuro-fuzzy techniques for intelligent highway pavement performance prediction model. *42nd Midwest Symposium on Circuits and Systems (Cat. No.99CH36356)*, 2, 922–924 vol. 2.
- Kaur, D., & Tekkedil, D. (2000). Fuzzy expert system for asphalt pavement performance prediction. *ITSC2000. 2000 IEEE Intelligent Transportation Systems. Proceedings (Cat. No.00TH8493)*, 428–433.
- Kaya, O., Rezaei-Tarahomi, A., Ceylan, H., Gopalakrishnan, K., Kim, S., & Brill, D. R. (2018). Neural Network–Based Multiple-Slab Response Models for Top-Down Cracking Mode in Airfield Pavement Design. *Journal of Transportation Engineering, Part B: Pavements*, 144(2), 4018009.
- Ke-zhen, Y., Liao, H., Yin, H., Huang, L., & Engineers, A. S. of C. (2011). *Predicting the Pavement Serviceability Ratio of Flexible Pavement with Support Vector Machines*. pp 24-32.
- Kim, D.-H., Lee, S.-J., Moon, K.-H., & Jeong, J.-H. (2021). Prediction of Indirect Tensile Strength of Intermediate Layer of Asphalt Pavements Using Artificial Neural Network Model. *Arab. J. Sci. En*
- Kirbaş, U., & Karaşahin, M. (2016). Performance models for hot mix asphalt pavements in urban roads. *Constr Build Mater*, 116, 281–288
- Lea, J. D., Paige-Green, P., & Jones, D. (1998). *Neural networks for performance prediction on unsealed roads*. 1-16 (Session E).

- Lee, Y.-H., Ker, H.-W., Liu, Y.-B., & Engineers, A. S. of C. (2014). *Applications of Artificial Neural Networks to Pavement Prediction Modeling: A Case Study*. pp 289-295.
- Li, M., & Wang, H. (2018). Prediction of asphalt pavement responses from FWD surface deflections using soft computing methods. *J Transp Eng Part B Pavements*, 144(2).
- Li, M., & Wang, H. (2019). Development of ANN-GA program for backcalculation of pavement moduli under FWD testing with viscoelastic and nonlinear parameters. *Int. J. Pavement Eng.*, 20(4), 490–498.
- Li, N., Xie, W. C., & Haas, R. (1996). Reliability-based processing of Markov chains for modeling pavement network deterioration. *Transportation research record*, 1524(1), 203-213.
- Li, Y., Liu, C., Du, Y., & Jiang, S. (2020). A novel evaluation method for pavement distress based on impact of ride comfort. *Int. J. Pavement Eng.*
- Ling, M., Chen, Y., Hu, S., Luo, X., & Lytton, R. L. (2019). Enhanced model for thermally induced transverse cracking of asphalt pavements. *Constr Build Mater*, 206, 130–139.
- Liu, G., Niu, F., & Wu, Z. (2020). Life-cycle performance prediction for rigid runway pavement using artificial neural network. *Int. J. Pavement Eng.*, 21(14), 1806–1814.
- Liu, Y., & Sun, M. (2007). Fuzzy optimization BP neural network model for pavement performance assessment. *2007 IEEE International Conference on Grey Systems and Intelligent Services*, 1031–1034.
- Maadani, O., Abd El Halim, A. O., & Mostafa, N. (2015). Instrumentation for monitoring pavement performance in cold regions. *Journal of cold regions engineering*, 29(4), 04014017.
- Maalouf, M., Khoury, N., Laguros, J. G., & Kumin, H. (2012). Support vector regression to predict the performance of stabilized aggregate bases subject to wet-dry cycles. *Int. J. Numer. Anal. Methods Geomech.*, 36(6), 675–696.
- Mahmood, M., Rahman, M., & Mathavan, S. (2020). Multi-Types of Flexible Pavement Deterioration Prediction Models. *2020 6th International Engineering Conference "Sustainable Technology and Development" (IEC)*, 7-12.

- Makendran, C., Vignesh Kumar, M., Mahalingam, B., Packialakshmi, S., & Palani, T. (2020). Roughness prediction models based on variable distress parameters using neural network and MLRA for PMGSY roads. *Int. J. Adv. Sci. Technol.*, 29(7 Special Issue), 2208–2218.
- Marcelino, P., de Lurdes Antunes, M., Fortunato, E., & Gomes, M. C. (2021). Machine learning approach for pavement performance prediction. *International Journal of Pavement Engineering*, 22(3), 341-354.
- Materials Engineering and Research Office (MTO) (2019). *Ontario's Default Parameters for AASHTOWare Pavement ME Design Interim Report*. Downsview, ON: Ministry of Transportation Ontario.
- Mazari, M., & Rodriguez, D. D. (2016). Prediction of pavement roughness using a hybrid gene expression programming-neural network technique. *J. Traffic Transp. Eng.*, 3(5), 448–455.
- Michigan Department of Transportation. (2017). *Asset Management Background Asset Management Background – International Roughness Index (IRI)*. Michigan Department of Transportation, November 2017
- Mirabdolazimi, S. M., & Shafabakhsh, G. (2017). Rutting depth prediction of hot mix asphalts modified with forta fiber using artificial neural networks and genetic programming technique. *Constr Build Mater*, 148, 666–674.
- Mitchell, T. M., & Mitchell, T. M. (1997). *Machine learning* (Vol. 1, No. 9). New York: McGraw-hill.
- Mohammad, L. N., Puppala, A. J., & Kathavate, S. (1994). Design and Reliability Assessment of Data Acquisition System for Louisiana Accelerated Loading Device. *Transportation Research Record*, (1435).
- Nabipour, N., Karballaezadeh, N., Dineva, A., Mosavi, A., Mohammadzadeh S., D., & Shamshirband, S. (2019). Comparative analysis of machine learning models for prediction of remaining service life of flexible pavement. *Mathematics*, 7(12).

- Nega, A., & Nikraz, H. (2017). Evaluation of tire-pavement contact stress distribution of pavement response and some effects on the flexible pavements. In *Airfield and Highway Pavements 2017* (pp. 174-185).
- Okuda, T., Suzuki, K., & Kohtake, N. (2017). Proposal and evaluation of pavement deterioration prediction method by recurrent neural network. *IJARE*, 3, 4.
- Okuda, T., Suzuki, K., & Kohtake, N. (2017). Proposal and Evaluation of Prediction of Pavement Rutting Depth by Recurrent Neural Network. *Proc. - IIAI Int. Congr. Adv. Appl. Inf., IIAI-AAI*, 1053–1054.
- Okuda, T., Suzuki, K., & Kohtake, N. (2018). Non-parametric Prediction Interval Estimate for Uncertainty Quantification of the Prediction of Road Pavement Deterioration. *2018 21st International Conference on Intelligent Transportation Systems (ITSC)*, 824–830.
- Oladele, A. S. (2013). Improved intelligent pavement performance (IIPP) modeling for Botswana district Gravel road networks. *Airfield Highw. Pavement: Sustainable Effic. Pavements - Proc. Airfield Highw. Pavement Conf.*, 1358–1369.
- Pallas-Areny, R., & Webster, J. G. (2012). *Sensors and signal conditioning*. John Wiley & Sons.
- Pavements and Foundation Section (MTO). (2008). *Adaptation and verification of aashto pavement design guide for ontario conditions*. Downsview, ON: Ministry of Transportation Ontario.
- Pedregosa, F., Varoquaux, Ga"el, Gramfort, A., Michel, V., Thirion, B., Grisel, O., ... others. (2011). Scikit-learn: Machine learning in Python. *Journal of Machine Learning Research*, 12(Oct), 2825–2830.
- Piryonesi, S. M., & El-Diraby, T. (2018). *Using Data Analytics for Cost-Effective Prediction of Road Conditions: Case of The Pavement Condition Index:[summary report]* (No. FHWA-HRT-18-065). United States. Federal Highway Administration. Office of Research, Development, and Technology.
- Piryonesi, S. M., & El-Diraby, T. E. (2017). A data analytics solution for predicting the condition of roads using the most affordable attributes. *CSCE-CRC Int. Constr. Spec. Conf. - Held Part Can. Soc. Civ. Eng. Annu. Conf. Gen. Meet., 1*, 39–48.

- Piryonesi, S. M., & El-Diraby, T. E. (2020). Data analytics in asset management: Cost-effective prediction of the pavement condition index. *Journal of Infrastructure Systems*, 26(1), 04019036.
- Piryonesi, S. M., & El-Diraby, T. E. (2021). Using machine learning to examine impact of type of performance indicator on flexible pavement deterioration modeling. *Journal of Infrastructure Systems*, 27(2), 04021005.
- Plati, C., Georgiou, P., & Papavasiliou, V. (2016). Simulating pavement structural condition using artificial neural networks. *Struct. Infrastructure Eng.*, 12(9), 1127–1136.
- Pu, Z., Liu, C., Wang, Y., Shi, X., Zhang, C., & Board, T. R. (2019). *Road Surface Condition Prediction using Long Short-Term Memory Neural Network based on Historical Data*. 6p-.
- Pulugurta, H., Shao, Q., & Chou, Y. J. (2009). Pavement condition prediction using Markov process. *Journal of Statistics and Management Systems*, 12(5), 853-871.
- Qiao, Y., Zhang, Y., Elshaer, M., & Daniel, J. S. (2017). A method to assess climate change induced damage on flexible pavements with machine learning. *Bear. Capacit. Roads, Railw. Airfld. - Proc. Int. Conf. Bear. Capacit. Roads, Railw. Airfld.*, 2103–2108.
- Queiroz, C. (1983). A mechanistic analysis of asphalt pavement performance in Brazil. *Journal of Association of Asphalt Paving Technology*, 52, 474-488.
- Rabe, R. (2013). Measuring pavement response—Design, development and application of sensors and data evaluation for test and in-service pavements. In *Proceedings of the international conferences on the bearing capacity of roads, railways and airfields* (pp. 465-474).
- Radwan, M. M., Abo-Hashema, M. A., Faheem, H. P., & Hashem, M. D. (2019, November). ANN-based fatigue and rutting prediction models versus regression-based models for flexible pavements. In *International Congress and Exhibition " Sustainable Civil Infrastructures "* (pp. 117-133). Springer, Cham.
- Ren, J., Vanapalli, S. K., Han, Z., Omenogor, K. O., & Bai, Y. (2019). The resilient moduli of five Canadian soils under wetting and freeze-thaw conditions and their estimation by using an artificial neural network model. *Cold Reg. Sci. Technol.*, 168.

- Rezaei-Tarahomi, A., Kaya, O., Ceylan, H., Kim, S., Gopalakrishnan, K., & Brill, D. R. (2017). Development of rapid three-dimensional finite-element based rigid airfield pavement foundation response and moduli prediction models. *Transp. Geotech.*, 13, 81–91.
- Rigabadi, A., Rezaei Zadeh Herozi, M., & Rezagholilou, A. (2021). An attempt for development of pavements temperature prediction models based on remote sensing data and artificial neural network. *Int. J. Pavement Eng.*
- Rosada, A., Arliansyah, J., & Buchari, E. (2019). Evaluation Pavement Deteriorating Condition on Surface Distress Index (SDI) Data Using Radial Basis Function Neural Networks (RBFNN). *J. Phys. Conf. Ser.*, 1198(3).
- Saghafi, B., Hassani, A., Noori, R., & Bustos, M. G. (2009). Artificial neural networks and regression analysis for predicting faulting in jointed concrete pavements considering base condition. *Int. J. Pavement Res. Technol.*, 2(1), 20–25.
- Saleh, M. (2015). Prediction of rigid pavement responses under axle loads using artificial neural network. *Int. J. Pavement Res. Technol.*, 8(1), 10–16.
- Saltan, M., & Sezgin, H. (2007). Hybrid neural network and finite element modeling of sub-base layer material properties in flexible pavements. *Mater. Des.*, 28(5), 1725–1730.
- Shahnazari, H., Tutunchian, M. A., Mashayekhi, M., & Amini, A. A. (2012). Application of soft computing for prediction of pavement condition index. *J. Transp. Eng.*, 138(12), 1495–1506.
- Sharma, S., & Das, A. (2008). Backcalculation of pavement layer moduli from falling weight deflectometer data using an artificial neural network. *Can. J. Civ. Eng.*, 35(1), 57–66.
- Shen, D.-H., & Du, J.-C. (2004). Grey model for asphalt pavement performance prediction. *Proceedings. The 7th International IEEE Conference on Intelligent Transportation Systems (IEEE Cat. No.04TH8749)*, 668–672.
- Simpson, A. L., Daleiden, J. F., & Hadley, W. O. (1995). RUTTING ANALYSIS FROM A DIFFERENT PERSPECTIVE. *Transportation Research Record*, 1473, 9–17.
- Sollazzo, G., Fwa, T. F., & Bosurgi, G. (2017). An ANN model to correlate roughness and structural performance in asphalt pavements. *Constr Build Mater*, 134, 684–693.

- Tabatabaee, N., & Sebaaly, P. (1990). State-of-the-art pavement instrumentation. *Transportation Research Record*, 1260, 246-255.
- Tabatabaee, N., Al-Qadi, I. L., & Sebaaly, P. E. (1992). Field evaluation of pavement instrumentation methods. *Journal of testing and evaluation*, 20(2), 144-151.
- Tabatabaee, N., Ziyadi, M., & Shafahi, Y. (2013). Two-stage support vector classifier and recurrent neural network predictor for pavement performance modeling. *J. Infrastruct. Syst.*, 19(3), 266–274.
- Taddesse, E. (2017). Pavement rutting prediction models for the coastal roads of southern Norway. In *Bearing Capacity of Roads, Railways and Airfields* (pp. 1375-1382). CRC Press.
- Taddesse, E. (2017). Pavement rutting prediction models for the coasroads of southern norway. *Bear. Capacit. Roads, Railw. Airfld. - Proc. Int. Conf. Bear. Capacit. Roads, Railw. Airfld.*, 1375–1382.
- Tarahomi, A., Kaya, O., Ceylan, H., Gopalakrishnan, K., Kim, S., & Brill, D. R. (2022). ANNFAA: artificial neural network-based tool for the analysis of Federal Aviation Administration’s rigid pavement systems. *International Journal of Pavement Engineering*, 23(2), 400-413.
- Terzi, S. (2007). Modeling the pavement serviceability ratio of flexible highway pavements by artificial neural networks. *Constr Build Mater*, 21(3), 590–593.
- Thube, D. T. (2012). Artificial neural network (ANN) based pavement deterioration models for low volume roads in India. *International Journal of Pavement Research and Technology*, 5(2), 115.
- Tighe, S. (2013). *Pavement Asset Design and Management Guide*. Ottawa, ON: Transportation Association of Canada.
- Tıldemir, M. (2014). Re-evaluation of the AASHTO-flexible pavement design equation with neural network modeling. *PLoS ONE*, 9(11).
- Transport Canada. “Road Transportation.” Transport Canada, March 5, 2021. <https://tc.canada.ca/en/corporate-services/policies/road-transportation-0>.

- Ullah, S., Tanyu, B. F., & Zainab, B. (2020). Development of an artificial neural network (ANN)-based model to predict permanent deformation of base course containing reclaimed asphalt pavement (RAP). *Road Mater. Pavement Des.*, 1–19.
- Ullah, S., Tanyu, B. F., & Zainab, B. (2021). Development of an artificial neural network (ANN)-based model to predict permanent deformation of base course containing reclaimed asphalt pavement (RAP). *Road Materials and Pavement Design*, 22(11), 2552-2570.
- Wang, H., Li, M., Szary, P., & Hu, X. (2019). Structural assessment of asphalt pavement condition using backcalculated modulus and field data. *Constr Build Mater*, 211, 943–951.
- Wang, L., Wenjing, X., Druta, C., & Wang, D. (2012). Integration of structural health monitoring and asset management.
- Wang, W.-N., & Tsai, Y.-C. J. (2013). Back-propagation network modeling for concrete pavement faulting using LTPP data. *International Journal of Pavement Research and Technology*, 6(5), pp 651-657.
- Wang, W., Qin, Y., Li, X., Wang, D., & Chen, H. (2017). Comparisons of Faulting-Based Pavement Performance Prediction Models. *Adv. Mater. Sci. Eng.*, 2017.
- Wei-dong, Q. (2010). Study on the Prediction and Evaluation of Composite Pavement Combination Property. *2010 International Conference on Artificial Intelligence and Computational Intelligence*, 2, 488–491.
- Wu, D., Zhao, H., Zeng, M., Zou, D., Tian, Y., & Board, T. R. (2019). *Assessment of Concrete Pavement Support Conditions Using Distributed Optical Sensing Fiber and a Neural Network*. 17p-.
- Xu, G., Bai, L., & Sun, Z. (2014). Pavement deterioration modeling and prediction for Kentucky interstate and highways. *IIE Annual Conf. Expo*, 993–1002.
- Yamany, M. S., Saeed, T. U., Volovski, M., & Ahmed, A. (2020). Characterizing the performance of interstate flexible pavements using artificial neural networks and random parameters regression. *Journal of Infrastructure Systems*, 26(2), 04020010.

- Yamany, M. S., Saeed, T. U., Volovski, M., & Ahmed, A. (2020). Characterizing the Performance of Interstate Flexible Pavements Using Artificial Neural Networks and Random Parameters Regression. *J. Infrastruct. Syst.*, 26(2).
- Yamany, M. S., Saeed, T. U., Volovski, M., & Board, T. R. (2019). *Performance Prediction of Interstate Flexible Pavement Across the Midwestern United States: Random-Parameter Regression vs Artificial Neural Network*. 7p
- Yan, K.-Z., Xu, H.-B., & Shen, G.-H. (2014). Novel approach to resilient modulus using routine subgrade soil properties. *Int. J. Geomech.*, 14(6).
- Yan, W., Peng, W., & Huaiyu, X. (2012). Research of Pavement Performance Evaluation and Prediction System of Highway Based on Linear Regression Method. *2012 International Conference on Communication Systems and Network Technologies*, 982–986.
- You, L., Yan, K., & Liu, N. (2020). Assessing artificial neural network performance for predicting interlayer conditions and layer modulus of multi-layered flexible pavement. *Front. Struct. Civ. Eng.*, 14(2), 487–500.
- Younos, M. A., Abd El-Hakim, R. T., El-Badawy, S. M., & Afify, H. A. (2020). Multi-input performance prediction models for flexible pavements using LTPP database. *Innov. Infrastruct. Solut.*, 5(1).
- Zeida, W., Dabous, S. A., Hamad, K., Al-Ruzouq, R., & Khalil, M. A. (2020). Machine learning for pavement performance modelling in warm climate regions. *Arabian journal for science and engineering*, 45(5), 4091-4109.
- Zeida, W., Hamad, K., Omar, M., Underwood, B. S., Khalil, M. A., & Karzad, A. S. (2019). Investigation and modelling of asphalt pavement performance in cold regions. *International journal of pavement engineering*, 20(8), 986-997.
- Zeida, W., Hamad, K., Omar, M., Underwood, B. S., Khalil, M. A., & Karzad, A. S. (2019). Investigation and modelling of asphalt pavement performance in cold regions. *Int. J. Pavement Eng.*, 20(8), 986–997.
- Zhang, W., Chen, X., Shen, S., Mohammad, L. N., Cui, B., Wu, S., & Raza Khan, A. (2021). Investigation of Field Rut Depth of Asphalt Pavements Using Hamburg Wheel Tracking Test. *J Transp Eng Part B Pavements*, 147

- Zhang, W., Shen, S., Faheem, A., Basak, P., Wu, S., & Mohammad, L. (2017). Predictive quality of the pavement ME design program for field performance of warm mix asphalt pavements. *Construction and Building Materials*, *131*, 400-410.
- Ziari, H., Sobhani, J., Ayoubinejad, J., & Hartmann, T. (2016). Prediction of IRI in short and long terms for flexible pavements: ANN and GMDH methods. *International Journal of Pavement Engineering*, *17*(9), pp 776-788.
- Zou, W.-L., Han, Z., Ding, L.-Q., & Wang, X.-Q. (2021). Predicting resilient modulus of compacted subgrade soils under influences of freeze–thaw cycles and moisture using gene expression programming and artificial neural network approaches. *Transp. Geotech.*, *28*.

Appendix

Material Property for ABAQUS from AASHTOWare ME Design Manual

Asphalt Mixes

Table B-1: Design Details for the Mixes

| Mix Code | Mix | PG Grade | Traffic Level | Highway Class | RAP Mix | Anti-stripping Additive | Warm Mix Additive & Modified |
|----------|------------|----------|---------------|-------------------|---------|-------------------------|------------------------------|
| 1 | SP12.5 FC2 | 70-28 | D | Freeway | - | - | - |
| 2 | | 64-28 | E | Freeway | - | 1% hydrated lime | - |
| 3 | | 64-28 | D | Freeway | 15% | - | - |
| 4 | | 64-34 | E | Freeway | - | 1% hydrated lime | - |
| 5 | SP12.5 FC1 | 64-28 | D | King's Highway | 15% | - | - |
| 6 | | 58-34P | C | King's Highway | 20% | 0.5% Adhere LOF 65-00 | 0.5% Evotherm |
| 7 | | 58-34P | D | King's Highway | - | 1% Adhere LOF 65-00 | Polymer |
| 8 | SP12.5 | 64-34 | D | King's Highway | - | 0.5% Adhere LOF 77-00 | Polymer |
| 9 | | 58-28 | C | King's Highway | 20% | - | - |
| 10 | | 58-34 | C | King's Highway | - | 0.5% Adhere LOF 77-00 | - |
| 11 | | 58-34 | C | King's Highway | - | - | 0.3% Evotherm |
| 12 | | 58-40 | B | Secondary Highway | - | 0.5% Adhere LOF 77-00 | - |
| 13 | | 52-34 | B | Secondary Highway | - | 0.5% Redicote 2914 | - |
| 14 | SP19.0 | 64-28 | E | King's Highway | 20% | - | - |
| 15 | | 64-34P | D | King's Highway | 20% | 0.5% Adhere LOF 77-00 | Polymer |
| 16 | | 58-28 | D | King's Highway | 20% | 0.5% Adhere LOF 65-00 | - |
| 17 | | 58-34P | C | King's Highway | 15% | 0.5% Adhere LOF 65-00 | Polymer |
| 18 | | 58-34 | D | King's Highway | 10% | 1% Adhere LOF 65-00 | - |
| 19 | | 52-34 | B | King's Highway | 30% | - | - |
| 20 | SP25.0 | 58-28 | D | Freeway | 15% | - | - |
| 21 | SMA | 70-28 | E | Freeway | - | 1% hydrated lime | - |

Dynamic Modulus of Asphalt Mixes

| | | Frequency, Hz | | | | | |
|--------------|------------|---------------|---------|---------|---------|---------|---------|
| Temp. °C | | 0.1 | 0.5 | 1 | 5 | 10 | 25 |
| Mix 1 | -10 | 13312.5 | 15744.7 | 16945.3 | 19552.1 | 20779.9 | 22172.2 |
| | 4 | 6286.3 | 7804.9 | 8530.1 | 10784.0 | 11878.2 | 12963.0 |
| | 21 | 2526.8 | 3286.9 | 3623.5 | 4963.6 | 5642.0 | 6243.8 |
| | 37 | 1099.0 | 1368.2 | 1495.1 | 2111.3 | 2499.9 | 2747.6 |
| | 54 | 419.5 | 523.9 | 576.5 | 895.5 | 1093.4 | 1019.8 |
| Mix 2 | -10 | 11273.0 | 13670.4 | 14837.8 | 17595.2 | 19008.1 | 20801.5 |
| | 4 | 5305.6 | 6688.2 | 7339.5 | 9463.2 | 10474.1 | 11655.5 |
| | 21 | 2161.4 | 2769.9 | 3038.2 | 4188.6 | 4804.6 | 5532.4 |
| | 37 | 1009.0 | 1229.3 | 1325.3 | 1820.9 | 2167.1 | 2491.3 |
| | 54 | 409.8 | 502.4 | 535.9 | 801.1 | 957.0 | 1038.2 |
| Mix 3 | -10 | 13134.7 | 15546.5 | 16671.8 | 19321.8 | 20500.9 | 21863.6 |
| | 4 | 6585.0 | 8524.4 | 9481.9 | 12078.5 | 13447.5 | 15023.3 |
| | 21 | 2498.1 | 3252.4 | 3564.9 | 5095.7 | 5904.7 | 6822.2 |
| | 37 | 1246.3 | 1542.7 | 1675.3 | 2362.6 | 2801.4 | 3169.3 |
| | 54 | 467.3 | 557.7 | 598.4 | 887.8 | 1029.5 | 987.8 |

Dynamic Modulus of Asphalt Mixes

| | Temp. °C | Frequency, Hz | | | | | |
|---------------|------------|---------------|---------|---------|---------|---------|---------|
| | | 0.1 | 0.5 | 1 | 5 | 10 | 25 |
| Mix 12 | -10 | 6435.7 | 8143.4 | 8945.2 | 11565.4 | 12818.6 | 14145.4 |
| | 4 | 3205.2 | 3376.1 | 3680.2 | 5037.5 | 5752.9 | 6545.4 |
| | 21 | 1368.9 | 1540.2 | 1663.4 | 2199.7 | 2563.9 | 3064.3 |
| | 37 | 716.5 | 855.2 | 907.6 | 1178.6 | 1384.6 | 1595.6 |
| | 54 | 263.3 | 312.2 | 329.1 | 471.7 | 552.2 | 527.4 |
| Mix 13 | -10 | 10335.1 | 12721.1 | 13862.7 | 16636.5 | 17895.8 | 19415.7 |
| | 4 | 4302.2 | 5662.6 | 6242.6 | 8600.4 | 9706.7 | 10638.7 |
| | 21 | 1685.2 | 2309.6 | 2561.9 | 3891.1 | 4666.5 | 5442.5 |
| | 37 | 656.5 | 808.7 | 885.7 | 1259.7 | 1565.2 | 1955.1 |
| | 54 | 220.4 | 271.0 | 289.5 | 420.2 | 507.0 | 549.2 |
| Mix 14 | -10 | 20072.5 | 22733.7 | 23882.0 | 26408.4 | 27463.0 | 29145.7 |
| | 4 | 10320.7 | 12739.5 | 13963.0 | 16878.6 | 18308.5 | 20215.8 |
| | 21 | 4114.6 | 5424.9 | 5930.2 | 8264.1 | 9435.7 | 10822.8 |
| | 37 | 1627.0 | 2162.1 | 2386.5 | 3558.0 | 4290.9 | 4759.3 |
| | 54 | 486.7 | 634.8 | 706.0 | 1108.5 | 1353.2 | 1413.8 |
| Mix 15 | -10 | 10527.3 | 12891.6 | 14052.4 | 16871.2 | 18209.8 | 19898.5 |
| | 4 | 4708.1 | 6169.8 | 6857.9 | 9171.6 | 10317.9 | 11401.2 |
| | 21 | 1738.7 | 2242.8 | 2474.5 | 3555.9 | 4202.6 | 4983.7 |
| | 37 | 850.0 | 1007.8 | 1089.0 | 1487.6 | 1795.6 | 2144.6 |
| | 54 | 330.4 | 385.8 | 416.2 | 596.5 | 721.6 | 795.3 |
| Mix 16 | -10 | 13778.3 | 16271.5 | 17365.0 | 19886.1 | 20993.4 | 22577.9 |
| | 4 | 6745.4 | 8681.3 | 9553.0 | 12368.6 | 13554.7 | 14573.6 |
| | 21 | 2625.4 | 3415.9 | 3830.9 | 5621.2 | 6611.7 | 7441.6 |
| | 37 | 998.2 | 1292.3 | 1381.5 | 2034.5 | 2532.8 | 2915.8 |
| | 54 | 350.0 | 465.8 | 491.8 | 750.1 | 975.9 | 940.7 |

Base and Subbase Material Properties

| Unbound | Granular A | Granular B-I | Granular B-II | Granular B-III | Granular O | |
|---|------------------|-----------------|------------------|-------------------|---------------|------|
| Layer Thickness (mm) | Project specific | | | | | |
| Poisson's Ratio | 0.35 | | | | | |
| Coefficient of Lateral Pressure (k_o) | 0.5 | | | | | |
| Modulus | | | | | | |
| Resilient Modulus ^{Note 1} (MPa) | 250 | 150 | 200 | 150 | 200 | |
| Sieve | | | | | | |
| Gradation and other engineering properties | | | | | | |
| Aggregate Gradation (percent passing) | 75 μ m | 5 | 4 | 5 | 4 | 2.5 |
| | 300 μ m | 13.5 | 33.5 | 13.5 | 18.5 | - |
| | 1.18 mm | 27.5 | 55 | 25 | 35 | 7.5 |
| | 4.75 mm | 45 | 60 | 37.5 | 55 | 32.5 |
| | 9.5 mm | 61.5 | - | - | 66 | 60 |
| | 13.2 mm | 77.5 | - | - | - | 70 |
| | 19.0 mm | 92.5 | - | - | - | 87.5 |
| 25 mm | 100 | 75 | 75 | 75 | 97.5 | |
| Liquid Limit | 6 | 11 | 11 | 11 | 6 | |
| Plasticity Index | 0 | | | | | |
| Is layer compacted | Yes | | | | | |
| Maximum dry unit weight (kg/m^3) | Calculated | | | | | |
| Saturated hydraulic conductivity (m/hr) | Calculated | | | | | |
| Specific gravity of solids | Calculated | | | | | |
| Optimum gravimetric water content (T) | Calculated | | | | | |

Note 1: The resilient moduli shown are based on new materials. Reduction in resilient modulus for existing granular can be up to 40% depending on the condition of materials.

Ontario Subgrade Soil Classification

| Brief Description | Category No. | MTO Classification (MTO, 1980) | Drainage Characteristics | Susceptibility at Frost Action | M _R (MPa) Good | M _R (MPa) Fair | M _R (MPa) Poor |
|---|--------------|--------------------------------|-------------------------------|--------------------------------|---------------------------|---------------------------|---------------------------|
| Rock, rock fill, shattered rock, boulders/cobbles | 1 | Boulders/cobbles | Excellent | None | 90 | 80 | 70 |
| Well graded gravels and sands suitable as granular borrow | 2 | GW, SW | Excellent | Negligible | 80 | 70 | 50 |
| Poorly graded gravels and sands | 3 | GP, SP | Excellent to fair | Negligible to slight | 70 | 50 | 35 |
| Silty gravels and sands | 4 | GM, SM | Fair to semi-impervious | Slight to moderate | 50 | 35 | 30 |
| Clayey gravels and sands | 5 | GC, SC | Practically impervious | Negligible to slight | 40 | 30 | 25 |
| Silts and sandy silts | 6 | ML, MI | Typically poor | Severe | 30 | 25 | 18 |
| Low plasticity clays and compressible silts | 7 | CL, MH | Practically impervious | Slight to severe | 35 | 20 | 15 |
| Medium to high plasticity clays | 8 | CI; CH | Semi-impervious to impervious | Negligible to severe | 30 | 20 | 15 |

Ontario Subgrade Material Property

| | Subgrade Type | | | | | | | | | | | |
|---|---------------------------------------|-----|-----|-------|-----------|-----|-----|-----|---|--|--|--|
| | CL | CI | CH | CL-ML | ML | MI | MH | SM | SC | | | |
| Unbound | | | | | | | | | | | | |
| Layer Thickness (mm) | Semi-infinite | | | | | | | | | | | |
| Poisson's Ratio ^{vi} | 0.45 (saturated) 0.2 (unsaturated) | | | | 0.325 | | | | 0.3 (dense) 0.15 (coarse-grained) 0.25 (fine-grained) | | | |
| Coefficient of Lateral Pressure (k ₀) | 0.52-0.60 | | | | 0.47-0.58 | | | | 0.4-0.53 | | | |
| Modulus | Refer to Table 21 | | | | | | | | | | | |
| Resilient Modulus (MPa) | | | | | | | | | | | | |
| Gradation and other engineering properties | | | | | | | | | | | | |
| Aggregate Gradation (percent passing) | 30 | 37 | 60 | 16 | 11 | 25 | 40 | 8 | 13 | | | |
| 0.075 mm | 80 | 88 | 92 | 84 | 74 | 82 | 84 | 29 | 32 | | | |
| 0.180 mm | 84 | 92 | 94 | 89 | 86 | 91 | 91 | 58 | 48 | | | |
| 0.425 mm | 91 | 95 | 96 | 92 | 91 | 95 | 96 | 72 | 56 | | | |
| 2.00 mm | 95 | 98 | 98 | 96 | 95 | 98 | 99 | 84 | 86 | | | |
| 4.75 mm | 97 | 99 | 99 | 98 | 96 | 100 | 100 | 90 | 93 | | | |
| 9.5 mm | 99 | 100 | 100 | 99 | 100 | 100 | 100 | 94 | 100 | | | |
| 12.5 mm | 100 | 100 | 100 | 100 | 100 | 100 | 100 | 97 | 100 | | | |
| 19.0 mm | 100 | 100 | 100 | 100 | 100 | 100 | 100 | 98 | 100 | | | |
| 25.0 mm | 100 | 100 | 100 | 100 | 100 | 100 | 100 | 100 | 100 | | | |
| Liquid Limit | 26 | 41 | 67 | 22 | 26 | 42 | 53 | 18 | 22 | | | |
| Plasticity Index | 12 | 21 | 43 | 6 | 3 | 15 | 21 | 4 | 10 | | | |
| Is layer compacted | Yes | | | | | | | | | | | |
| Maximum dry unit weight (kg/m ³) | Calculated | | | | | | | | | | | |
| Saturated hydraulic conductivity (m/hr) | Calculated | | | | | | | | | | | |
| Specific gravity of solids | Calculated | | | | | | | | | | | |
| Optimum gravimetric water content (T) | Calculated | | | | | | | | | | | |